

 Open access • Report • DOI:10.2172/1785330

Aeroacoustic Assessment of Wind Plant Controls — [Source link](#)

Nicholas Hamilton, Pietro Bortolotti, Dave Jager, Yi Guo ...+2 more authors

Institutions: National Renewable Energy Laboratory

Published on: 01 May 2021

Related papers:

- [Design and performance of the aeroacoustic wind tunnel in SUSTech](#)
- [The present situation and development of modern aeroacoustic wind tunnel technique](#)
- [Experimental characterization of the aeroacoustic behavior of a low speed wind tunnel](#)
- [Development and Validation of a Semi-Empirical Wind Turbine Aeroacoustic Code](#)
- [Progress in Aeroacoustic and Climatic Wind Tunnels for Automotive Wind Noise and Acoustic Testing](#)

Share this paper:    

View more about this paper here: <https://typeset.io/papers/aeroacoustic-assessment-of-wind-plant-controls-1emi1f14ft>



Aeroacoustic Assessment of Wind Plant Controls

Nicholas Hamilton, Pietro Bortolotti, Dave Jager, Yi Guo, Jason Roadman, and Eric Simley

National Renewable Energy Laboratory

**NREL is a national laboratory of the U.S. Department of Energy
Office of Energy Efficiency & Renewable Energy
Operated by the Alliance for Sustainable Energy, LLC**

This report is available at no cost from the National Renewable Energy Laboratory (NREL) at www.nrel.gov/publications.

Contract No. DE-AC36-08GO28308

Technical Report
NREL/TP-5000-79664
May 2021



Aeroacoustic Assessment of Wind Plant Controls

Nicholas Hamilton, Pietro Bortolotti, Dave Jager, Yi Guo, Jason Roadman, and Eric Simley

National Renewable Energy Laboratory

Suggested Citation

Hamilton, Nicholas, Pietro Bortolotti, Dave Jager, Yi Guo, Jason Roadman, Eric Simley. 2021. *Aeroacoustic Assessment of Wind Plant Controls*. Golden, CO: National Renewable Energy Laboratory. NREL/TP-5000-79664. <https://www.nrel.gov/docs/fy21osti/79664.pdf>.

**NREL is a national laboratory of the U.S. Department of Energy
Office of Energy Efficiency & Renewable Energy
Operated by the Alliance for Sustainable Energy, LLC**

This report is available at no cost from the National Renewable Energy Laboratory (NREL) at www.nrel.gov/publications.

Contract No. DE-AC36-08GO28308

Technical Report
NREL/TP-5000-79664
May 2021

National Renewable Energy Laboratory
15013 Denver West Parkway
Golden, CO 80401
303-275-3000 • www.nrel.gov

NOTICE

This work was authored by the National Renewable Energy Laboratory, operated by Alliance for Sustainable Energy, LLC, for the U.S. Department of Energy (DOE) under Contract No. DE-AC36-08GO28308. Funding provided by the U.S. Department of Energy Office of Energy Efficiency and Renewable Energy Wind Energy Technologies Office. The views expressed herein do not necessarily represent the views of the DOE or the U.S. Government.

This report is available at no cost from the National Renewable Energy Laboratory (NREL) at www.nrel.gov/publications.

U.S. Department of Energy (DOE) reports produced after 1991 and a growing number of pre-1991 documents are available free via www.OSTI.gov.

Cover Photos by Dennis Schroeder: (clockwise, left to right) NREL 51934, NREL 45897, NREL 42160, NREL 45891, NREL 48097, NREL 46526.

NREL prints on paper that contains recycled content.

Executive Summary

The Aeroacoustic Assessment project aims to quantify changes in aeroacoustic noise generation by a utility-scale wind turbine operating under imposed yaw offsets common for wake steering and wind plant control strategies. Although active plant control utilizing wake deflection control strategies has been shown experimentally and computationally to reliably produce 1%–2% of additional annual energy production without significant changes in turbine structural loads, the potential impact on aeroacoustic emissions has yet to be quantified or completely understood. Yawed operation of a wind turbine changes the three-dimensional aerodynamic interaction between the rotor blades and the incoming atmospheric flow, leading to changes in noise generation. This work quantifies the extent to which active control induces additional aeroacoustic emissions from additional separation and other flow interaction dynamic effects. Given public concerns about wind turbine noise and the need for observational data required for regulators to establish noise restrictions, we must understand potential acoustic emissions resulting from active control prior to commercial deployment and the development of practical noise reduction methods and technologies.

The work outlined in this report details the new aeroacoustic measurement capability developed at the National Renewable Energy Laboratory (NREL) and its application to making full-field observations of noise from a utility-scale wind turbine. Preliminary noise modeling with the aeroacoustics module in OpenFAST helped to establish the design of the experiment, specifically targeting the noise recorded at observers distributed around the U.S. Department of Energy (DOE)-owned GE 1.5-MW wind turbine. Low-frequency and infrasound measurement capabilities implemented in this project establish an operational baseline for the wind turbine, setting the stage for future control, rotor blade, and turbine design research.

Noise generated by a wind turbine operating in yawed conditions is dominated by the turbulent inflow/leading edge interactions and by the trailing edge contributions. Modeled equivalent sound pressure levels (SPLs) and noise spectra match observed quantities for yaw offsets less than 20° , yielding a slight decrease in wind turbine noise, related to reduced tip speeds. At more aggressive yaw offsets— 25° as investigated in this work—the models suggest that wind turbine noise should increase overall. However, observations at this yaw offset demonstrate reductions in wind turbine noise of up to 6 dB for particular wind speeds and observer locations. The experimental evidence in this study suggests that operating wind turbines under modern wind plant control strategies is unlikely to lead to additional noise emissions that could adversely impact wind plant operation.

A quality-controlled data set containing the results of this work is hosted on the Atmosphere to Electrons (A2e) Data Archive Portal (DAP). The data set includes SPLs for all microphones, noise spectra, operational data from the wind turbine, and meteorological data from a met mast. These data are publicly available without charge and are intended to support the advancement of aeroacoustics research for wind energy. Data can be found at: <https://a2e.energy.gov/projects/aawpc>. Please cite this report if using the data for any research publications or reporting.

Acknowledgments

This project would not have been possible without the support and guidance from Mike Robinson and Ben Hallisey from DOE. The expertise in aeroacoustic modeling from Pat Moriarty and in wind turbine noise testing from Arlinda Huskey were instrumental in the successful design and execution of the project. Jason Roadman and Casey Nichols developed the distributed data acquisition system needed to collect data from 11 acoustic measurement stations, an in situ met tower, and wind turbine operational parameters. Andrew Simms, Dave Jager, and Troy Boro were critical to deploying, calibrating, and managing equipment in the field. Pietro Bortolotti and Yi Guo developed aeroacoustic modeling codes in the OpenFAST platform and simulated the experimental matrix to pinpoint measurement locations. Eric Simley processed an enormity of instrument data, developed processing techniques, and teased out key results.

Acronyms

A2e	Atmosphere to Electrons
DAP	Data Archive Portal
DAS	data acquisition system
DOE	U.S. Department of Energy
IEC	International Electrotechnical Commission
IEPE	integrated electronic piezo-electric
NI	National Instruments
NREL	National Renewable Energy Laboratory
SFR	standard frequency range
SPL	sound pressure level
TBL-TE	turbulent boundary layer trailing edge
TDMS	Technical Data Management Streaming
TI	turbulence intensity
UDP	universal datagram protocol

Table of contents

Executive Summary	iv
Acknowledgments	v
Acronyms	vi
1 Introduction	4
2 Design of Experiment	5
2.1 Measurement Locations	5
2.2 Measurement Requirements	7
2.3 Equipment Selection	8
2.3.1 Microphones	8
2.3.2 Data Acquisition Systems	9
2.4 Wind Turbine	10
3 Analysis Methods	14
3.1 Data Reduction	14
3.1.1 File Conversion	14
3.1.2 NoiseLAB	14
3.1.3 Noise and SCADA Data Synchronization	16
3.2 IEC 61400-11 Acoustic Noise Analysis	16
3.2.1 Sound Power Level vs. Wind Speed	18
3.2.2 Tonality	19
3.3 Low-Frequency Noise and Infrasound	19
3.4 Impulsivity	20
3.5 Amplitude Modulation	20
4 Numerical Models for Aeroacoustics Noise	22
4.1 Aeroacoustics Noise Generation	22
4.2 Impact of Yaw Misalignment on Noise	22
4.3 Noise Propagation	23
4.4 Infrasound and Low-Frequency Noise	23
5 Results	24
5.1 Preliminary Modeling	24
5.2 Experimental Results	24
5.3 Model Validation	38
6 Conclusions	41
6.1 Aeroacoustics Multi-Year Research Objectives	41
6.1.1 Airfoil Level Research	42
6.1.2 Wind-Plant-Level Research	42
6.1.3 Human Response	43

Bibliography	44
Appendix A Wind Turbine Noise Spectra	46
Appendix B Data Channels	56
Appendix C Acoustic Instrumentation Data Sheets	69

List of Figures

Figure 1. Seasonal wind roses at 80 m at the Flatirons Campus	5
Figure 2. Experimental design around the DOE 1.5	6
Figure 3. Modeled SPL field with measurement points	7
Figure 4. Line diagram of DAS subsystems	10
Figure 5. DOE-owned 1.5-MW wind turbine located at site 4.0 at the FC.	12
Figure 6. Map of the FC, including the DOE 1.5 located in the northeast corner of the facility.	13
Figure 7. High-level data processing procedure	15
Figure 8. IEC 61400-11 data reduction procedure	17
Figure 9. Pre-experiment model results for the DOE 1.5 at the yaw offsets selected for testing	24
Figure 10. Number of valid 10-sec SPL slices obtained for each 1 m/s wind speed bin for background and normal operation periods	25
Figure 11. Distribution of background noise by wind speed (left) and median background noise for each microphone (right)	26
Figure 12. Comparison of background noise and overall noise recorded at each microphone. Each subfigure is arranged in the relative position of the respective microphone in the experiment. Refer to Figure 2b.	27
Figure 13. Individual and mean spectra for standard frequency microphones (left) and low-frequency microphones (right)	28
Figure 14. Overall and background spectra at 9 m/s for all microphones.	29
Figure 15. Distributions of SPL vs. wind speed for each yaw offset	31
Figure 16. Equivalent A-weighted SPL at each microphone location for 8 m/s for each yaw offset	32
Figure 17. SPL vs. wind speed for each yaw offset	33
Figure 18. Change in SPL from the 0° yaw case	34
Figure 19. Distributions of high-speed shaft RPM of the DOE 1.5 operating at 0°yaw and 25°yaw, taken as a proxy for rotor speed. Red triangles indicated mean shaft rotational speeds.	35
Figure 20. Changes in audible noise spectra with yaw for Mic 01N in the north (left) and Mic 06S in the south (right)	35
Figure 21. Wind turbine noise spectra at the IEC test location (Mic 04C) by wind speed and yaw offset	36
Figure 22. Wind turbine noise spectra from the low-frequency noise microphone at the South DAS node (Mic 13S) by wind speed and yaw offset. Green and blue bands indicate infrasound and low-frequency noise ranges of the spectra.	37

Figure 23.	Comparison of measured and modeled equivalent SPL for SFR microphones	38
Figure 24.	Profiles of turbulence intensity by wind speed during aeroacoustic measurement campaign	39
Figure 25.	Measured vs. modeled wind turbine noise spectra at the IEC test location, Mic 04C	40
Figure 26.	Overall and background spectra at 5 m/s for all microphones.	46
Figure 27.	Overall and background spectra at 6 m/s for all microphones.	47
Figure 28.	Overall and background spectra at 7 m/s for all microphones.	48
Figure 29.	Overall and background spectra at 8 m/s for all microphones.	49
Figure 30.	Overall and background spectra at 9 m/s for all microphones.	50
Figure 31.	Overall and background spectra at 10 m/s for all microphones.	51
Figure 32.	Overall and background spectra at 11 m/s for all microphones.	52
Figure 33.	Overall and background spectra at 12 m/s for all microphones.	53
Figure 34.	Overall and background spectra at 13 m/s for all microphones.	54
Figure 35.	Overall and background spectra at 14 m/s for all microphones.	55

List of Tables

Table 1.	Yaw Offset Schedule for Experiment	7
Table 2.	Measurement Requirements for IEC-Compliant Wind Turbine Noise Testing	7
Table 3.	Test Turbine Configuration	11
Table 4.	Data channel names, descriptions, and units for the public dataset	56

1 Introduction

Wind plant control strategies are used more and more to mitigate wake losses within wind plants. The most commonly implemented strategy for wake loss mitigation is that of wake steering—introducing lateral deflections to the momentum-deficit characterizing the wake by intentionally yawing a wind turbine with respect to the incoming wind direction. Wake steering has been shown experimentally and computationally to increase annual energy production of a wind plant by 1%–2% reliably, with the potential for much greater gains under conditions where wake losses are most pronounced. As wake steering becomes a common and accepted operational strategy for large wind plants, external effects must be quantified to ensure that the strategy remains viable moving forward.

External or secondary effects of wake steering include the potential for increased structural loads, which could increase operations and maintenance costs, and increased aeroacoustic noise generation, which could impose additional operational constraints. To meet local constraints on noise generation, wind turbines may be operated at a reduced tip speed, impacting the mechanical efficiency of the machine and the levelized cost of energy. For wake steering to be widely applied as a strategy to mitigate wake losses, changes in the aeroacoustic noise emissions of utility-scale wind turbines under yawed operation must be quantified.

The primary goal of the Aeroacoustic Assessment project is to characterize the acoustic emissions of the GE 1.5-MW SLE wind turbine owned by the U.S. Department of Energy (DOE 1.5) at the National Renewable Energy Laboratory’s (NREL) Flatirons Campus (FC) to determine the nature and degree of changes of acoustic emissions produced when operating a utility-scale wind turbine according to modern wind plant control strategies.

Aeroacoustic noise observations include multiple point-measurements located to sample the acoustic emissions, including points required and suggested in the International Electrotechnical Commission (IEC) Standard, Wind Turbines Part 11: Acoustic Noise Measurement Techniques, IEC 61400-11, Edition 3.1 IEC 2020, hereafter referred to simply as the Standards. This report documents the measurement techniques, test equipment, and analysis procedures for quantifying changes in the aeroacoustic noise generation of a utility-scale wind turbine operated under yawed conditions. Measurement data are used to validate aeroacoustics models underlying the Standards and incorporated in a module to interface with NREL’s multiphysics modeling platform, OpenFAST (Bortolotti et al. 2020).

A data set containing acoustic observations, met mast data, and wind turbine data has been made available to the public on the A2e Data Archive Portal (DAP). This is a unique data set that will support aeroacoustic noise model development and validation efforts by the wind turbine noise research community. Data from the Aeroacoustic Assessment project is located at <https://a2e.energy.gov/projects/aawpc>.

The aeroacoustic assessment project objectives are focused on quantifying the changes in acoustic emissions introduced by implementing modern wind turbine and wind plant control strategies. The main objectives of the project are to:

1. Experimentally quantify the operational aeroacoustic emissions from a utility-scale turbine operating under active wind plant control strategies and ascertain the extent to which nominal operating emissions are modified.
2. Validate aeroacoustic models against experimental data, identify sources of uncertainty, and calibrate emission and propagation models.
3. Create a publicly available data set containing aeroacoustic noise data, meteorological data, and turbine operating data for the wind turbine noise research community.

2 Design of Experiment

2.1 Measurement Locations

Figure 1 shows wind roses for the autumn quarter (October–December) and for the winter quarter (January–March), respectively. Both figures show that the prevailing wind direction is from the direction bin of 280° to 290° . In the figure, only the wind speed bins called out in Table 1 have been colored to highlight the conditions relevant for aeroacoustic testing.

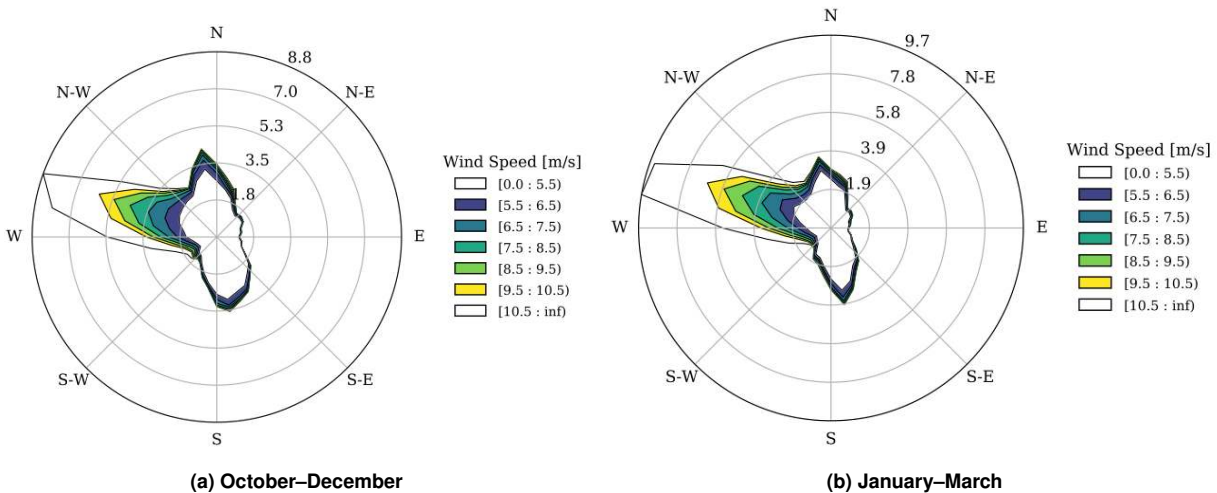


Figure 1. Seasonal wind roses at 80 m at the Flatirons Campus

Measurement (sound board) locations are shown in Figure 2a relative to the location of the DOE 1.5 wind turbine (green marker) and the prevailing wind direction during the fall and winter, 285° . This is the wind direction with the greatest representation from data recorded at hub height (H , 80 m) by the cup anemometer on the met mast M5. Other markers on the figure represent locations of interest for recording aeroacoustic noise. The black dot connected to the turbine by a dashed line indicates the measurement location required by the IEC Standard for noise testing and is $H + D/2$ downstream of the turbine in the prevailing wind direction, where $D = 77$ m is the rotor diameter of the DOE 1.5. Points on the innermost circle correspond to additional suggested measurement locations in the IEC Standard, also $H + D/2$ away from the rotor but offset $\pm 45^\circ$ from the prevailing wind direction. All other points indicate locations designed to measure the sound pressure level (SPL) field produced by the DOE 1.5. In Figure 2a, red markers indicate the locations of subsystems of the data acquisition system (DAS), as well as approximate locations of the three low-frequency noise measurement stations.

Figures 2a and 2b show the arrangement of microphones and DAS favorable for sampling the overall sound output of the DOE 1.5. Standard frequency range (SFR) microphones specified to comply with the wind turbine noise measurement standards (20 Hz–11.2 kHz) will be deployed at the black points. SFR mics will be placed to evenly sample the overall SPL directivity. Spacing between proximal locations are shown with black lines and annotations. The average SPL difference between neighboring points is expected to be at least 3 dB, enough to ensure a detectable difference in SPL and quantify the changes induced to the directivity from wind plant control (see Figure 3).

Low-frequency noise microphones were specified to quantify the noise emissions of the DOE 1.5 in the subaudible frequency range. Low-frequency noise measurements require specialized equipment, including microphones specifically designed to sample pressure field fluctuations, preamplifiers, and powered signal conditioning units that ensure a flat frequency response down to 0.1 Hz. In the current work, low-frequency mics measure audio signals as low as 1 Hz. Due to the requirement of additional power supply to the low-frequency noise microphone setups, they were located near each DAS, indicated as red dots in Figure 2a. Red dashed lines indicate connections between microphones

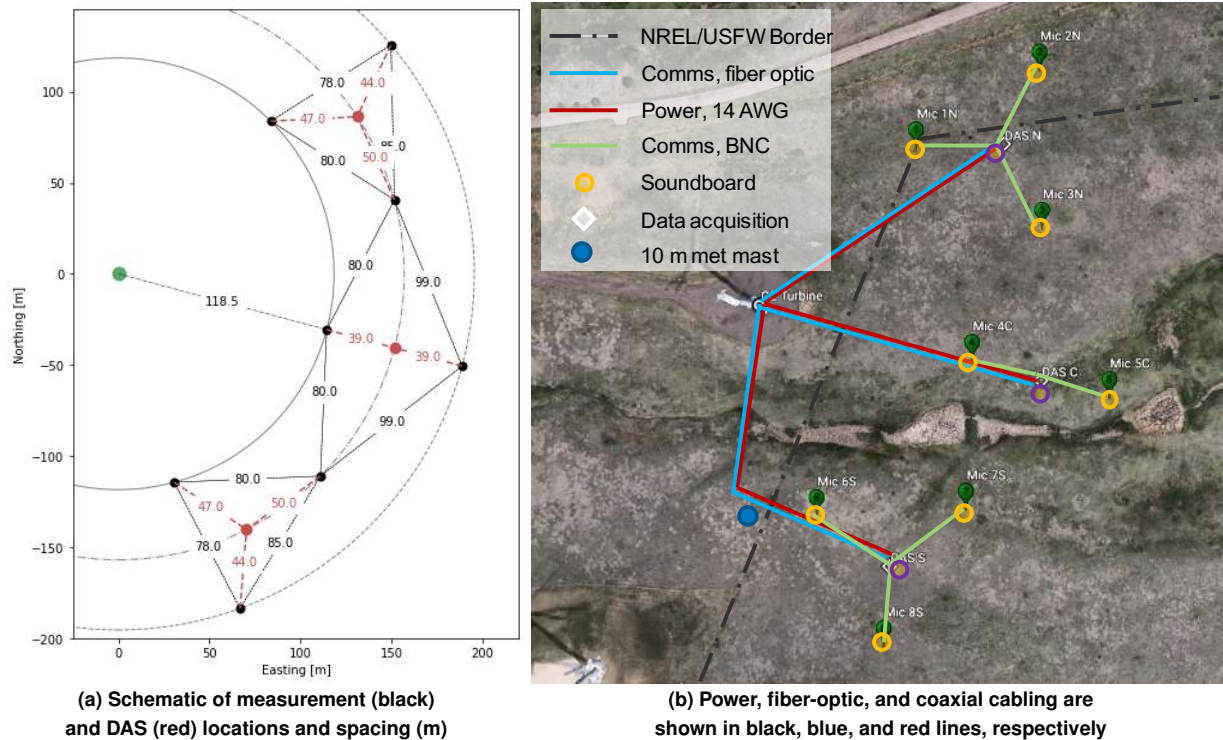


Figure 2. Experimental design around the DOE 1.5

and DAS subsystems.

To ensure that the acoustic data collected during the project are accurately analyzable in both the time domain and frequency domain, extra care was taken with regard to the design of the DAS. Each microphone communicated with a DAS subsystem over coaxial (BNC) connection. Signal degradation was mitigated in the instrumentation plan by limiting BNC cable lengths to a maximum of 50 m (red dashed lines in Figure 2a). Communication from each DAS location to a central data storage server occurred over fiber-optic cables, which can transmit over much longer distances (easily up to 1 km) without signal degradation.

Yaw offsets were achieved on the DOE 1.5 using National Instruments (NI)-based hardware to subtract the desired offset from the wind vane signal before it is input to the turbine's yaw control system. This strategy induces a yaw offset in the turbine without requiring modification of the yaw control algorithm. Based on the interest in implementing wake steering using positive yaw offsets (a counter-clockwise rotation of the nacelle relative to the wind direction seen from above), the experiment was focused on positive yaw offsets. However, for model validation, a single negative yaw offset was also evaluated. As explained in Fleming et al. (2019), based on a loads analysis of the DOE 1.5 under different amounts of yaw misalignment in Damiani et al. (2018), a limit of 20° was chosen for implementation of wake steering at a commercial wind farm. However, previous yaw misalignment experiments on the DOE 1.5 have used yaw offsets up to $\pm 25^\circ$ (Damiani et al. 2018; Annoni et al. 2018). To capture the expected range of yaw offsets that will be implemented by wake steering controllers, as well as a negative yaw offset and a larger positive yaw offset for model validation, the yaw offset schedule in Table 1 was implemented in the field experiment.

The yaw controller cycled between each yaw offset, holding each value for 30 min and repeating the schedule every 2.5 hours. The specific order of yaw offsets was intended to reduce the magnitude of the most extreme change in yaw orientation. The first 5 min of data after a new yaw offset were discarded to account for yaw positioning transients and the audible mechanical noise associated with the yaw maneuver.

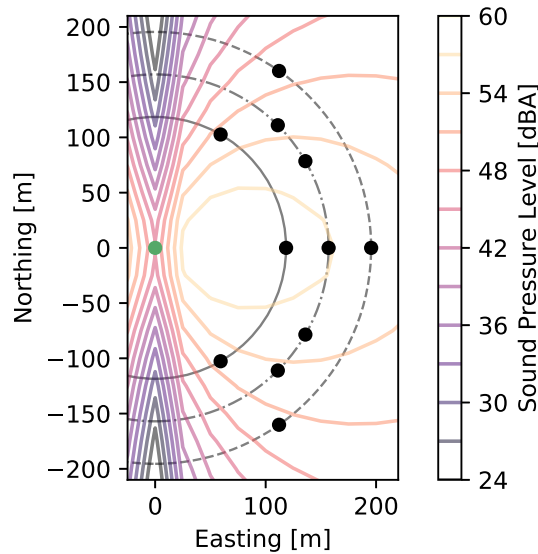


Figure 3. Modeled SPL field with measurement points

Table 1. Yaw Offset Schedule for Experiment

Yaw Offset	-18°	0°	25°	18°	10°
Duration	30 min	30 min	30 min	30 min	30 min

2.2 Measurement Requirements

The field experiment was conducted over selected days with favorable atmospheric conditions. Table 2 lists the minimum required observations according to the IEC Standard. These requirements were duplicated for each yaw offset position in the experiment. To fulfill the test requirements, only data corresponding to a mean wind direction within $\pm 15^\circ$ of the prevailing wind direction of 285° were considered.

Acoustic signals for all 11 microphones and from all measurement periods were recorded in the field and stored for later review and analysis. The recorded signals from microphone 02N were reviewed to identify and eliminate intruding noise. Microphone 02N was selected as the reference microphone because it was located closest to the Flatirons Campus access road, and was thus expected to be most sensitive to intruding noise. Throughout the experi-

Table 2. Measurement Requirements for IEC-Compliant Wind Turbine Noise Testing

Measurement Type	Requirements
Overall measurements	At least thirty 1-min averages
For A-weighted SPL: (for turbine and background measurements)	At least 3 min of data with wind speeds ± 0.5 m/s of the integer values of 6, 7, 8, 9, and 10 m/s
For octave or third octave band measurements: (for turbine and background measurements)	At least 3 min of data with wind speeds ± 0.5 m/s of the integer values of 6, 7, 8, 9, and 10 m/s
N ¹ band measurements: (for turbine and background measurements)	At least 2 min of data with wind speeds ± 0.5 m/s of the integer values of 6, 7, 8, 9, and 10 m/s

ment, the complete measurement chain was calibrated at the beginning and end of every measurement period. After completing the baseline data requirements in Table 2, and observing that the microphone calibration constants had not changed throughout the experiment, the recordings were allowed to proceed overnight in order to collect additional data. In every case, the full system was calibrated again the following morning. The same procedure was followed when recording background noise levels. To the greatest degree possible, data were collected for each of the specified yaw offsets and with the turbine parked over a similar range of atmospheric conditions. Microphone calibration was performed by providing a reference signal (1,000 Hz, 94 dB) to each microphone with a B&K 4231 Sound Calibrator (see Appendix C for additional detail on acoustic equipment). When possible, multiple calibrators were used in parallel to reduce downtime for the measurement system.

2.3 Equipment Selection

2.3.1 Microphones

Microphone requirements are specified under the Standards for wind turbine noise (IEC 61400-11) as well as for sound level metering (IEC 61672) and measurement microphones (IEC 61094-4). Standards indicate that microphones must meet the Class 1 requirements for reliable measurement systems and traceable calibration. All the requirements for acoustic instrumentation under the Standard are found in Section 6.1: Acoustic Instruments. Relevant excerpts are reproduced below from IEC 61400-11 Edition 3.1 2018-06 (Final Version). The Standards indicate that:

6.1.2 Equipment for the determination of the equivalent continuous A-weighted SPL: “The diameter of the microphone diaphragm shall be no greater than 13mm” (paragraph 6.1.2). The equipment shall meet the requirements relevant to this document of an IEC 61672 class 1 sound level meter.

6.1.3 Equipment for the determination of A-weighted 1/3-octave band spectra: The filters shall meet the requirements relevant to this document of IEC 61260 for class 1 filters.

6.1.4 Equipment for the determination of narrow band spectra: The equipment shall fulfil the relevant requirements for IEC 61672 series class 1 instrumentation in the 20 Hz to 11 200 Hz frequency range.

6.1.6 Acoustical calibrator: The calibrator shall fulfill the requirements of IEC 60942:2003 class 1, and shall be used within its specified environmental conditions.

6.1.7 Data recording/playback systems: A data recording/playback system is a required part of the measurement instrumentation. If used for analysis (other than re-listening), the entire chain of measurement instruments shall fulfill the relevant requirements of IEC 61672 series, for class 1 instrumentation.

Technical specifications for all microphones and acoustic measurement components are located in Appendix C.

Standard-Frequency Microphones

The requirements for IEC 61400-11 noise measurements are satisfied by the Brüel og Kjær (B&K) 4966-H-041, which combines a Type 4966 prepolarized, free-field microphone and a Type 1706 microphone preamplifier. Specifically, the 4966-H-041 delivers flat frequency response within the required range of 20 Hz–11.2 kHz. Additionally, the 4966-H-041 complies with the Class 1 specifications in IEC Standard 61672, and has an appropriate dynamic range and operating temperature range for all conditions at the NREL FC. Finally, the 4966-H-041 is an integrated electronic piezo-electric (IEPE) microphone, which allows microphones to be powered through BNC cables used for signal transmission.

Low-Frequency Microphones

Specialized microphones are required to collect pressure-field measurements as specified in the Standards for low-frequency noise and infrasound (ANSI/ASA S12.9-2016). Low-frequency noise measurements require additional care in terms of both the acoustic recordings and signal conditioning. To make low-frequency noise measurements, B&K Type 4964 microphones were selected to make measurements down to 1 Hz as specified in the experimental plan. These microphones have a similar dynamic range and operating temperature range as the IEPE mics above. However, measuring the low-frequency content of the acoustic emissions required that the Type 4964 microphones

be connected to a Type 2669 preamplifier and a Type 1708 signal conditioner. Because each signal conditioner required an additional supply of external power (i.e., not powered over the communication line like IEPE microphones), low-frequency noise measurements were made in proximity to the DAS subsystems (red markers in Figure 2a).

2.3.2 Data Acquisition Systems

The distribution of measurement points over a large area behind the DOE 1.5 required a similarly distributed data acquisition system. Reconciling this requirement against the need to keep cable runs short enough to minimize signal degradation pointed to the assembly of three DAS subsystems. Each subsystem was constructed on a National Instruments (NI) CompactRIO (cRIO) chassis that combines a real-time controller with a platform for adding signal input/output modules. The chassis selected for the Aeroacoustics project (cRIO-9042) contains sufficient processing power and a modular design to ensure that they will meet the needs for the measurements outlined above and be usable for other measurement campaigns in coming years. Each DAS subsystem consisted of a cRIO outfitted with three NI C-series modules:

NI-9250 Sound and vibration module with four BNC input terminals. This module is capable of powering the IEPE microphone/preamp combos and processing the acoustic data for the specified frequency range.

NI-9239 Analog voltage input module. This module interfaced with the B&K signal conditioning unit for each low-frequency measurement station. A separate module was used to ensure that each type of observation could be configured independently.

NI-9467 GPS time synchronization module. All data needed to be time-stamped locally to ensure that data can be accurately compared for subsequent time-domain analysis. Using a GPS timestamp allowed for a distributed system without the need for a wired clock signal shared among the cRIOs or the complexity associated with network timing. GPS is also extremely accurate for time synchronization.

An example DAS subsystem and measurement devices are shown in a line diagram in Figure 4.

The DAS consisted of three subsystems in the configuration described above, each interfacing with a host computer in the base of the DOE 1.5 turbine. Power and network connections are run to each subsystem and the cRIO, and associated hardware are housed in a weather-tight enclosure with desiccant inside. Inside each subsystem enclosure was another MOXA Ethernet-to-fiber-media converter and two separate DC-DC power supplies. A CUI Inc model PQDE6W-Q24-S5-DIN provided power for the low-frequency noise microphones and converted the incoming 10–36 VDC to 5 VDC. A CUI Inc model VHK100W-Q24-S28-DIN provided power for the MOXA converter and the NI Chassis and converted the incoming 9–36 VDC to 28 VDC. The effects of voltage drop in the long (210–230 m, 700–750 ft) DC power cable runs were negligible due to using wide input range DC–DC converters. At the base of the DOE 1.5 turbine was an enclosure that housed the AC–DC power supplies (XP Power model SHP350PS36). These supply the AC 120V line voltage to 36 VDC for each DAS subsystem. The 36 VDC provided power to a MOXA IMC-21GA Industrial Gigabit Ethernet-to-fiber-media converter at the turbine base and to each of the three subsystems.

The data acquisition code is written as a custom program in LabVIEW. This code was adapted from existing MV-DAS infrastructure at NREL (Shah et al. 2019). Each subsystem ran an identical instance of the subsystem program and interfaces over User Datagram Protocol (UDP) with the host program. Data were stored locally on each subsystem and later downloaded after recording. Record and stop commands were issued over UDP along with subsystem status back to the host. The software had the capability to start each subsystem recording individually or issue a command to start recording simultaneously using the GPS clock. The DAS also had functionality to check and record microphone calibration signals in real time. Host code interfaced with turbine controller signals to plot real-time SPLs from all microphones against wind speed to provide situational awareness for decision-making throughout the duration of the experiment.

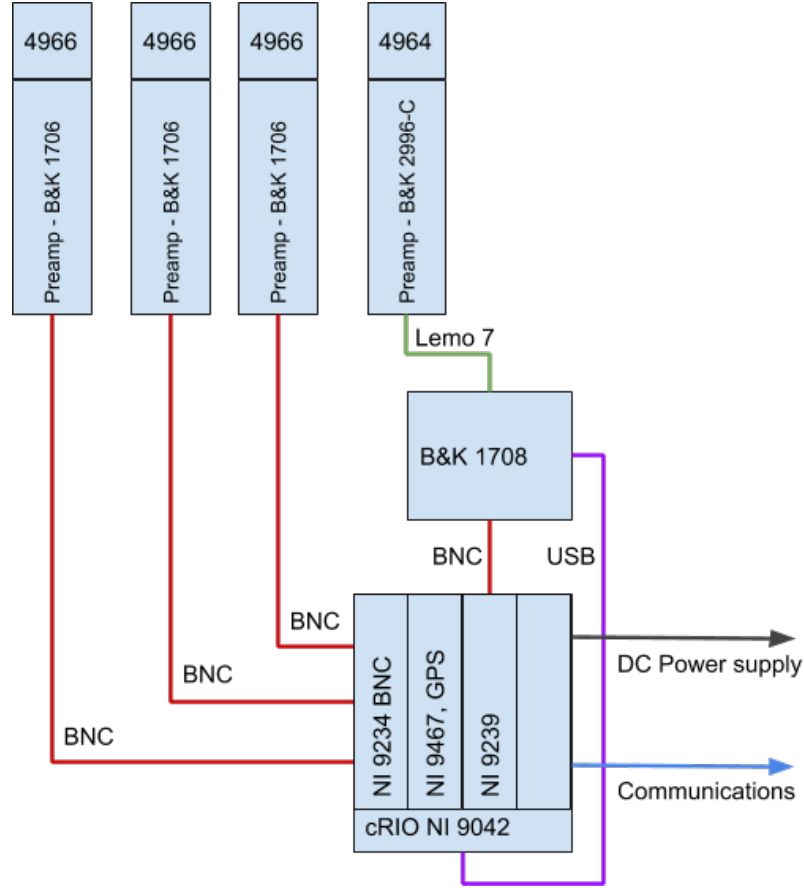


Figure 4. Line diagram of DAS subsystems

2.4 Wind Turbine

Aeroacoustic measurements were made around the DOE 1.5 turbine, which is representative of a large segment of installed wind capacity; more than 18,000 turbines of this make and model are currently in operation in the United States. The DOE 1.5 is built on the platform of GE's 1.5-MW SLE commercial wind turbine model and was installed at NREL's FC with the objective of supporting DOE Wind Program research initiatives such as Atmosphere to Electrons (A2e). The DOE 1.5 is a horizontal-axis, three-bladed, upwind turbine with full span pitch control. Table 3 provides the key descriptive information of the test turbine.

The turbine is located 8 miles south of Boulder, Colorado, at the FC, on test site 4.0. Figure 5 shows the test turbine and the area downstream according to the prevailing wind direction on site ($\approx 285^\circ$). Instrumentation was arrayed in the area downstream of the DOE 1.5. Figure 6 shows the test site with respect to the surrounding geography and the rest of the FC. Red dots indicate the locations of utility-scale and small wind turbines on site; green triangles indicate locations of meteorological masts (met masts).

Table 3. Test Turbine Configuration

Turbine manufacturer and address	GE Energy 300 Garlington Rd., P.O. 648 Greenville, SC 29602-0648
Model	GE 1.5-MW SLE
Rated power (kW)	1,500
Rated wind speed (m/s)	14
Serial number	N000780-N / TB059-3
Blade make, type, and serial number	GE37c, fiberglass, S00028, S00029, S00030
Generator make, type, and serial number	Winergy, doubly-fed induction, JFEC-500SS-06A
Gearbox make, type, and serial number	Winergy multistage planetary/helical model PEAB 4410.4, serial number NFR-W-111620
Control software	WindSCADA
Wind turbine type	Horizontal axis, upwind
Tower type	Tubular
Number of blades	3
Hub height (m)	80
Rotor diameter (m)	77
Horizontal distance from rotor center to tower axis (m)	3.8
Speed control	Pitch control
Constant or variable speed	Variable
Rotational speeds at standardized integer wind speeds from 6 m/s to 10 m/s (rpm)	10–20



Figure 5. DOE-owned 1.5-MW wind turbine located at site 4.0 at the FC. Photo credit: Jeroen van Dam, NREL

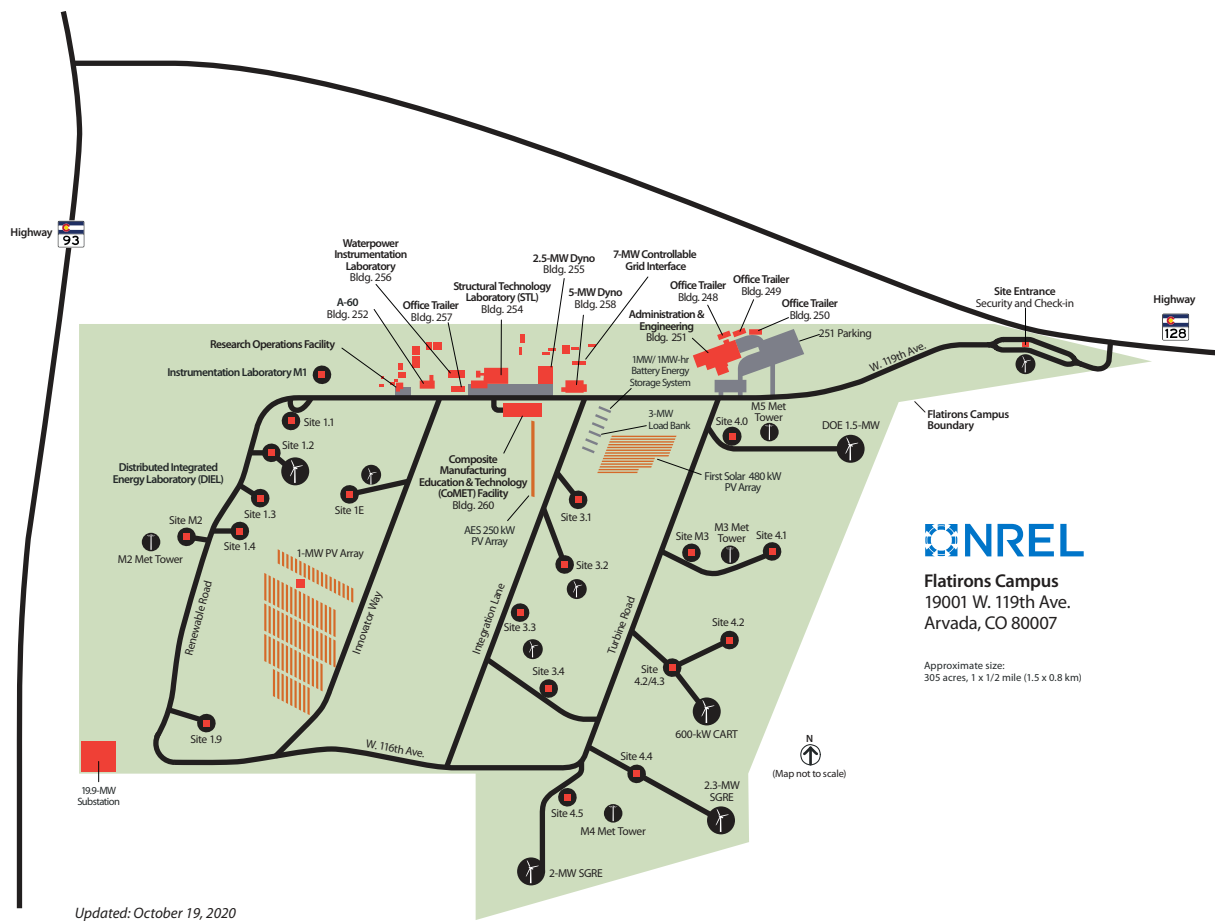


Figure 6. Map of the FC, including the DOE 1.5 located in the northeast corner of the facility.

3 Analysis Methods

This section contains a description of the data processing procedure for deriving acoustic quantities of interest. Section 3.1 outlines the data reduction process for transforming raw acoustic, turbine, and meteorological (met mast) data into the required inputs for further noise analysis. The IEC Standard acoustic noise analysis process is described in Section 3.2, where the procedures for deriving sound power levels for different wind speeds and analyzing tonality are explained. Section 3.3 discusses the analysis of low-frequency and infrasound noise that is performed for the three low-frequency microphones. Finally, Sections 3.4 and 3.5 provide an overview of impulsivity and amplitude modulation characterization, respectively. These latter two categories are optional analyses that will be performed pending successful completion of the IEC Standard as well as low-frequency and infrasound analyses.

3.1 Data Reduction

Prior to performing the IEC Standard and low-frequency noise analyses, raw data from the microphone measurements, DOE 1.5 turbine SCADA system, and met mast must be combined and reduced to 10-sec averages (slices). The workflow for reducing the 51.2-kHz audio recordings for each microphone and 1-Hz SCADA data—containing turbine and met mast variables—to appropriate 10-sec slices is outlined in Figure 7. Intermediate steps for converting the microphone recordings to noise and calibration tone files; calculating total SPL and SPL in 1/3-octave bands for 10-sec slices using the NoiseLAB software (DELTA Acoustics and Vibration 2014); and synchronizing the acoustic, turbine, and met data are explained in Sections 3.1.1–3.1.3, respectively.

3.1.1 File Conversion

As illustrated in Figure 7, audio recordings for each microphone channel are converted from the NI Technical Data Management Streaming (TDMS) file format, in which they are saved by the DAS, to WAV files to be imported into NoiseLAB. A Python script was developed to convert the 51.2-kHz TDMS audio files to WAV file format. Further, the script identifies calibration tone periods from the audio recordings and saves the clips as separate WAV files to facilitate efficient calibration of noise levels in NoiseLAB. Specifically, when a 1-kHz, 94-dB calibration tone is identified in an audio file, the corresponding audio clip is extracted and saved as a new file.

3.1.2 NoiseLAB

The DELTA NoiseLAB acoustic noise analysis software (DELTA Acoustics and Vibration 2014) is used to derive acoustic quantities of interest in 10-sec slices from the converted WAV files and export the derived values as CSV files. First, audio recordings for each microphone along with accompanying calibration files are imported into NoiseLAB for the recording period(s) of interest. For each audio file, the file containing the most recent calibration tone for the corresponding microphone is selected and used to calibrate the absolute noise level of the recording. Once the recordings for each microphone channel are calibrated, the following three analyses are performed using NoiseLAB:

A-weighted total and 1/3-octave band SPL. The recordings for each microphone are divided into 10-sec slices.

For each slice, the A-weighted SPL is calculated for the total frequency range as well as 1/3-octave bands from 20 Hz to 10 kHz. A CSV file is saved containing the A-weighted total and 1/3-octave band SPL values for all 10-sec slices and microphone channels.

A-weighted narrowband spectra. The recordings for each microphone are divided into 10-sec slices, and A-weighting is applied. For each slice, the narrowband spectrum is calculated for frequencies up to 10 kHz with a frequency resolution of 3 Hz. A CSV file is saved containing the A-weighted narrowband spectra for all 10-sec slices and microphone channels.

Unweighted total and 1/3-octave band SPL for low-frequency and infrasound noise analysis. The recordings for the three low-frequency microphones are divided into 10-sec slices. For each slice, the unweighted SPL is calculated for the total frequency range as well as 1/3-octave bands from 1 Hz to 10 kHz. Additionally, the G-weighted (infrasound weighting) total SPL is calculated. A CSV file is saved containing the unweighted total and 1/3-octave band SPL values and G-weighted total SPL values for all 10-sec slices and microphone channels.

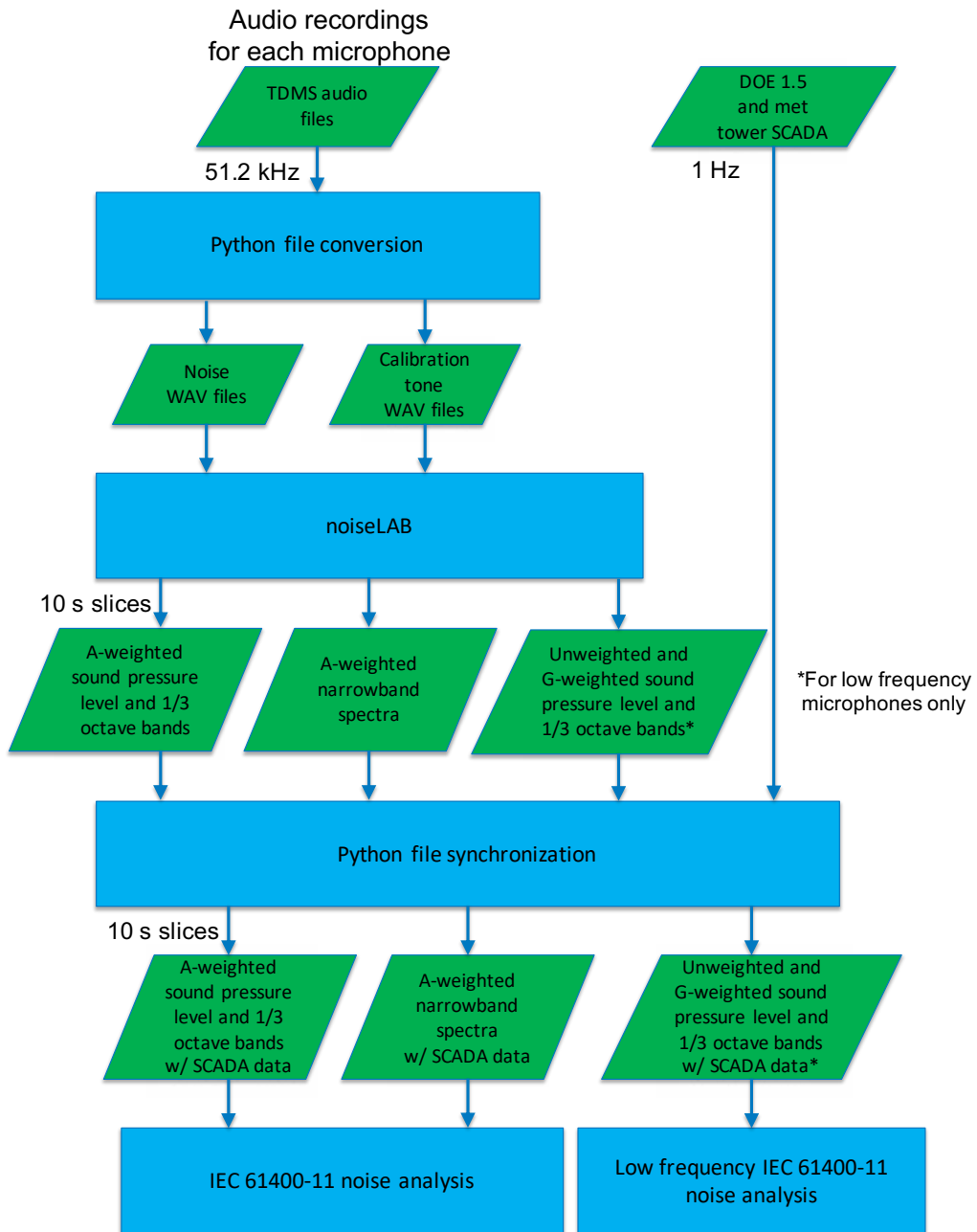


Figure 7. High-level data processing procedure

3.1.3 Noise and SCADA Data Synchronization

After CSV files containing the relevant SPL values and narrowband spectra are exported from NoiseLAB, they are synchronized and merged with turbine and met mast data to characterize the turbine operating state and atmospheric conditions corresponding to each 10-sec slice. This synchronization step is performed using a Python script that saves the combined data as a Pandas DataFrame (The Pandas Development Team 2020). For each CSV file produced using NoiseLAB in the previous step, 1-Hz SCADA data files containing the DOE 1.5 turbine and met mast variables are imported for the corresponding time range. Next, for each 10-sec slice of acoustic data, the corresponding 10-sec average values of relevant turbine and met mast variables are calculated. Specifically, the following variables are combined with the acoustic data:

Turbine variables:

- Active power
- Rotor speed
- Blade pitch angle
- Turbine status (to filter for normal operation)
- Nacelle position
- Nacelle wind speed
- Nacelle wind vane
- Yaw offset command (see Table 1).

Met mast variables:

- Wind speed at 80-m height (hub height)
- Wind direction at 87-m height (the nearest measurement to hub height)
- Temperature (for normalizing wind speed to standard atmospheric conditions)
- Air pressure (for normalizing wind speed to standard atmospheric conditions).

Lastly, the synchronized 10-sec acoustic, turbine, and met mast data are merged and appended to a Pandas DataFrame comprising all recording periods to date.

As indicated in Figure 7, the synchronized 10-sec A-weighted SPL values (total and 1/3-octave band), narrowband spectra, and SCADA data act as inputs to the IEC Standard acoustic noise analysis procedure, discussed in Section 3.2. Additionally, for the three low-frequency microphones, the combined unweighted SPL values (total and 1/3 octave band), G-weighted total SPL values, and SCADA data serve as inputs to the low-frequency and infrasound noise analysis procedure described in Section 3.3.

3.2 IEC 61400-11 Acoustic Noise Analysis

The IEC Standard acoustic noise analysis procedure (IEC 2020) is followed to determine (1) the total and 1/3-octave band A-weighted sound power level as a function of wind speed, and (2) tonality in the acoustic emissions from the wind turbine. The presentation of the results is similar to the 2011 DOE 1.5 acoustic noise test reported by Roadman and Huskey (2015). However, whereas the 2011 test assessed acoustic noise using a single microphone downstream of the wind turbine, measurements from 11 microphones are analyzed in this experiment to reveal directivity of the noise emissions (see Figure 2a). Additionally, sound power level and tonality are assessed for each of the five yaw offsets listed in Table 1. Figure 8 contains a flowchart outlining the IEC Standard acoustic noise analysis procedure followed for each microphone channel, beginning with the synchronized 10-sec acoustic, turbine, and met mast data described in Section 3.1.3. The individual steps of the analysis procedure are briefly described in this section, but full details can be found in the IEC 61400-11 Standard document (IEC 2020).

Before the IEC Standard analysis procedure splits into separate sound power level and tonality analyses, the 10-sec data are binned by wind speed, as shown in Figure 8. Additionally, the data are filtered to remove periods when the wind direction—as determined by the measured nacelle position—is more than 15° away from the prevailing wind direction of 285°, as discussed in Section 2.1. Wind speed is determined differently depending on whether the turbine is operating and the specific region of the power curve in which the turbine is operating. For below-rated wind speeds where the slope of the power curve is sufficiently steep (IEC 2020), wind speed is estimated from the

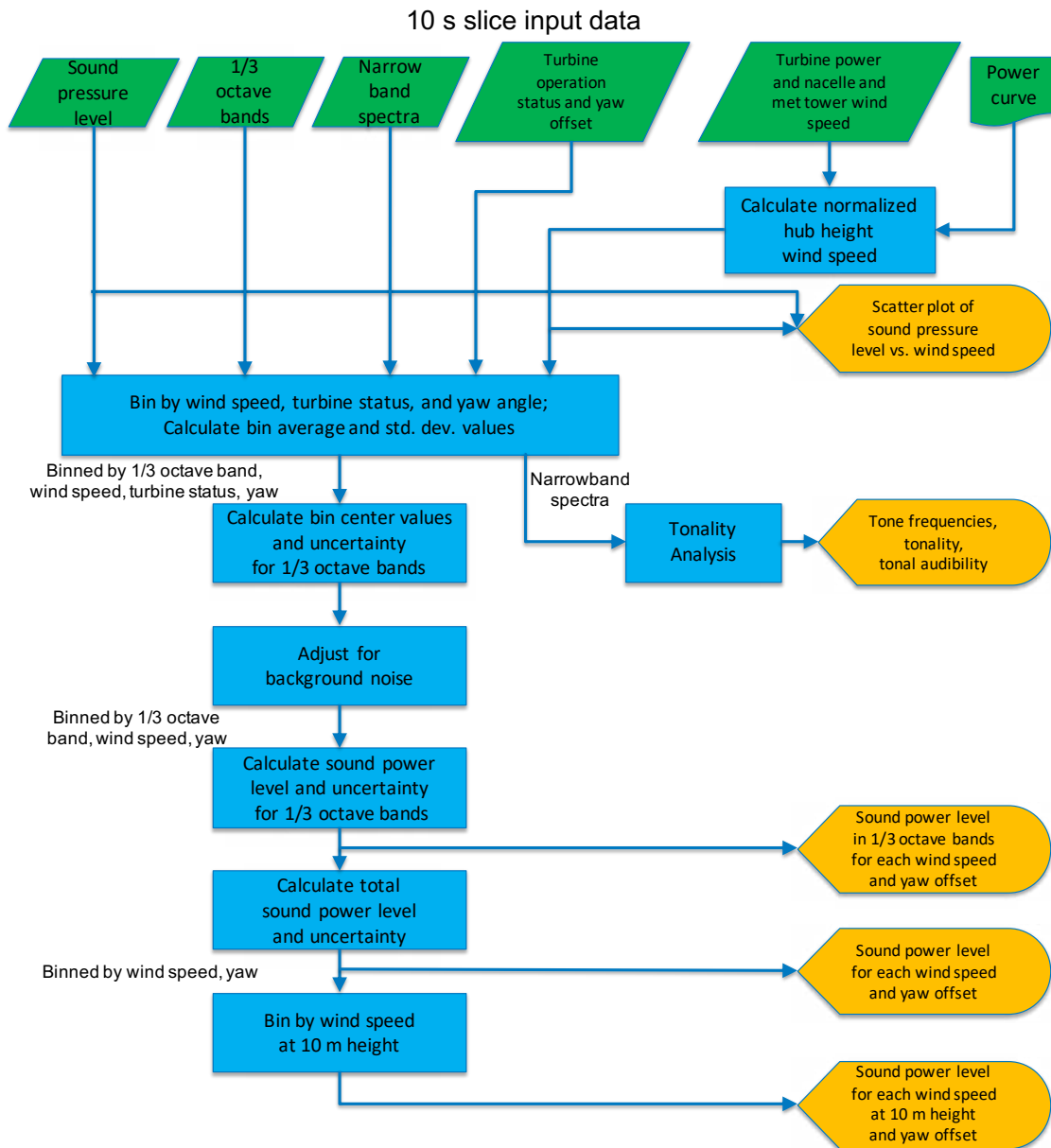


Figure 8. IEC 61400-11 data reduction procedure

measured turbine power via the turbine's measured power curve, ideally calculated based on the IEC 61400-12-1 Standard (IEC 2005). For higher wind speeds when the slope of the power curve is too small to yield an unambiguous wind speed for a given measured power, wind speed is measured using the turbine's nacelle anemometer. However, the measurement is corrected using the ratio between the wind speed estimated from the power curve and the nacelle anemometer wind speed when the slope of the power curve is sufficiently steep. Similarly, for background noise measurements when the turbine is not operating, wind speed is measured using the met mast anemometer at 80-m height (hub height). Again, the measurement is corrected using the ratio between the wind speed estimated from the power curve and the met mast wind speed when the slope of the power curve is sufficiently steep. All wind speed measurements are normalized to standard atmospheric conditions (15° and 101.3 kPa) using the temperature and atmospheric pressure measurements from the met mast.

Once the reference wind speed is calculated, the data are binned by wind speed—in increments of 0.5 m/s—as well as turbine status (operating or not operating) and yaw offset. Following guidance in the IEC Standard, measurements are analyzed for wind speeds between 0.8 and 1.3 times the wind speed when the turbine generates 85% of rated power; for the DOE 1.5 turbine, this corresponds to wind speed bins between 8.5 m/s and 14 m/s. For each wind speed/turbine status/yaw offset bin, the average A-weighted 1/3-octave band SPL values and wind speed are calculated along with the corresponding standard deviations. Note that prior to averaging, the total SPL for each measurement period is used to normalize the 1/3-octave band SPL values reported by NoiseLAB so that the sum of the 1/3-octave band SPL matches the total SPL. Next, if at least ten 10-sec periods are available for a given wind speed/yaw offset bin when the turbine is both operating and stopped, the sound power level is determined for the bin. Similarly, if at least ten 10-sec periods are available when the turbine is operating, tonality analysis is performed for the bin.

3.2.1 Sound Power Level vs. Wind Speed

Total and 1/3-octave band sound power levels are calculated as a function of wind speed for each yaw offset along with the accompanying uncertainty. The IEC Standard analysis procedure described in this section is repeated for each of the five yaw offset values. First, within each wind speed bin, the uncertainty associated with the average SPL is calculated for each 1/3-octave band. Uncertainty is also calculated for the average wind speed value within each bin. As specified in the IEC Standard, the calculated uncertainty is composed of type A uncertainty components (statistical uncertainty determined from the standard deviation of SPL and wind speed within each bin) as well as type B uncertainty (based on the assumed measurement uncertainty corresponding to each stage of the measurement chain). At this point, the average wind speed within each wind speed bin may not correspond to the bin center (e.g., the average wind speed in the 10 m/s wind speed bin might be 10.1 m/s). Therefore, linear interpolation is used to provide SPL values at the desired bin center wind speeds, based on the average wind speed and SPL values for neighboring bins. The corresponding uncertainty is interpolated as well.

Next, for each bin and 1/3-octave band, the SPL attributed to the wind turbine noise is calculated by subtracting the background SPL (when the turbine is stopped) from the combined SPL (when the turbine is operating). The uncertainty of the resulting background corrected SPL values is calculated as well using the uncertainty of the background and combined SPL components. Note that background corrected SPL values corresponding to bins and 1/3-octave bands for which the difference between the combined and background SPL is less than 3 dB should be treated as less reliable.

The sound power level of the noise emitted by the wind turbine is then calculated for each bin and 1/3-octave band by adjusting the background corrected SPL values for (1) propagation losses associated with the distance between the rotor center and the microphone location, and (2) approximate pressure doubling at the microphone locations caused by the measurement boards. The sound power spectrum in 1/3-octave bands is provided as an analysis output for each wind speed and yaw offset, along with accompanying uncertainty.

Subsequently, the total sound power level associated with the wind turbine noise is calculated for each wind speed bin and yaw offset by summing the individual sound power levels for each 1/3-octave band. Likewise, the uncertainty associated with the total sound power level is calculated based on the uncertainty corresponding to each 1/3-octave band. The total sound power level as a function of wind speed bin and yaw offset is reported as a standard

analysis output, along with accompanying uncertainty, as long as the difference between the total combined and background noise is greater than 3 dB.

Finally, the total sound power level is calculated for integer 10-m height equivalent wind speed bins. Measured hub height wind speeds corresponding to the 10-m height equivalent wind speeds are determined by assuming a logarithmic wind shear profile with a roughness length of 0.05 m. The 10-m height equivalent sound power levels are found using linear interpolation by repeating the relevant steps of the analysis procedure described in this section for hub height wind speeds corresponding to the integer 10-m height wind speeds. The total sound power level as a function of 10-m height wind speed and yaw offset is then reported as an analysis output together with the calculated uncertainty.

3.2.2 Tonality

Using the A-weighted narrowband spectra corresponding to periods when the turbine is operating, the IEC Standard tonality analysis procedure (IEC 2020) is performed for each hub height wind speed bin and yaw offset. The goal of the tonality analysis is to identify and characterize tones in the wind turbine noise that can be perceived by the human ear. For each wind speed/yaw offset bin, the following procedure is performed. Further details can be found in the IEC Standard document (IEC 2020).

- For each 10-sec period, potential tones are identified. First local maxima in the spectrum are found and a critical band is calculated around each maximum point. If the local maxima are at least 6 dB above the average energy in the critical band, the point is considered a potential tone.
- For each potential tone, further analysis is performed to determine if the local maximum qualifies as a tone. Within the critical band surrounding each potential tone, each frequency component is classified as a “masking” frequency, a tone, or neither, based on its relative energy content.
- If several frequencies are identified as tones within the critical band, the frequency of the component with the highest energy is considered the tone frequency. The tone level is calculated as the sum of the energy of all tones identified in the critical band.
- The *tonality* of the tone is calculated as the difference between the tone level and the average energy content of the masking noise.
- *Tonal audibility* is calculated by subtracting a frequency-dependent audibility criterion from the tonality. This term accounts for the sensitivity of the human ear to tonality at different frequencies.
- The tonal audibility values corresponding to the same tone origin identified in all 10-sec periods are averaged to form a single tonal audibility value. The tone frequency and its tonal audibility are reported if the tone origin is identified in at least six 10-sec periods and is present in at least 20% of all 10-sec periods within the wind speed/yaw offset bin.

Finally, a table including the identified tone frequencies, tonality, and tonal audibility values for each wind speed/yaw offset bin is provided as an analysis output.

3.3 Low-Frequency Noise and Infrasound

Measurements from the three low-frequency microphones discussed in Section 2.3.1 are used to characterize the low-frequency and infrasound noise emitted by the wind turbine. Low-frequency noise is defined as noise in the frequency band between 20 Hz and 200 Hz, whereas infrasound noise consists of frequencies below 20 Hz. For each low-frequency microphone, low-frequency and infrasound noise are characterized by performing the IEC Standard noise analysis procedure outlined in Section 3.2. However, unweighted SPL values are used in place of the traditional A-weighted SPL (A-weighting heavily filters the low frequencies of interest in this analysis). Additionally, total sound power level is calculated using G-weighted SPL values to characterize total infrasound emissions. Further, only 1/3-octave bands between 1 Hz and 200 Hz are considered.

For each wind speed bin and yaw offset, reported low-frequency and infrasound quantities include unweighted 1/3-octave band sound power levels between 1 Hz and 200 Hz, unweighted total sound power levels for frequencies

below 20 Hz and frequencies between 20 Hz and 200 Hz, and G-weighted total sound power level. These data are not reviewed in this report, but have been made available through the public data set hosted on the DAP.

3.4 Impulsivity

Impulsivity analysis is used to identify impulsive sounds emitted from the wind turbine (i.e., sounds with a sudden onset). The impulsivity analysis procedure used for this experiment follows the guidelines presented in the Nordtest method document (Nordtest 2002). The Nordtest method establishes a procedure for quantifying the prominence of impulsive sounds, characterizing the degree of annoyance caused by impulses. An adjustment to the average A-weighted SPL of the measured environment is then recommended to account for the added annoyance.

To identify impulsive sounds, the microphone recordings are divided into A-weighted total SPL time series with a sampling period of 10–25 ms. Impulses are defined as periods when the slope of the SPL signal exceeds 10 dB/s. For each impulse, the *onset rate* is calculated as the slope of the least-squares best fit line derived from the SPL time series during the full impulse period. The *level difference* is calculated as the difference in dB between the SPL at the end and starting points of the impulse. Once an impulse has been identified, the *predicted prominence* of the impulse—used to quantify the perceived annoyance of the impulse—is calculated as a linear combination of the logarithm of the onset rate and level difference. Increases in either onset rate or level difference result in a higher predicted prominence value. Lastly, if a predicted prominence value exceeds 5, an adjustment term (in dB) is calculated based on the prominence, which can be added to the average A-weighted SPL level to account for the annoyance created by the impulse.

The Nordtest method suggests using the maximum prominence from all impulses identified in a 30-min measurement period to calculate an adjustment term to be added to the 30-min average SPL. However, in this experiment the prominence of impulses detected for each microphone are grouped by the wind speed bin and yaw offset during which they occurred. The maximum prominence and the recommended SPL adjustment term are reported for each wind speed/yaw offset bin as long as the maximum prominence exceeds 5. The audio recordings will be examined to ensure that the reported impulses are associated with wind turbine noise as opposed to background noise (e.g., cars or birds).

3.5 Amplitude Modulation

Amplitude modulation is defined as periodic fluctuations in the level of noise emitted by a wind turbine occurring at the blade passing frequency (Institute of Acoustics IOA Noise Working Group (Wind Turbine Noise) 2016). Although high-frequency “blade swishing” is one form of amplitude modulation, periodic low-frequency “whoomphing” is more problematic because it can persist over greater distances. The *Reference Method* published by the UK Institute of Acoustics Amplitude Modulation Working Group (IOA AMWG) is used in this experiment to identify and characterize amplitude modulation related to low-frequency “whoomphing” noise (Institute of Acoustics IOA Noise Working Group (Wind Turbine Noise) 2016). The method identifies the presence and level of amplitude modulation present in 10-min measurement periods. Note that the IOA AMWG suggests measuring amplitude modulation at least 500 m from the wind turbine, which is not possible in this experiment given the locations of the microphones.

The IOA AMWG method begins by dividing each 10-min measurement period into sixty 10-sec slices. For each 10-sec slice, a time series of A-weighted 1/3-octave band SPL values is calculated in 100 ms periods, yielding a 100-sample sequence. The amplitude modulation procedure is then performed using the sum of the 1/3-octave band SPL values for three different frequency ranges: 50–200 Hz, 100–400 Hz, and 200–800 Hz. For each frequency range, the resulting SPL time series is detrended and transformed to the frequency domain using Fourier analysis. If a sufficiently prominent peak is identified in the spectrum near the expected blade passing frequency, amplitude modulation is attributed to the 10-sec slice. Next, a filtered time series is calculated using the inverse Fourier transform, including only the peak frequency component and the second and third harmonics (if they are sufficiently prominent) as well as all adjacent frequency components. The degree of amplitude modulation is then calculated as the difference between the 95th and 5th percentiles of the SPL of the reconstructed time series. If amplitude modulation is identified in at least 50% of the individual 10-sec slices within a 10-min period, the 10-min period is classified as exhibiting amplitude modulation. The level of amplitude modulation for the 10-min period is quantified as the 90th

percentile of the individual modulation amplitudes for each valid 10-sec slice. Finally, by analyzing all 10-min periods, the frequency range that tends to yield the highest level of amplitude modulation is chosen as the representative frequency range for reporting.

In this experiment, the level of amplitude modulation attributed to each 10-min period is binned by the 10-min average wind speed (calculated as explained in Section 3.2) and yaw offset for each microphone. The maximum amplitude modulation level identified for each wind speed/yaw offset bin is reported as an analysis output. Note that periods where amplitude modulation is identified are investigated further to ensure that wind turbine noise is the source of the amplitude modulation.

4 Numerical Models for Aeroacoustics Noise

This section contains a brief overview of the numerical models used to estimate the aeroacoustics noise of wind turbines. The discussion is divided into four subsections. First, the models to predict the noise generation in the acoustic range are presented. Next, the expected impact of yaw offsets in the output spectra is discussed. Third, the models to simulate how noise propagates in the atmosphere are introduced. Finally, the models to estimate infrasound noise are reviewed. Readers interested in the details of the models should refer to Bortolotti et al. (2020) and to the references listed in the next paragraphs.

4.1 Aeroacoustics Noise Generation

The emission of aeroacoustics noise of the DOE 1.5 turbine is simulated by running a numerical aeroacoustics model (Bortolotti et al. 2020). The model is part of the aeroservoelastic framework in OpenFAST, and it is run simulating noise generation during various wind conditions, rotor speeds, and yaw angles. The aeroacoustics model encompasses various mechanisms of noise generation. The aeroacoustics noise of the DOE 1.5 turbine is estimated combining a formulation for turbulent inflow (TI) noise and a formulation for the turbulent boundary layer trailing edge (TBL-TE) noise. The TI noise source is caused by the perturbation of the turbulent flow generated by each of the three rotor blades and is also known as leading edge noise. The second noise source belongs to the so-called airfoil self-noise mechanisms where noise originates from turbulent vortexes created past the trailing edge of the airfoils along the span of the blades. The aeroacoustics model implemented in OpenFAST also offers the possibility to predict noise generated from other sources, namely other airfoil self-noise mechanisms. As of now, these are believed to be irrelevant for modern multimegawatt wind turbines.

Literature presents various formulations of both TI noise and TBL-TE noise models. The implementation in OpenFAST currently includes two TI noise models, namely the original formulation from Amiet (1975) in its simplified and compact form, and the Amiet model with a correction to include the effects on noise of the finite thickness of the blade from Moriarty, Guidati, and Migliore (2005). The original Amiet model indeed assumes a flat plate and therefore neglects the shape of the leading edge of the airfoils. Note that the Amiet model also includes a correction term at lower frequencies and a correction for nonzero angles of attack (Bortolotti et al. 2020).

In the TBL-TE model, noise can be simulated either by adopting the original formulation defined by Brooks, Pope, and Marcolini (1989), the model commonly referred to as BPM, or by running the more recent and more computationally expensive formulation developed at the Dutch research institute TNO (Parchen 1998). The latter model requires the boundary layer characteristics of the airfoils along blade span. These can be automatically reconstructed by the code from the semi-empirical relations defined in the BPM model or can be provided as inputs by the user. In the latter case, the properties can be computed with numerical models at various fidelity level. In this project, the BPM noise model is adopted.

4.2 Impact of Yaw Misalignment on Noise

Both the TI and TBL-TE models are most sensitive to the rotational speed of the wind turbine rotor. Wind turbines operating under yaw offsets see a reduction of rotor speed at given wind conditions, and this effect is expected to reduce the generation of aeroacoustics noise. A counteracting effect is, however, expected from the higher angles of attack that misaligned rotors experience (Damiani et al. 2018). The angle of attack correction in the TI model and the effect of higher angles of attack in the separated flow noise BPM model are expected to possibly increase the noise spectra at the observer locations. Higher amplitude modulation may also be present.

In addition, noise is not emitted uniformly from each blade span section, and a noise directivity model from Brooks, Pope, and Marcolini (1989) is included in OpenFAST. At each instant of time, the model reconstructs a spanwise and a chordwise angle for each blade segment and each observer, and the model computes a directivity term that is applied to the SPLs. Operations under yaw offsets impact these angles and therefore the directivity terms. Aeroacoustics noise is expected to be highest in the observers lying perpendicular to the rotor plane, and be lowest in the observers lying in the rotor plane.

4.3 Noise Propagation

Similar to wind resource predictions for wind farm planning, noise evaluations for wind farms should be performed before the wind farm is built, such that inappropriate land-use planning can be avoided. In order to enable wind farm noise simulation capability, it is essential to capture noise propagation from individual wind turbines over a long distance and consider atmosphere and terrain conditions. Simulating noise propagation in the far field has historically been a difficult task because the ambient turbulence level, terrain geometry, and wake interaction between turbines and ground all can affect noise propagation over a long distance. A recent paper by Shen (Shen et al. 2020) compares low-fidelity models for noise propagation using the models named WindSTAR (Zhu et al. 2018), Nord2000 (Jonasson and Storeheier 2001), ISO 9613-2 (1996), and *DK-BEK135* for a single wind turbine located at a relatively flat terrain against experiment data in depth. The paper concludes that for the simple case taken into consideration, all models perform fairly well. More complex scenarios (such as in the presence of complex terrain) are, however, expected to affect the behavior of the low-fidelity models.

Higher-fidelity tools to simulate noise propagation over complex terrain also exist, such as OTL–Terrain developed by Economou and Peppin (2012). This tool utilizes sound ray modeling, which solves Helmholtz’s sound wave equation and thus accounts for sound diffraction to any order (the phenomenon of the bending of sound around objects). Furthermore, it accounts for sound wave reflection from finite size surfaces of finite impedance using Fresnel Zones and spherical wave reflection coefficient concepts, respectively. Model predictions of noise in far field matched well with experimental data. However, its applications so far are limited to simple noise resources and obstacles based on authors’ best knowledge. The model’s potential for wind turbine applications is yet to be explored.

At NREL, the model described in ISO 9613-2 (1996) has been recently implemented in a Python script and exercised assessing the sensitivity of the outputs to various inputs. The outputs are very sensitive to the parameters modeling ground attenuation. The atmospheric absorption is expected to play a role for distances beyond the measurement range planned in this project.

4.4 Infrasound and Low-Frequency Noise

The generation of infrasound noise from wind turbines is an open research question, and the physical phenomenon is less clear than in the audible acoustic range. In this project, one goal was to characterize the emission of infrasound noise experimentally. Achieving this, follow-on validation projects of the numerical models can be planned. This section reviews the models that have the potential to accurately estimate the low frequency emissions of wind turbines. None of these models are currently implemented at NREL.

Whereas models to estimate the audible aeroacoustics noise emitted by wind turbine rotors are frequency based, the numerical models to estimate the infrasound emissions of wind turbines are usually based on time-domain approaches. These methods are based on acoustic analogies, which use manipulations of classical fluid dynamic equations to calculate acoustic pressures. The most common model to estimate the low-frequency noise of wind turbines is the Ffowcs Williams-Hawkings (FW-H) (Williams and Hawkings 1969) model based on the Farassat 1A formulation (Farassat 2007). One example of its implementation is presented in Sucameli et al. (2018). This model requires the computation of thickness and loading noise on a control surface and neglects the contribution of the quadrupole term of the original FW-H formulation. This way, the method can use as input the pressure and velocity distributions measured directly on the blade surface. These can be obtained from the combination of a blade element momentum-based aeroelastic model such as OpenFAST and a boundary-layer airfoil solver such as XFOIL (Drela and Giles 1987). The latter is used to reconstruct pressure distributions on the blades from lift and drag coefficients. Alternatively, the FW-H model can be coupled to higher-fidelity solvers such as SOWFA (Klein et al. 2018) or NREL’s AMR-Wind. The latter family of approaches comes with a higher degree of fidelity at the cost of higher computational requirements. An implementation of the FW-H model is also available in the code WOPWOP, which was developed at the Pennsylvania State University in collaboration with NASA and the U.S. Army (Brentner et al. 2002).

5 Results

5.1 Preliminary Modeling

As part of the experimental design, the Aeroacoustics module in OpenFAST was used to preview experimental results. Figure 9 shows the overall SPLA at observer locations arrayed around the DOE 1.5 modeled with idealized settings. In each case, the rotor speed was held at a fixed value, wind speed was set to a constant 8 m/s, and the incoming TI and turbulence length scale were fixed at 10% and 40 m, respectively. The preliminary modeling results are included here to help contextualize the experimental results shown in Section 5.2.

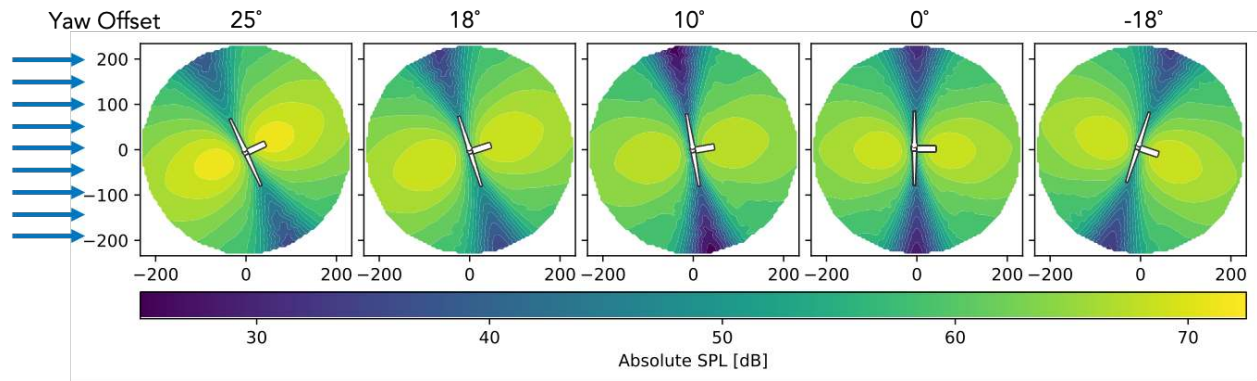


Figure 9. Pre-experiment model results for the DOE 1.5 at the yaw offsets selected for testing

Figure 9 indicates that the SPL around the turbine should change with yaw offset. The greatest part of the change is a rotation of the estimated SPL, arising from the directivity model implemented in OpenFAST. Directivity accounts for difference in SPL based on the relative orientation between an observer and the blades over their rotation. With the exception of a yaw offset of 25°, the magnitude of the overall SPL changes little from case to case. For more extreme yaw offsets, as is the case with 25°, the boundary layer may separate from the blades during their rotation, causing additional noise and leading to the higher SPL in the leftmost image in Figure 9.

Note that the modeling results shown in Figure 9 include observers very close to the turbine where the predicted noise is expected to be quite high (greater than 70 dB). The ambient turbulence level used in the simulations is also lower than observed in the field, causing the quiet region near the rotor plane to exhibit a lower overall SPL than observed in the field. Despite the differences in specific atmospheric and turbine operating conditions, the pre-experiment modeling results provide a qualitative guide to understanding the experimental results presented below.

5.2 Experimental Results

The experiment yielded more than 41 hours worth of quality-controlled aeroacoustic data binned in 10-sec intervals. Of the retained data, approximately 9 hours were of background noise (with the DOE 1.5 parked) and 32 hours of data were collected with the turbine operating. Figure 10 shows the accumulated quality-controlled background and operational data by wind speed. Background data include observations recorded for all wind directions, while operational data was constrained to times when the wind direction was within the sector of $285^\circ \pm 15^\circ$, following guidance in the Standards.

The dashed line near the bottom of each histogram indicates the required number of observations for each wind speed bin. With the exception of hub-height wind speeds above 15 m/s, the quality controlled data from the field experiment greatly outstrips the requirements outlined in the Standards. In the reference case of 0° yaw, the majority of data were collected at wind speeds below 8 m/s. At all other yaw offsets, the final data set has more observations for wind speeds between 8 m/s and 14 m/s. Background noise measurements are fairly even across the range of 6 m/s to 14 m/s, which is the range of focus for much of the following analysis.

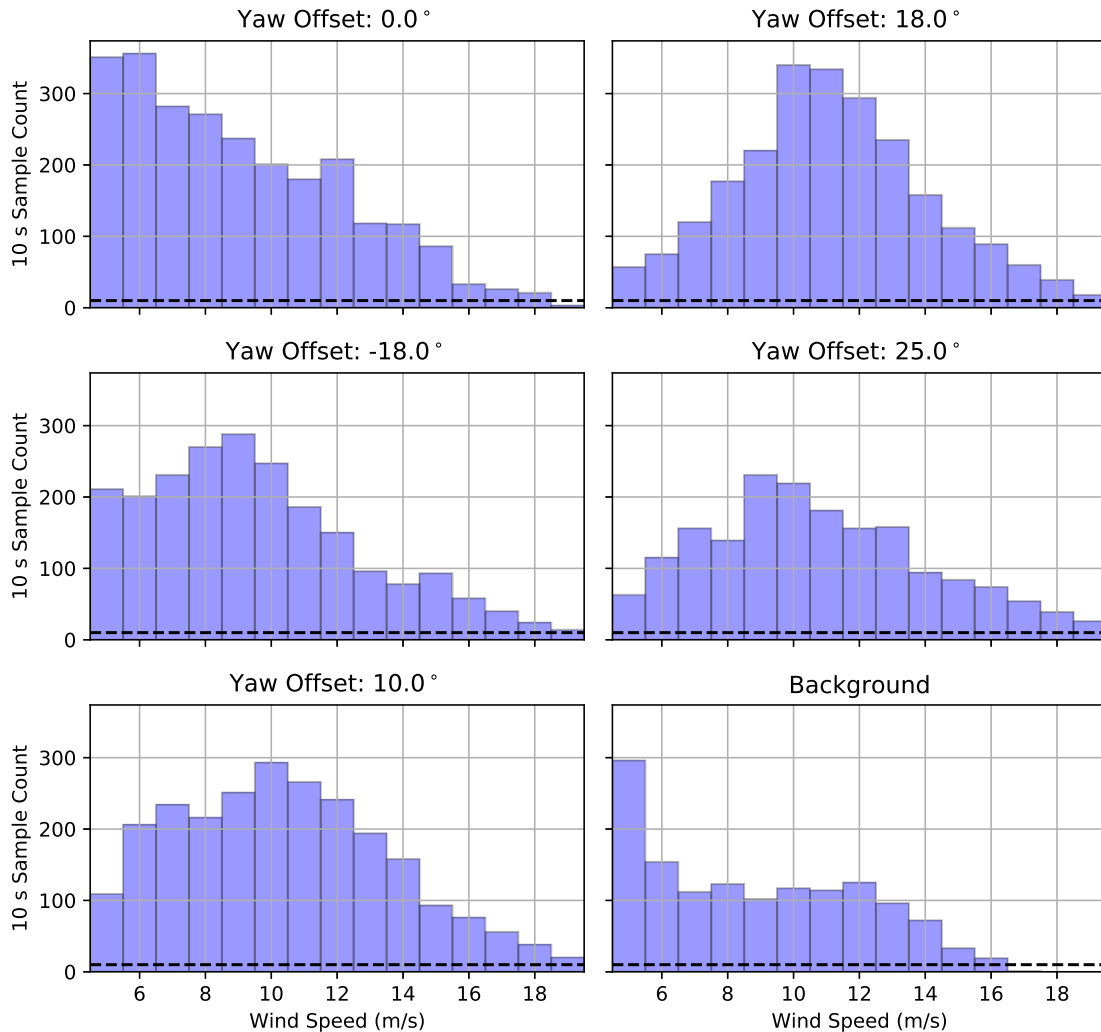


Figure 10. Number of valid 10-sec SPL slices obtained for each 1 m/s wind speed bin for background and normal operation periods

Characterizing the background noise in the area is crucial to be able to correctly assess aeroacoustic noise generated by the wind turbine. Background noise recorded at each of the 11 microphones is shown in Figure 11. The boxplots on the left show the combined distribution of background noise levels from all SFR microphones together by wind speed. The whiskers in each plot indicate the valid range of observations—statistical outliers have been excluded from the figure for clarity. The valid range of noise measurements for each wind speed bin is fairly consistent, with span varying from 8 dB to 14 dB. The trends in the right plot of Figure 11 show the median A-weighted SPL at each microphone, including the low-frequency noise mics. All median SPL trends follow the pattern shown by the boxplots, with the exception of microphone 04C, which reported a higher median background noise level for wind speeds above 6 m/s.

Comparing the distribution of background noise and overall A-weighted SPL, as in Figure 12, provides a sense of the signal-to-noise ratio for each microphone. Microphone 04C (Figure 12(a)), which shows the greatest median background SPL with wind speeds greater than 6 m/s, also shows the a wider distribution of recorded SPLA. Whereas 04C shows a range of background SPLA on between 40 and 65 dBA for wind speeds greater than 9 m/s, other microphones show an much tighter distribution. Microphone 12C, for example, has a background noise range of 37 to 45 dBA at 9 m/s, a range of only about 8 dBA. Because the background noise for this microphone is so much higher

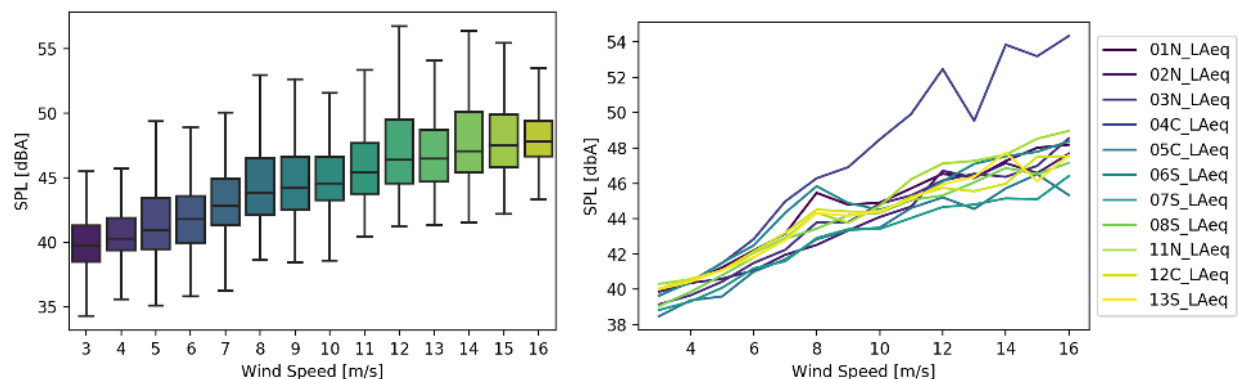
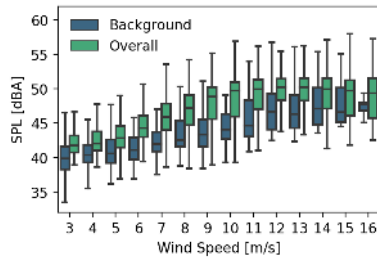


Figure 11. Distribution of background noise by wind speed (left) and median background noise for each microphone (right)

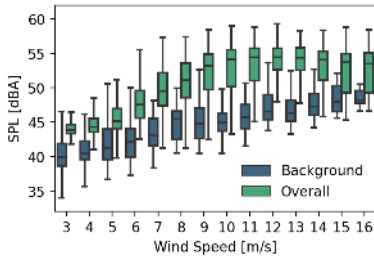
than four other measurement locations, the signal-to-noise ratio is comparatively small. The only other microphones with small signal-to-noise ratio's are microphone 02N and microphone 08S, both of which are located farthest from the turbine and the prevailing wind direction. In Figure 12, all equivalent SPL data have been A-weighted, so the low frequency microphones (mics 11N, 12C and 13S, center subfigures) do not show any significantly different trends than the SFR microphones.

Additional insight into the background noise are provided by looking at spectra. The collection of background noise spectra recorded at 8 m/s are shown in Figure 13 from all of the SFR microphones together (left) and the low-frequency noise microphones (right). In each plot, spectra calculated from 10-sec slices are shown in thin purple and blue lines for the SFR and low-frequency noise microphones respectively. Average background noise spectra are shown in thicker contrasting lines. Note that the differences between spectra are most evident at the low- and high-frequency ends of the spectrum. Standard frequency microphones do not have a flat frequency response below 20 Hz, and so under report sub-audible noise. In the low-frequency region, standard frequency microphones do accurately reflect low-frequency noise emitted by the wind turbine. Both the SFR and the low-frequency noise microphones overestimate high-frequency noise as well. Noted in the equipment specifications in Appendix C, microphone response above 9 or 10 kHz is typically over-reported.

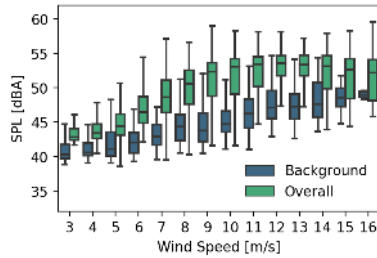
Background and overall noise spectra are shown in Figure 14 each microphone at a wind speed of 9 m/s. Each sub figure is arranged placing data for each microphone in the respective position during the experiment. Spectra from 10-sec slices are shown in thin blue and green lines for the background and overall noise spectra, respectively. Thicker lines indicate the average spectra for each microphone at 9 m/s. The infrasound range below 20 Hz has been excluded for all SFR microphones. Low frequency microphones, in the center sub figures, extend down to 1 Hz. Every microphone recorded a peak in background noise around 350 Hz, with the exception of microphone 04C. Microphone 04C, at the IEC test location, reports a higher background SPL for frequencies below 100 Hz. This contribution is likely to have produced the unusually high background noise SPLA shown in Figures 11 and 12. The difference between the average spectra represents the noise contributed to the recordings from the wind turbine itself. Appendix A contains additional plots like those in Figure 14 for other wind speeds part of the experiment.



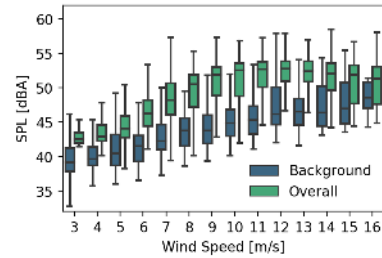
(a) Microphone 02N



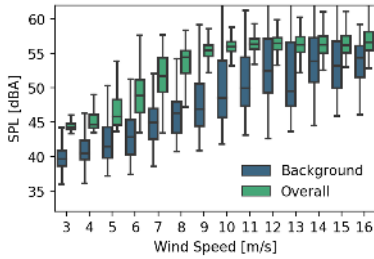
(b) Microphone 01N



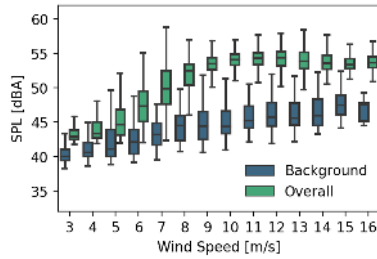
(c) Microphone 11N



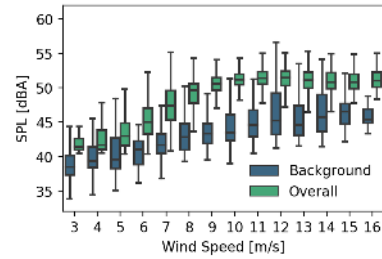
(d) Microphone 03N



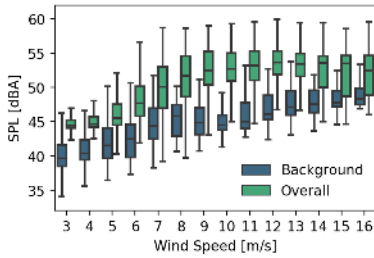
(e) Microphone 04C



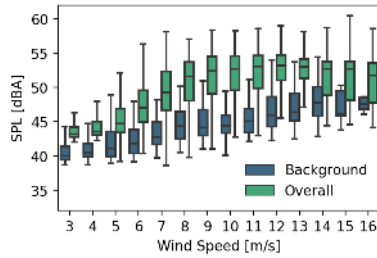
(f) Microphone 12C



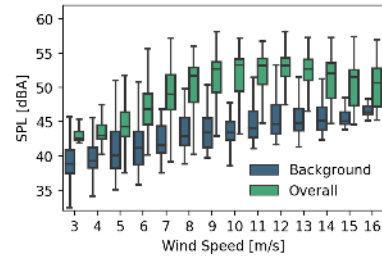
(g) Microphone 05C



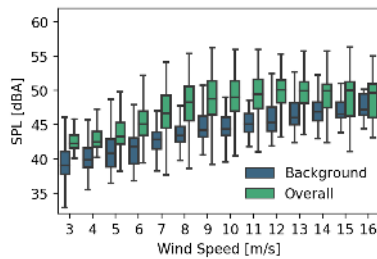
(h) Microphone 06S



(i) Microphone 13S



(j) Microphone 07S



(k) Microphone 08S

Figure 12. Comparison of background noise and overall noise recorded at each microphone. Each subfigure is arranged in the relative position of the respective microphone in the experiment. Refer to Figure 2b.

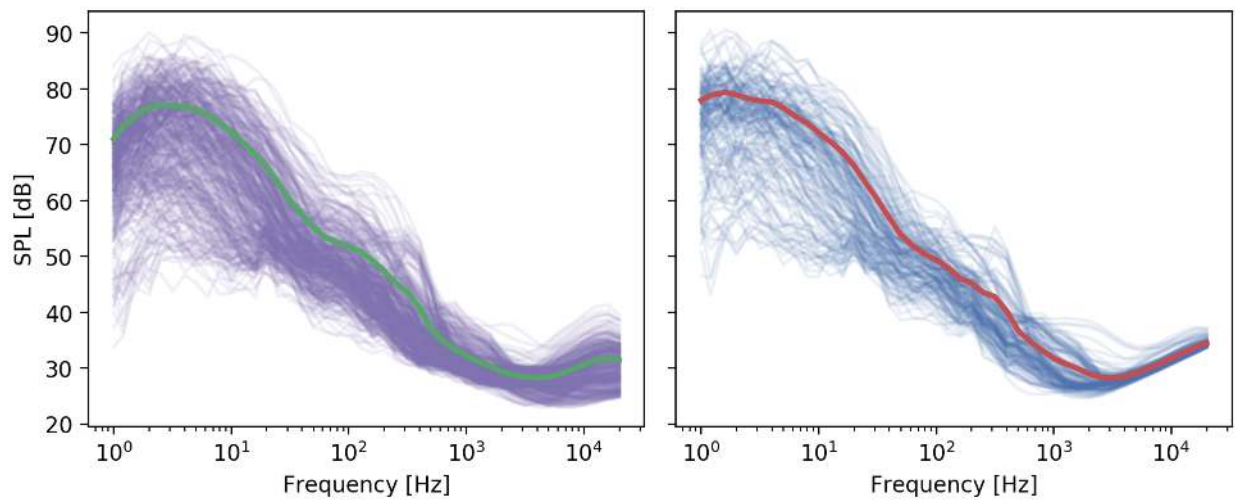


Figure 13. Individual and mean spectra for standard frequency microphones (left) and low-frequency microphones (right)

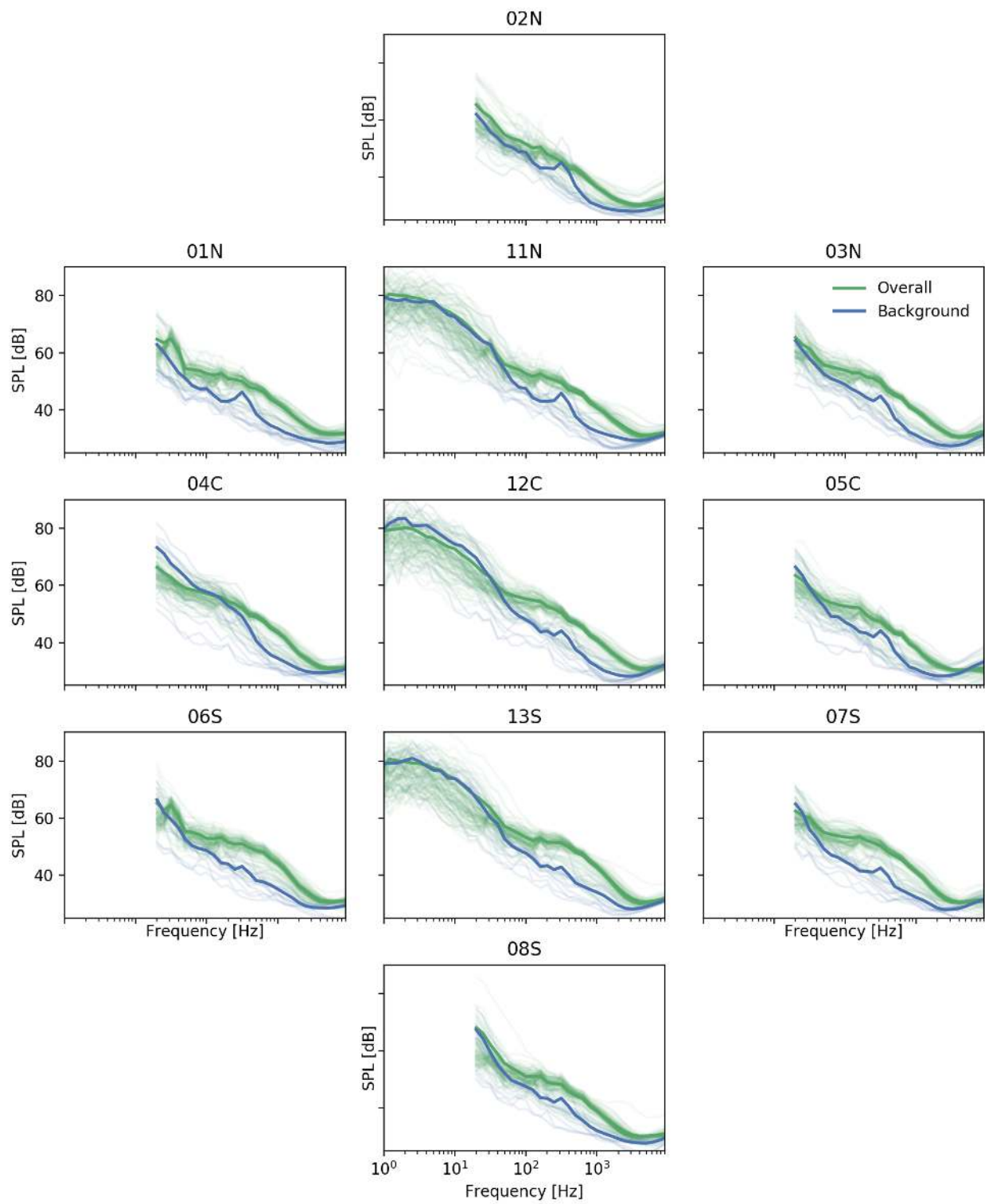


Figure 14. Overall and background spectra at 9 m/s for all microphones.

During normal operation, aeroacoustic noise generated by the wind turbine and background noise are both present. Only by removing the background noise signature from the overall SPL recorded by each microphone can the noise of the wind turbine be identified. For all of the equivalent SPL and noise spectra results in this report, the wind turbine noise is calculated by averaging the operational noise observations less the mean of the background noise. In cases where the mean background noise is greater than the operational noise at any particular frequency, this yields negative values, which cannot be described in decibels. Thus, in calculating the wind turbine noise spectra, only observations that yield a positive wind turbine noise value are included. This methodology is likely to bias results to be on the high side, but results here show that in most cases the wind turbine noise at these frequencies is only marginally greater than the background. The same procedure was followed for the equivalent SPL reported by NoiseLAB.

Figure 15 summarizes the results of the entire experiment, showing the distributions of wind turbine aeroacoustic noise at each microphone and for each yaw offset. All microphones reported a similar trend in aeroacoustic noise with wind speed, increasing from around 42 dB to somewhere near 52 dB. The notable exception to this trend is microphone 04C located in the IEC-specified test location, which reports a maximum median SPL of nearly 57 dB. It should be noted here that microphone 04C also recorded the highest background noise, as shown in Figure 11.

Each cluster of box and whisker plots contains the distribution of recorded A-weighted SPL for a single yaw offset. The general trend shown by the field of measurements is that the northern set of microphones (01N, 02N, 03N, 11N) record SPL that increases with yaw offset. At a yaw offset of -18° , the northern mics all show a distribution with lower values than the reference of 0° . As the offset increases through 10° , 18° , and 25° , the median of the respective distributions also increases, matching the expected changes from the preliminary modeling in Figure 9. The opposite trend is seen for the set of microphones associated with the southern DAS node (06S, 07S, 08S, 13S). All southern microphones report greater SPL for negative yaw offsets than for the reference case or for positive yaw offsets.

While changes in recorded wind turbine noise match the expected qualitative trends from preliminary modeling, the results show some asymmetry with yaw offset that was not predicted ahead of the experiment. Comparing the trend shown for microphone 02N and 08S, which are located on opposite sides of the prevailing wind direction, the model results suggest that we should expect more or less equal, but opposite changes in the recorded SPL.

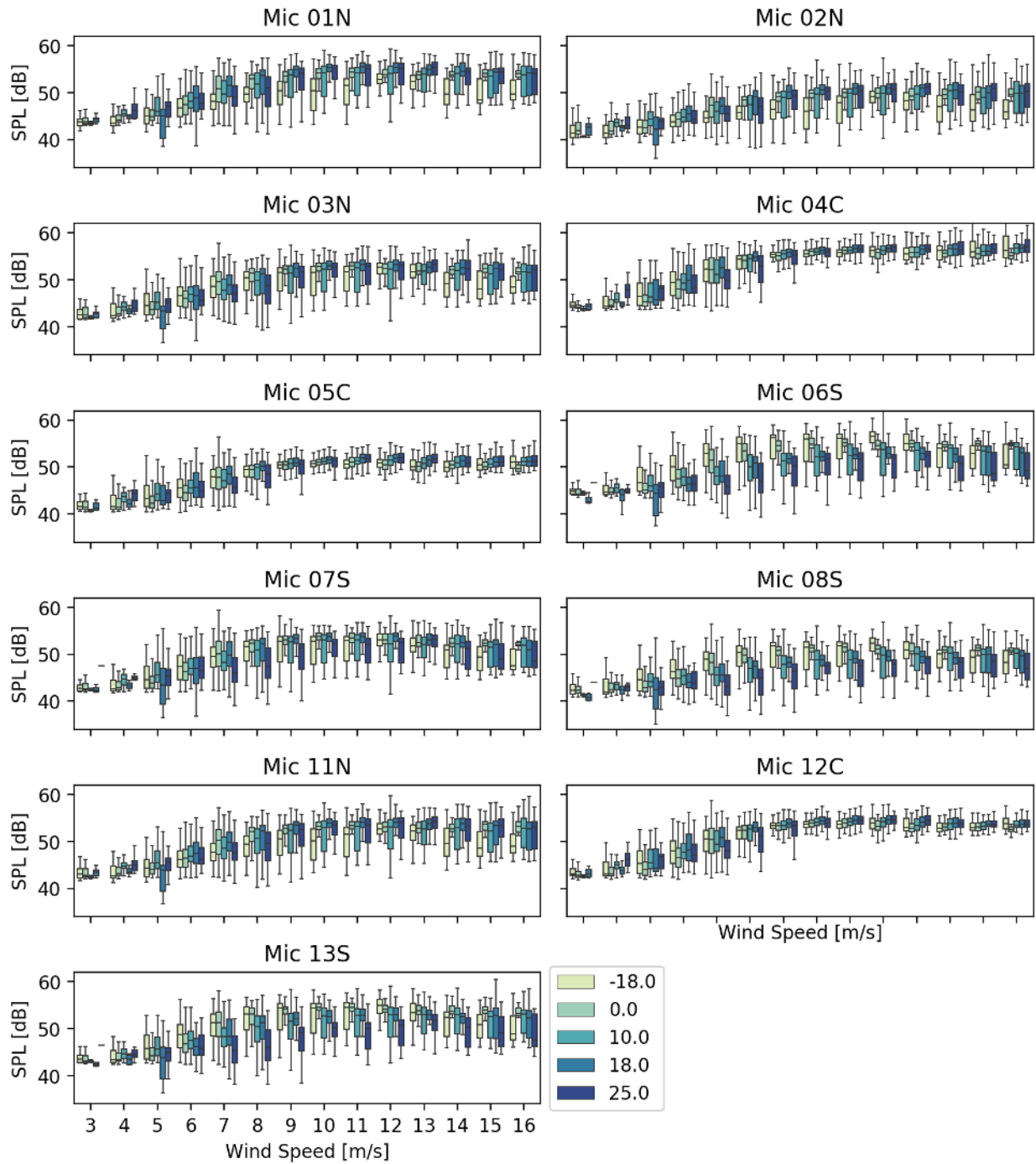


Figure 15. Distributions of SPL vs. wind speed for each yaw offset

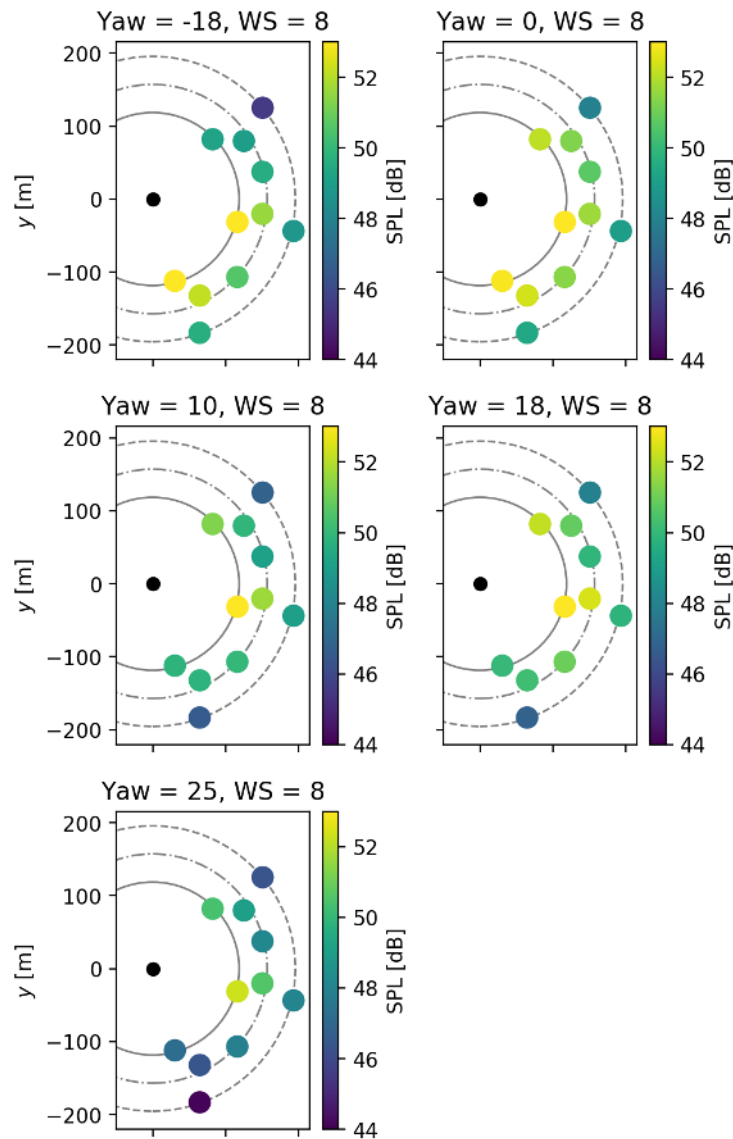


Figure 16. Equivalent A-weighted SPL at each microphone location for 8 m/s for each yaw offset

However, the experimental results show a much greater sensitivity to yaw offset for mic 08S than for mic 02N. In the north, the total change in median SPL from a yaw offset of -18° to 25° is about 5 dB, with only small changes for positive yaw offsets. Microphone 08S, in contrast, shows a nearly linear dependence on yaw offsets over the full range of tested conditions. These trends were not anticipated from the modeling, and should be investigated in greater detail to tease out the root cause.

Figure 16 shows the spatial distribution of changes in equivalent A-weighted SP by mapping results onto the location of each microphone. At 8 m/s, the reference case with 0° yaw offset (upper right corner) shows a peak SPL of approximately 53 dB at the 04C location and decreasing values moving both outward from the wind turbine and azimuthally away from the prevailing wind direction. At the negative yaw offset of -18° (upper left), the southern microphones show slightly elevated A-weighted SPL, the report of the central microphones is approximately unchanged, and the northern microphones report an SPL approximately 4 dB lower than at the reference yaw, conforming to the OpenFAST predictions shown in Figure 9. During operation at negative yaw offsets, the mics located in

the north are closer to the rotor plane, where the directivity model suggests lower overall SPL. Similarly for positive yaw settings, the SPL reported in the south decreases as microphones in that region are closer to the rotor plane. For moderate positive yaw offsets of 10° and 18°, the experimental results show similar trends to the expected changes in directivity from the preliminary modeling, where overall SPL for mics in south decreases, and overall SPL for mics in the north increase. At the more aggressive yaw offset of 25°, there is a substantial change in the noise recordings at all microphone locations, including those in the north, by as much as 7 dB. This finding was not predicted by the OpenFAST model, which suggested we should expect noise emissions to increase at 25°.

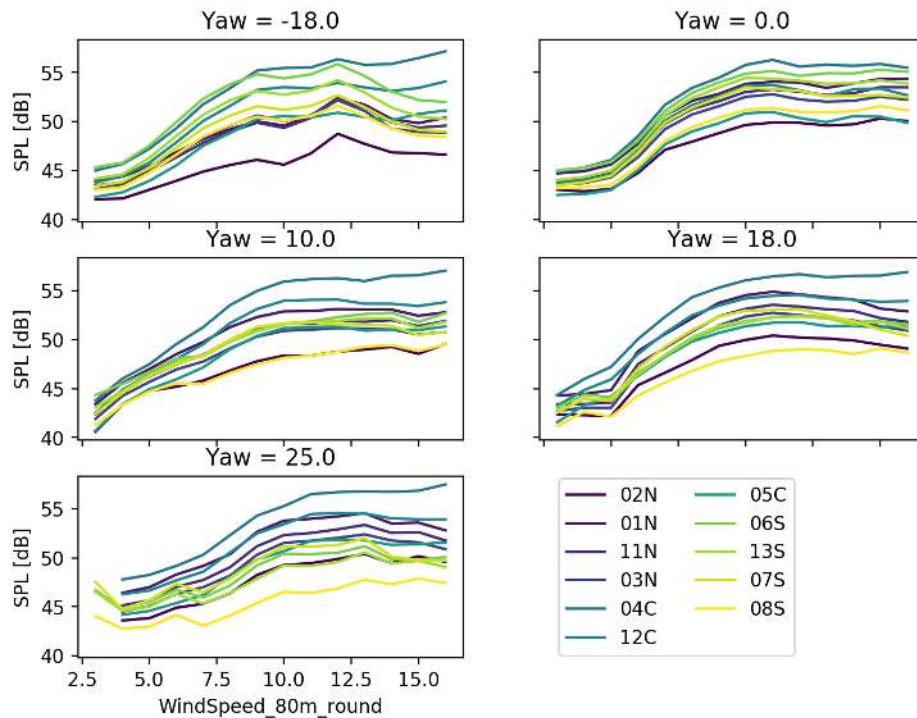


Figure 17. SPL vs. wind speed for each yaw offset

Figure 17 compares the A-weighted SPL from each microphone over the full range of wind speeds analyzed in the experiment. This view of the data does not convey the spatial distribution of A-weighted SPL, but rather assigns each microphone a color. In Figure 17, purple lines are microphones in the north, blue line those connected to the central node, and yellow/green those in the south. In a general sense, the aeroacoustic noise recorded by each microphone behaves similarly. At low wind speeds (below 5 m/s), every microphone shows the reported SPL leveling off in the range of 42–47 dB. Noise reported at these speeds is near the cut-in wind speed of the DOE 1.5, when tip speeds are relatively low. With increasing wind speeds, the aeroacoustic noise for each microphone also rises until around 10 m/s, where the SPL levels off between 47 and 57 dB, depending on the microphone location and yaw offset.

Changes in aeroacoustic noise reported by the microphones are summarized in Figure 18. In the figure, each plot shows the difference between the A-weighted SPL at each yaw offset and the reference case of yaw = 0°. For the intermediate positive yaw offsets of 10° and 18°, the overall trend is a decrease in the detected SPL, mostly observed in the southern set of microphones (yellow/green lines). These changes are attributed mostly to a decrease in rotor speed under yawed operation (see Figure 19). At the more extreme yaw offsets of -18° and 25°, the northern (purple) and southern mics (yellow/green), respectively, show a sizable decrease in SPL greater than 4 dB for some wind speeds. Asymmetry observed between the positive and negative yaw offsets is attributed to a difference in aerodynamic interactions between the blades and the inflow. The rotational sense of the rotor leads to different angles of attack for the blades at positive and negative yaw offsets. For positive values of yaw, the blades rise into the coming wind, increasing the angle of attack relative to the non-yawed case.

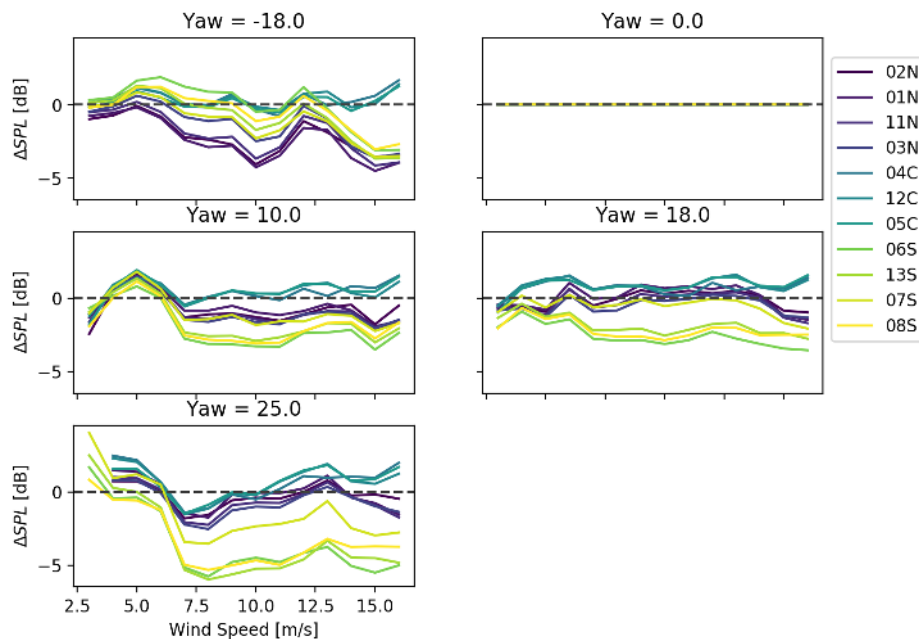


Figure 18. Change in SPL from the 0° yaw case

To highlight changes in aeroacoustic emissions from the DOE 1.5, Figure 20 compares the spectra from the two SFR microphones showing the greatest changes with yaw. Spectra from Mic 01N show less variation with yaw than those from Mic 06S. Because of its placement to the south of the prevailing wind direction, Mic 06S is closer to the rotor plane for the yaw positive offsets chosen for this project. Mic 06S shows decreases of as much as 10 dB for frequencies in the range of 300–900 Hz for a yaw offset of 25°. Intermediate positive yaw offsets (10° and 18°) show decreases of 4–5 dB over the same range of frequencies. Similar changes are evident in the spectra of Mic 01N, but to a lesser degree and only for the negative yaw offset. Positive yaw offsets do not induce the same magnitude of changes as seen for the southern microphone.

Figures 21 and 22 show the aeroacoustic noise spectra for microphones 04C and 13S, respectively. In these figures, each image compares the spectra at increasing wind speed (with brightening colors) for a given yaw setting, noted in the titles. Echoing results seen in previous figures, the spectra are spread out for wind speeds below 9 m/s, where the overall SPL at each microphone is more sensitive to wind speed. Above 10 m/s, the spectra overlap over most of the frequency range. Missing parts in the spectra are areas where the background noise spectrum was *higher* than the spectra when the DOE 1.5 was operating. In these cases, the difference (i.e., the wind turbine aeroacoustic noise) would be negative, and is undefined in dB.

The images in Figure 21 include a band that highlights the low-frequency noise region of the spectra. For standard microphones, the frequency response is not flat below 20 Hz, reflected in the results as a decrease in SPL. As a comparison, Figure 22 shows the spectra from a low-frequency noise microphone, with a flat frequency response down to 0.1 Hz, well below the audible range. In Figure 22, the low-frequency noise appears to level off around 80 dB for wind speeds greater than 7 m/s. The images for yaw offsets of -18° and 25° also indicate that frequencies below 100 Hz may be increased for low wind speeds.

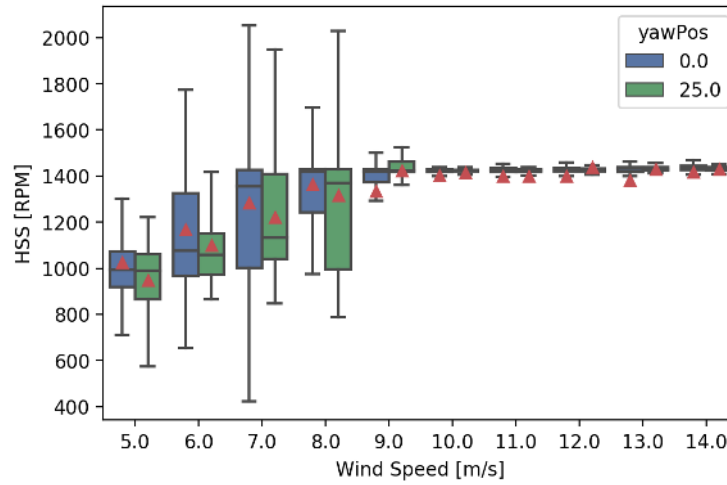


Figure 19. Distributions of high-speed shaft RPM of the DOE 1.5 operating at 0° yaw and 25° yaw, taken as a proxy for rotor speed. Red triangles indicated mean shaft rotational speeds.

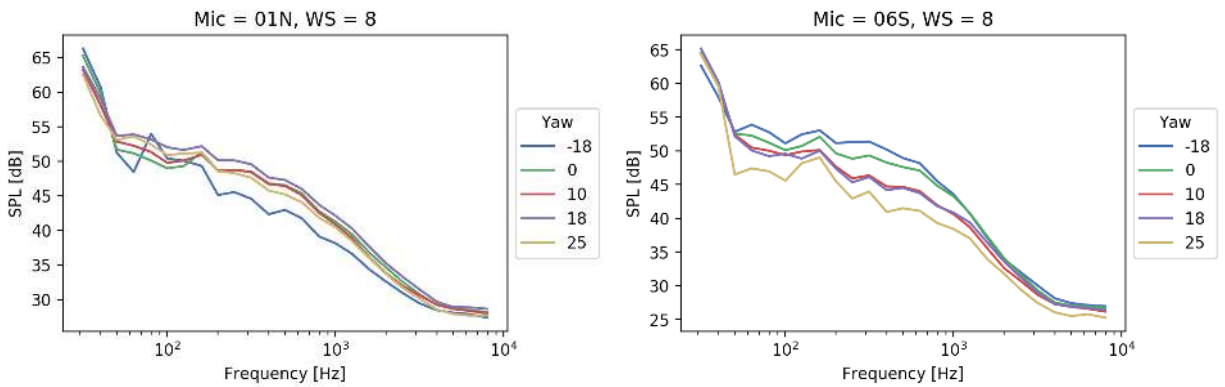


Figure 20. Changes in audible noise spectra with yaw for Mic 01N in the north (left) and Mic 06S in the south (right)

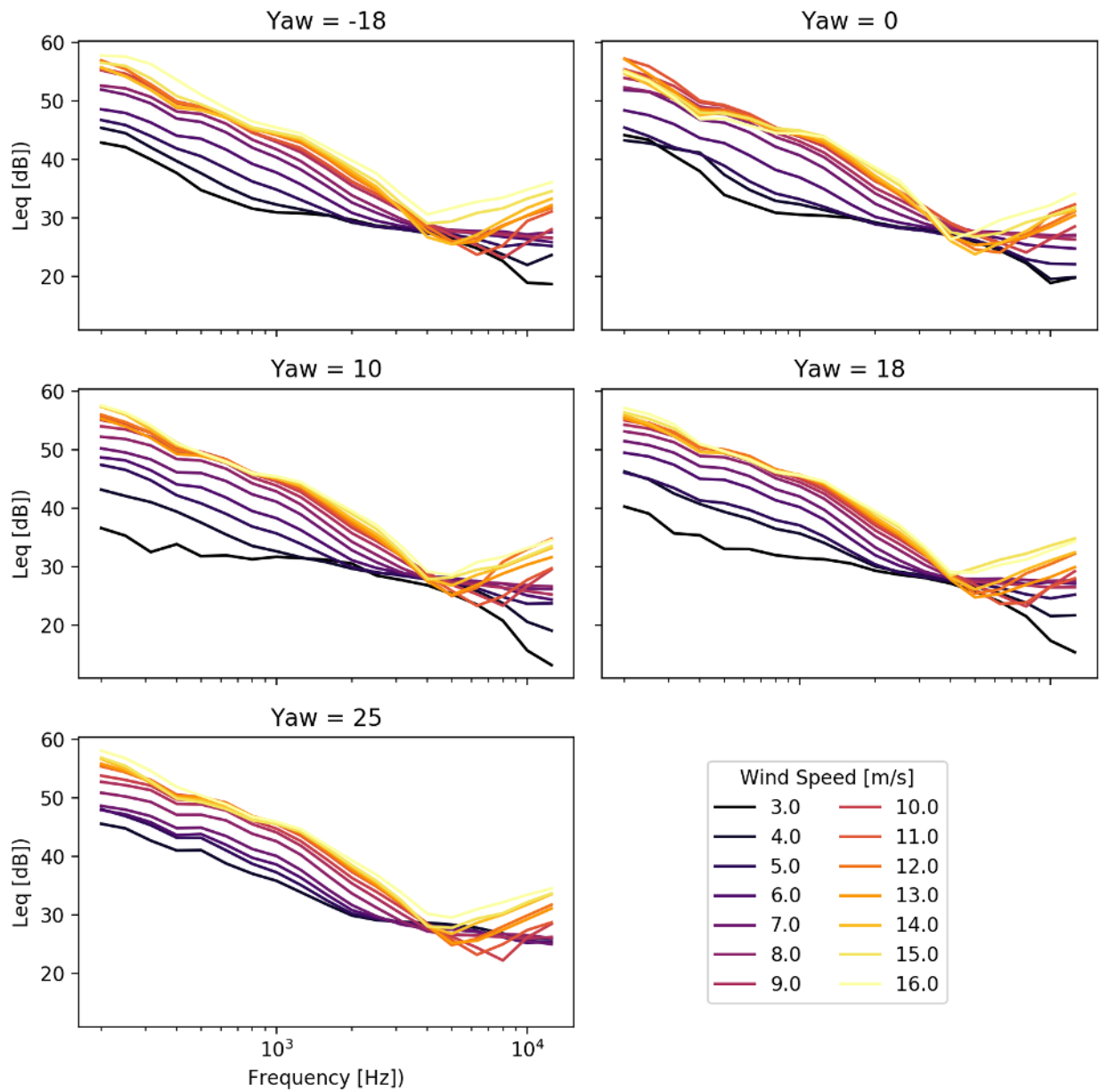


Figure 21. Wind turbine noise spectra at the IEC test location (Mic 04C) by wind speed and yaw offset

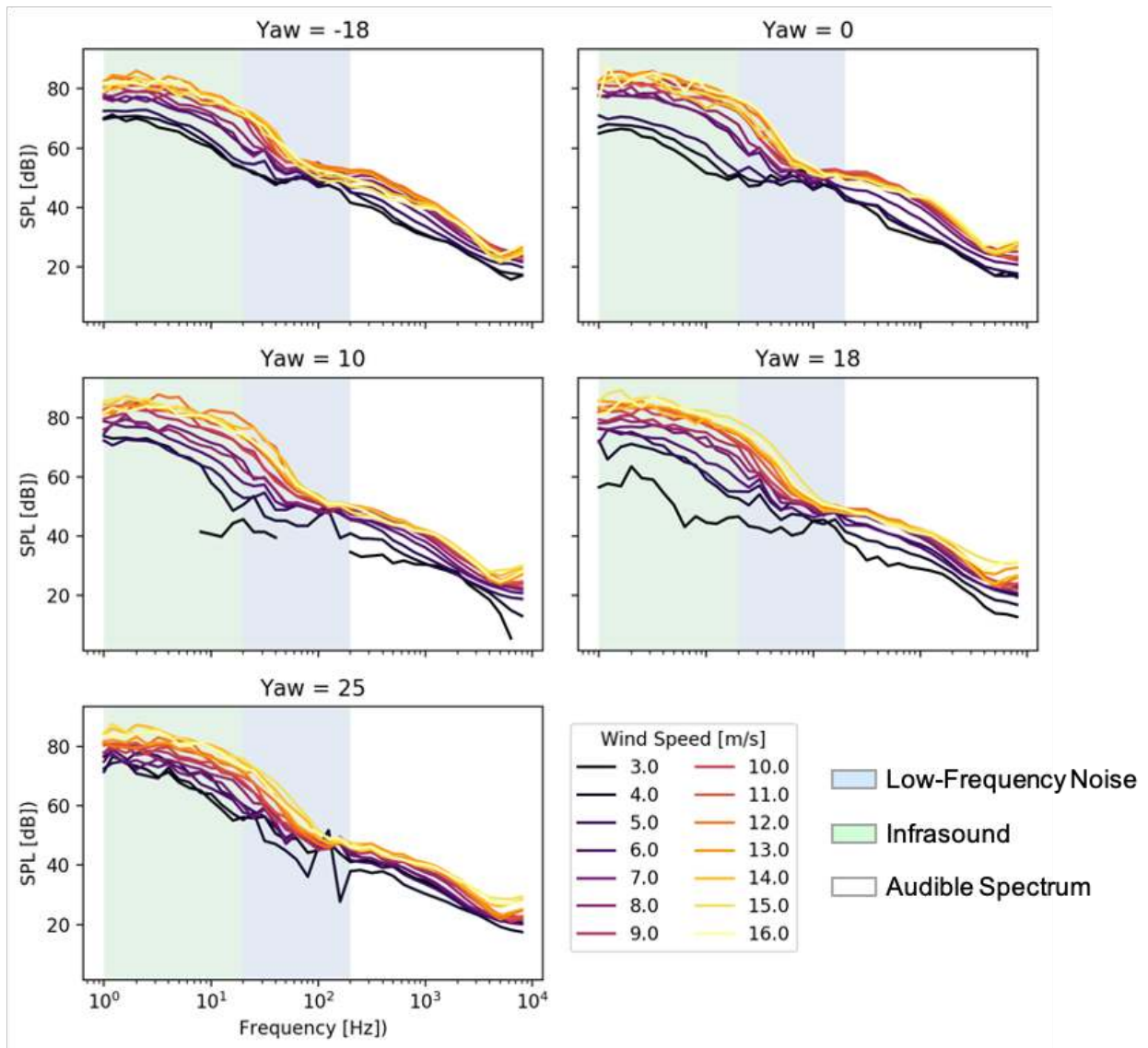


Figure 22. Wind turbine noise spectra from the low-frequency noise microphone at the South DAS node (Mic 13S) by wind speed and yaw offset. Green and blue bands indicate infrasound and low-frequency noise ranges of the spectra.

5.3 Model Validation

The comparison of equivalent SPL for each microphone location in Figure 23 highlights differences between model predictions (blue) and experimental results (red). For all microphone positions, the equivalent SPL for wind speeds above 9 m/s are more accurately matched than for the lower wind speeds. Microphones located in the north show the best agreement between experimental results and modeled SPL. Recalling that the microphone at the IEC test location (microphone 04C) consistently showed the highest noise levels of all test locations, it is not surprising that the model predictions are somewhat low for that measurement location.

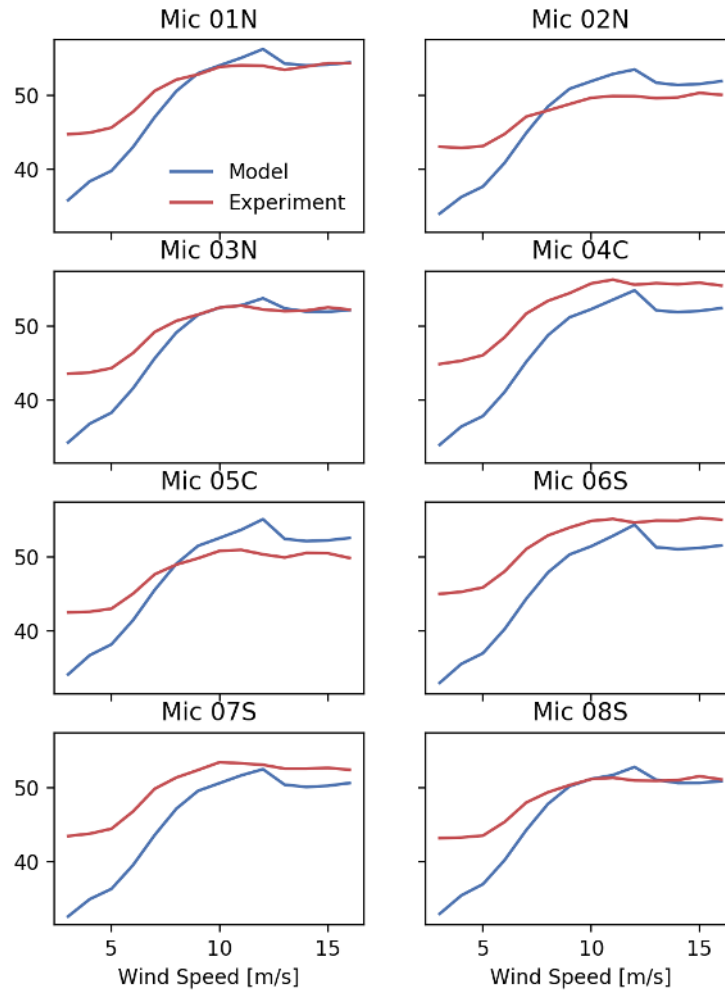


Figure 23. Comparison of measured and modeled equivalent SPL for SFR microphones

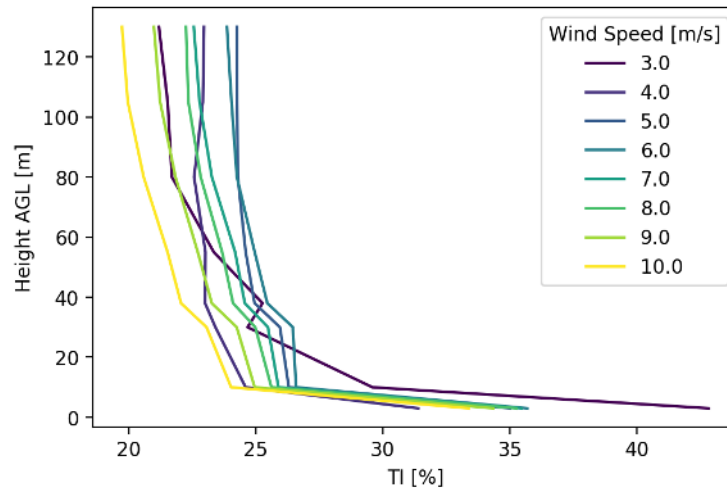


Figure 24. Profiles of turbulence intensity by wind speed during aeroacoustic measurement campaign

The results in Figure 23 show that the aeroacoustics models consistently underpredict noise at low wind speeds. The cause for this underprediction is not entirely clear. It may be that the models are not valid for utility-scale wind turbines at low speed. As an alternative, it may be that the particular conditions at the NREL FC are simply not well represented in the models. Discussed at length in Hamilton and Debnath (2019), the atmospheric conditions at the FC are fairly unconventional, exhibiting more extreme conditions, gusty winds, and high-turbulence conditions than would be normal for many wind plants. Figure 24 shows the average profiles of TI by wind speed recorded by the met mast. As expected, the TI increases close to the ground and levels off around 80 m. The TI is generally lower at greater wind speeds, but does not drop far below 20%. The relatively high level of turbulence arises from the unique geographic and atmospheric conditions at the FC. In all simulations, the turbulence intensity profiles shown in Figure 24 and the IEC specified turbulence length scale were used as inputs. As with the rest of the analysis contained in this report, observations were divided only by background wind speed and wind direction, not by atmospheric stability or time of day. Additional filtering of the atmospheric conditions will decrease the uncertainty in model input parameters, and lead to greater agreement between experiment and simulation results.

Microphones located within the gully behind the wind turbine are also not as accurately predicted by the OpenFAST model. For these microphones (Mics 05C, 06S, and 07S), the local terrain is not included in the model setup, nor is it explicitly accounted for in any of the noise models directly. In particular, Mic 05C is on the lee side of a hill and may have been protected from some of the wind turbine noise, evidenced by the lower values of SPL across the wind speed range. The opposite is true for Mics 06S and 07S, which are located on a slope facing toward the DOE 1.5, leading to slightly higher values of SPL.

Figure 25 compares noise spectra for the IEC test location, Mic 04C. Modeled wind turbine noise spectra shown in the figure is the sum of the two dominant noise generation mechanisms. The solid line combines the training edge noise and the leading edge noise contributions. For each of the modeled wind speeds, the trailing edge noise component peaks between 800 and 1,000 Hz. For wind speeds above 8 m/s, the model accurately predicts the peak in the spectra within the same frequency range.

The leading edge noise model is sensitive to both the ambient turbulence intensity and the turbulence integral length scale. The characteristic length scale of turbulent eddies incident on the leading edge of the rotor blades tends to be similar to the diameter of the leading edge, causing an interaction that leads to audible noise. The measured noise spectra shown in Figure 25 include all of the observed noise spectra within the specified wind speed bins, and are not filtered based on turbulence characteristics. Additional filtering of the observed noise spectra based on atmospheric conditions such as stability or incident turbulent intensity is expected to improve accuracy of the modeled wind turbine noise.

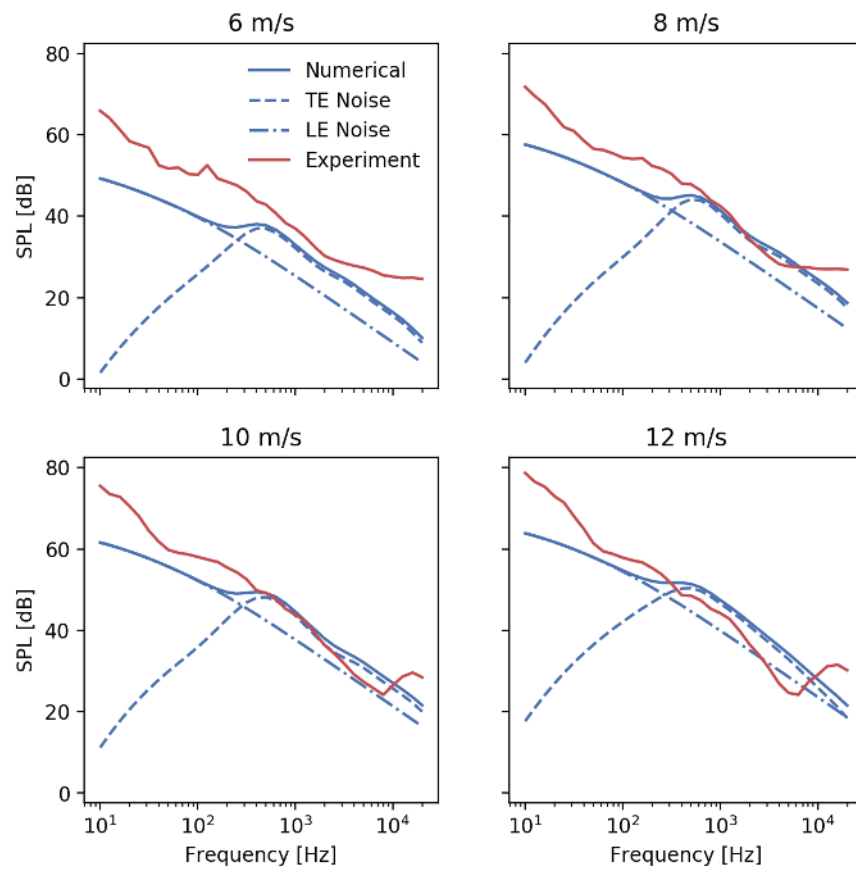


Figure 25. Measured vs. modeled wind turbine noise spectra at the IEC test location, Mic 04C

6 Conclusions

The Aeroacoustic Assessment of Wind Plant Controls Project included the development of new noise measurement capabilities at NREL that can be deployed in the support of a wide range of science goals for future wind turbine noise research. The distributed DAS can be reconfigured to flexibly deploy microphones around a utility-scale wind turbine in regions of interest supporting detailed examinations of any of the primary noise generation mechanisms summarized in Chapter 4. The measurement capability at NREL goes far beyond the requirements outlined in the IEC Standard on wind turbine noise characterization, and includes full-field observation locations and low-frequency microphones. Validation of the directivity model implemented in the OpenFAST framework required the multi-point full-field measurement capability developed at NREL. In addition, experimental results suggest that the reduction in noise when operating under yaw would not have been detected with a single point observation.

The experimental evidence gathered in this project indicate that imposing yaw offsets for wind plant control may systematically decrease the emitted aeroacoustic noise. However, the benefits to aeroacoustic noise may not be uniformly distributed over the range of expected yaw offsets. This experiment indicates that positive yaw offsets are more likely to contribute to a decrease in the overall SPL from a utility-scale wind turbine. Negative yaw offsets have a smaller effect on observed noise behind the DOE 1.5.

Changes in the aeroacoustic noise arise from a change in the three-dimensional aerodynamic interaction between the rotor blades and the incoming atmospheric flow. When yawing a wind turbine with respect to the bulk flow direction, the projection of the wind speed perpendicular to the rotor decreases with the cosine of the yaw angle. With the reduced effective wind speed, the control point of the wind turbine leads to a decrease in rotor speed, and therefore a reduction in noise generation. This observation likely implies that an optimal set point for operation of a wind turbine under yaw may include increasing the tip speed of the rotor. A new operating point would capitalize on the reduction in noise generation to operate the turbine more efficiently.

Preliminary validation of the noise models implemented in the OpenFAST framework suggest that the dominant contributions of the leading edge and trailing edge generation mechanisms accurately represent the audible peaks and trends of wind turbine noise with wind speed. The directivity model that accounts for changes in observed noise of an observer with respect to the position of the rotor blades also accurately accounts for changes in noise emission due to yaw. Discrepancies seen in the overall sound pressure for aggressive yaw settings greater than 20° likely arise from a mischaracterization of the blade aerodynamics rather than a deficiency in the directivity model.

Data can be found at: <https://a2e.energy.gov/projects/aawpc>. Please cite this report if using the data for any research publications or reporting.

6.1 Aeroacoustics Multi-Year Research Objectives

The “Wind Energy Technologies Office Multi-Year Program Plan Fiscal Years 2021–2025” (2020) specifically cites aeroacoustic challenges among the issues facing the rapid development of onshore wind energy. The United States is in a period of rapid development of wind plants, which necessarily leads to development closer to human settlements where noise can be an issue. Because in some cases wind plants are already noise regulated, any additional understanding of wind turbine noise generation and propagation can only support optimal deployment and operation. The results of this study indicate that operating wind turbines with modern wind plant control strategies will not lead to significant increases in wind turbine noise emissions. To ensure that these results apply broadly, the experimental methods developed in this work should be leveraged in larger-scale projects in other operating environments.

The measurement capability that NREL has developed for aeroacoustics research dovetails with ongoing in planned research in wind energy. Looking forward, the laboratory has developed experimental plans across a wide range of scales, including aeroelastic rotor and blade, wake aerodynamics, and wind plant-scale experiments. Modern offshore wind turbines have extremely large rotors, with flexible blades operating in environments for which acoustic propagation is expected to be a major issue. Some offshore wind turbine designs are beginning to consider downwind configurations. In the past, downwind turbines were associated with unacceptable low-frequency noise generation. For future wind turbine designs to move forward and be broadly accepted, the aeroacoustic emissions from these turbines must be quantified. The specific aeroacoustics research domains outlined here are all relevant to the

rapid development of new onshore and offshore wind plants, and offer an ideal platform for collaborating with other U.S. and international research groups, and with the group supporting IEA Wind Task 39: Quiet Wind.

6.1.1 Airfoil Level Research

Aeroacoustic noise generated by wind turbines arises from the aerodynamic interaction between rotor blades and incoming atmospheric flow. To date, most noise-reduction methodologies for utility-scale wind turbines amount to modifications of the trailing edge of rotor blades (Oerlemans et al. 2009; Fischer et al. 2014; Avallone et al. 2018). Blades serrations have been shown experimentally to reduce noise emissions by as much as 3 dB over specific frequencies. Ongoing research into leading edge modifications (Wang, Liu, and Li 2021; Chong et al. 2018) also shows promising results in terms of disrupting the coherent turbulent structures whose interactions give rise to audible noise. NREL has extensive experience in airfoil research and design and has established relationships with academic research groups focused on aeroacoustics. Any advancement in wind turbine blade design that reduces noise emissions could benefit wind turbines that may be subject to noise-related curtailment, or to operate wind turbines more efficiently at the same level of noise emissions.

NREL's advanced high-performance computing research capabilities should be leveraged to investigate the generation and propagation of noise from wind turbine blades. High-fidelity modeling provides access to acoustic fields at a resolution that is out of reach of practical experimental methods. Coupling advanced wind turbine fluid simulations and computational aeroacoustics will lead to new parameterized model development and validation. Model development should be focused on noise propagation, taking into account ambient atmospheric conditions and topography for onshore settings.

6.1.2 Wind-Plant-Level Research

Aeroacoustics research should consider the noise generated by wind plants in addition to fundamental mechanistic noise generation. In wind plant settings, the collective noise generated by individual turbines may sum to make a greater overall impact through constructive wave interference or syncing between multiple sources. These physics are not well understood or predicted for wind plants, but offer an opportunity for wind plant control that could avoid noise-based curtailment. Consideration of wind plant noise will continue to impact the design, operation, and placement of terrestrial and offshore wind plants for the foreseeable future. Wind plant noise studies will need to consider the generation and propagation of low-frequency noise (20–200 Hz) and infrasound (<20 Hz) as well as the transmission of vibrations through the ground. In offshore settings, specific attention must be paid to the sea state and wind/wave interactions.

The implementation of the aeroacoustic models in OpenFAST does not currently include a propagation model. Noise traveling through the atmosphere is attenuated unevenly at different frequencies and is sensitive to humidity, temperature, and background turbulence. In addition, sound waves are reflected and refracted by obstructions including terrain features, vegetation, and other obstructions. Recent work (Sun et al. 2019; Cao et al. 2018) has shown that noise propagation through the atmosphere in offshore environments must take into account reflections of the sea surface and noise refraction due to the operation of wind turbines.

Recent research focused on multi-criteria wind farm design (Cao et al. 2020) has shown that noise emissions can have a significant impact on wind plant layout. Considering results from this work and from other research in the literature suggests that multi-objective optimization and control strategies including wind plant controls and noise emissions may lead to improved wind plant performance.

Development of offshore wind plants in the United States requires a new level of environmental impact research. Offshore wind turbines are larger, and operate at higher tip speeds, both contributing to greater aeroacoustic emissions. Coupled with the advanced propagation in offshore environment, noise impacts from offshore wind plants may be greater than previously estimated. To ensure the rapid deployment and success of U.S. offshore wind, aeroacoustic noise in offshore environments and potential environmental impacts must be thoroughly assessed.

Aeroacoustics research should expand to consider additional sources of noise in the primary aeroacoustic noise generation mechanisms. Vibrations are major contributors to overall wind turbine noise and may become more dominant noise sources overall given advancement and quiet operation of modern wind turbine airfoils. In offshore settings,

mechanical and acoustic noise generated within the sea environment is of particular importance and will require research attention as the U.S. develops more offshore wind plants. Environmental impact assessments for offshore wind plants may begin to consider the generation of noise under the sea surface. Subsurface noise propagation through holds a potential impact to sea life, communications, navigation, and other marine technology.

6.1.3 Human Response

The physics of amplitude modulation, impulsivity, infrasound, and tonality are not well understood, especially as they impact human wellness or annoyance factors. Social acceptance of wind turbines and wind plant development depends to some extent on the noise produced by wind turbines. However, sensitivity to wind turbine noise may also be driven partly by other social acceptance factors, such as visual impacts or local land-use policy, with lower acceptance driving greater sensitivity to such noise (Enevoldsen and Sovacool 2016; Hansen and Hansen 2020). The complex interactions of human perception require detailed research to investigate. This research domain offers NREL/DOE the opportunity to partner with other agencies and international partners to define the relevant metrics for quantifying human responses to wind turbine noise.

Bibliography

- Amiet, R. K. 1975. “Acoustic Radiation from an Airfoil in a Turbulent Stream”. *Journal of Sound and Vibration* 41 (4): 407–420. doi:[10.1016/S0022-460X\(75\)80105-2](https://doi.org/10.1016/S0022-460X(75)80105-2).
- Annoni, J., P. Fleming, A. K. Scholbrock, J. M. Roadman, S. Dana, C. Adcock, F. Porte-Agel, S. Raach, F. Haizmann, and D. Schlipf. 2018. “Analysis of control-oriented wake modeling tools using lidar field results”. *Wind Energy Science (Online)* 3 (NREL/JA-5000-72767).
- Avallone, F, W. Van Der Velden, D Ragni, and D Casalino. 2018. “Noise reduction mechanisms of sawtooth and combed-sawtooth trailing-edge serrations”. *Journal of Fluid Mechanics* 848:560–591.
- Bortolotti, P., E. Branlard, A. Platt, P. Moriarty, C. L. Bottasso, and C. Sucameli. 2020. *Aeroacoustics Noise Model of OpenFAST*. Tech. rep. National Renewable Energy Lab.(NREL), Golden, CO (United States).
- Brentner, K. S., G. A. Bres, G. Perez, and H. E. Jones. 2002. “Maneuvering rotorcraft noise prediction: A new code for a new problem”.
- Brooks, T. F., S. D. Pope, and M. A. Marcolini. 1989. *Airfoil Self-Noise and Prediction*. Tech. rep. NASA Reference Publication 1218.
- Cao, J. F., W. J. Zhu, W. Z. Shen, J. N. Sørensen, and Z. Y. Sun. 2020. “Optimizing wind energy conversion efficiency with respect to noise: A study on multi-criteria wind farm layout design”. *Renewable Energy* 159:468–485.
- Cao, J., W. Zhu, X. Wu, T. Wang, H. Xu, et al. 2018. “An aero-acoustic noise distribution prediction methodology for offshore wind farms”. *Energies* 12 (1): 1–16.
- Chong, T. P., T. Biedermann, O. Koster, and S. M. Hasheminejad. 2018. “On the effect of leading edge serrations on aerofoil noise production”. In *2018 AIAA/CEAS Aeroacoustics Conference*, 3289.
- Damiani, R. R., S. Dana, J. Annoni, P. A. Fleming, J. M. Roadman, J. J. van Dam, and K. L. Dykes. 2018. “Assessment of wind turbine component loads under yaw-offset conditions”. *Wind Energy Science Discussions* 3 (NREL/JA-5000-68866).
- DELTA Acoustics and Vibration. 2014. “noiseLAB User’s Guide for Version 4.0”. <https://noiselabdk.files.wordpress.com/2011/10/noiselab-4-0-users-guide.pdf>.
- DK-BEK135. Visited on 09/20/2020. <https://www.retsinformation.dk/eli/ta/2019/135>.
- Drela, M., and M. B. Giles. 1987. “Viscous-inviscid analysis of transonic and low Reynolds number airfoils”. *AIAA* 25 (10). doi:[10.2514/3.9789](https://doi.org/10.2514/3.9789).
- Economou, P., and R. J. Peppin. 2012. “A comparison of iso 9613-2 and advanced calculation methods: Predictions versus experimental results”. *Canadian Acoustics* 40 (3): 54–55.
- Enevoldsen, P., and B. K. Sovacool. 2016. “Examining the social acceptance of wind energy: Practical guidelines for onshore wind project development in France”. *Renewable and Sustainable Energy Reviews* 53:178–184. ISSN: 1364-0321. doi:<https://doi.org/10.1016/j.rser.2015.08.041>. <https://www.sciencedirect.com/science/article/pii/S1364032115009028>.
- Farassat, F. 2007. “Derivation of Formulations 1 and 1A of Farassat”.
- Fischer, A., F. Bertagnolio, W. Z. Shen, J. Madsen, H. A. Madsen, C. Bak, W. Devenport, and N. Intarapet. 2014. “Wind tunnel test of trailing edge serrations for the reduction of wind turbine noise”. In *INTER-NOISE and NOISE-CON Congress and Conference Proceedings*, 249:4620–4629. 3. Institute of Noise Control Engineering.
- Fleming, P., J. King, K. Dykes, E. Simley, J. Roadman, A. Scholbrock, P. Murphy, J. K. Lundquist, P. Moriarty, K. Fleming, et al. 2019. “Initial results from a field campaign of wake steering applied at a commercial wind farm—Part 1”. *Wind Energy Science (Online)* 4 (NREL/JA-5000-73991).
- Hamilton, N., and M. C. Debnath. 2019. *National Wind Technology Center-Characterization of Atmospheric Conditions*. Tech. rep. National Renewable Energy Lab.(NREL), Golden, CO (United States).
- Hansen, C., and K. Hansen. 2020. “Recent advances in wind turbine noise research”. In *Acoustics*, 2:172–207. 1. Multidisciplinary Digital Publishing Institute.
- IEC. 2005. “International Electrotechnical Commission (IEC) standard, Wind turbines part 12-1: Power performance measurements of electricity producing wind turbines”. IEC 61400-12-1, Edition 1.
- IEC, C. 2020. “International Electrotechnical Commission (IEC) standard, Wind turbines part 11: Acoustic Noise Measurement Techniques”. IEC 61400-11, Edition 3.1.

- Institute of Acoustics IOA Noise Working Group (Wind Turbine Noise). 2016. “Amplitude Modulation Working Group Final Report: A Method for Rating Amplitude Modulation in Wind Turbine Noise”.
- ISO 9613-2, A. 1996. “Attenuation of Sound During Propagation Outdoors—Part 2: A General Method of Calculation (ISO 9613-2)”. *ISO, Geneva, Switzerland*.
- Jonasson, H. G., and S. Storeheier. 2001. *Nord 2000. New Nordic prediction method for road traffic noise*.
- Klein, L., J. Gude, F. Wenz, T. Lutz, and E. Krämer. 2018. “Advanced computational fluid dynamics (CFD)—multi-body simulation (MBS) coupling to assess low-frequency emissions from wind turbines”. Publisher: Copernicus GmbH, *Wind Energy Science* 3 (2): 713–728.
- Moriarty, P. J., G. Guidati, and P. Migliore. 2005. “Prediction of Turbulent Inflow and Trailing-Edge Noise for Wind Turbines”. *11th AIAA/CEAS Aeroacoustics Conference*. doi:10.2514/6.2005-2881.
- Nordtest. 2002. “Nordtest Method, Acoustics: Prominence of Impulsive Sounds and for Adjustment of L_{Aeq} ”. (Espoo, Finland) NT ACOU 112, Approved 2002-05.
- Oerlemans, S., M. Fisher, T. Maeder, and K. Kögler. 2009. “Reduction of wind turbine noise using optimized airfoils and trailing-edge serrations”. *AIAA journal* 47 (6): 1470–1481.
- Parchen, R. R. 1998. *Progress Report DRAW: A Prediction Scheme for Trailing Edge Noise Based on Detailed Boundary Layer Characteristics*. Tech. rep. TNO Institute of Applied Physics.
- Roadman, J., and A. Huskey. 2015. *Acoustic noise test report for the U.S. Department of Energy 1.5-Megawatt Wind Turbine*. Tech. rep. NREL/TP-5000-63681. Golden, CO: National Renewable Energy Laboratory.
- Shah, S., P. Koralewicz, R. Wallen, and V. Gevorgian. 2019. “Impedance characterization of utility-scale renewable energy and storage systems”. In *2019 IEEE Energy Conversion Congress and Exposition (ECCE)*, 2609–2616. IEEE.
- Shen, W. Z., M. Sessarego, J. Cao, C. M. Nyborg, K. S. Hansen, F. Bertagnolio, H. A. Madsen, P. Hansen, A. Vignaroli, and T. Sørensen. 2020. “Validation of noise propagation models against detailed flow and acoustic measurements”. In *Journal of Physics: Conference Series*, 1618:052023. Issue: 5. IOP Publishing.
- Sucameli, C. R., P. Bortolotti, A. Croce, C. Bottasso, and others. 2018. “Comparison of some wind turbine noise emission models coupled to BEM aerodynamics”. In *Journal of Physics: Conference Series*, vol. 1037. Issue: 2.
- Sun, Z., W. J. Zhu, W. Z. Shen, E. Barlas, J. N. Sørensen, J. Cao, and H. Yang. 2019. “Development of an efficient numerical method for wind turbine flow, sound generation, and propagation under multi-wake conditions”. *Applied Sciences* 9 (1): 100.
- The Pandas Development Team. 2020. *pandas-dev/pandas: Pandas*. Version latest. doi:10.5281/zenodo.3509134. <https://doi.org/10.5281/zenodo.3509134>.
- Wang, L., X. Liu, and D. Li. 2021. “Noise reduction mechanism of airfoils with leading-edge serrations and surface ridges inspired by owl wings”. *Physics of Fluids* 33 (1): 015123.
- Williams, J. F., and D. L. Hawkings. 1969. “Sound generation by turbulence and surfaces in arbitrary motion”. Publisher: JSTOR, *Philosophical Transactions for the Royal Society of London. Series A, Mathematical and Physical Sciences*: 321–342.
- “Wind Energy Technologies Office Multi-Year Program Plan Fiscal Years 2021–2025”. 2020 (). <https://www.osti.gov/biblio/1760301>.
- Zhu, W. J., W. Z. Shen, E. Barlas, F. Bertagnolio, and J. N. Sørensen. 2018. “Wind turbine noise generation and propagation modeling at DTU Wind Energy: A review”. Publisher: Elsevier, *Renewable and Sustainable Energy Reviews* 88:133–150.

Appendix A Wind Turbine Noise Spectra

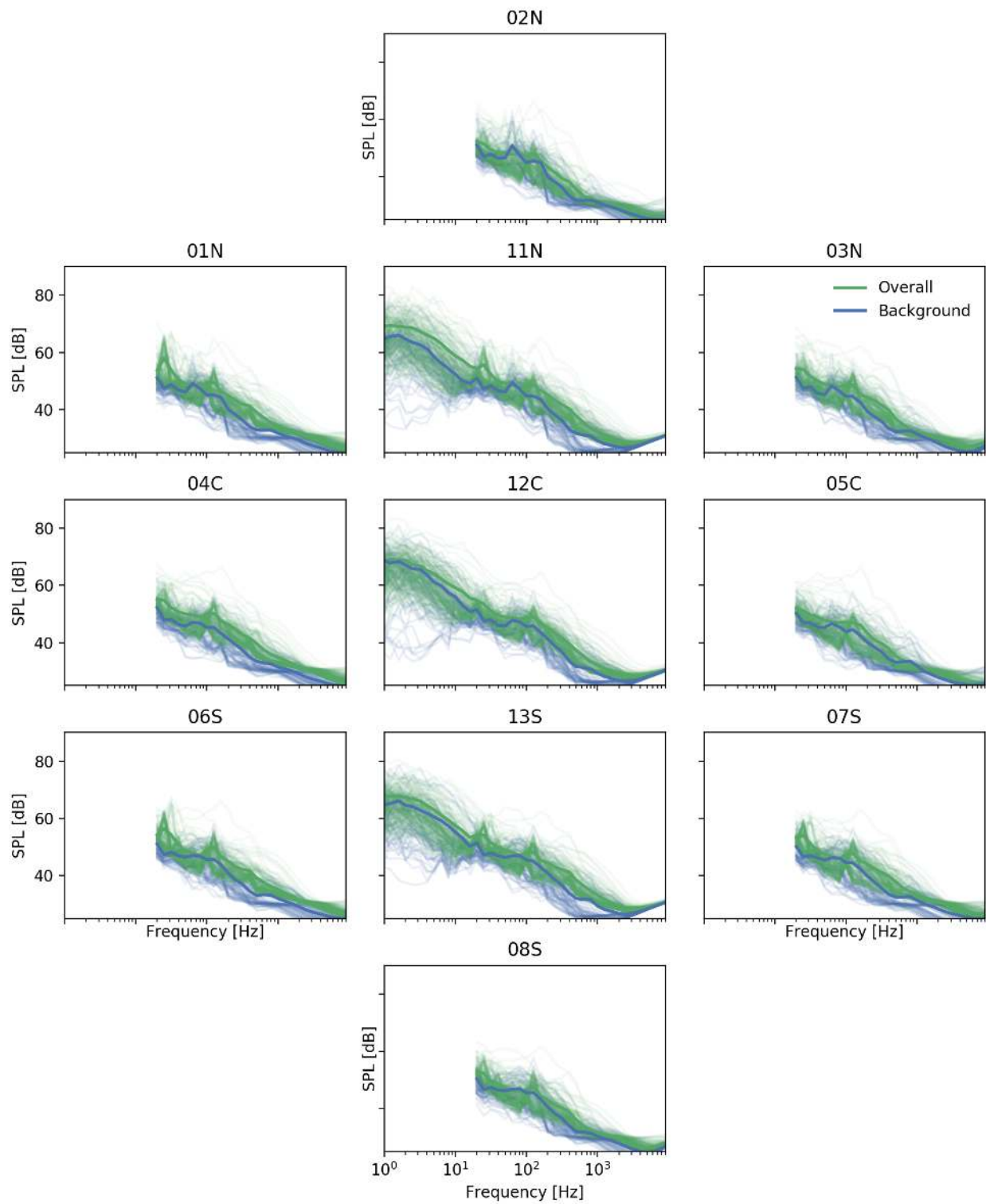


Figure 26. Overall and background spectra at 5 m/s for all microphones.

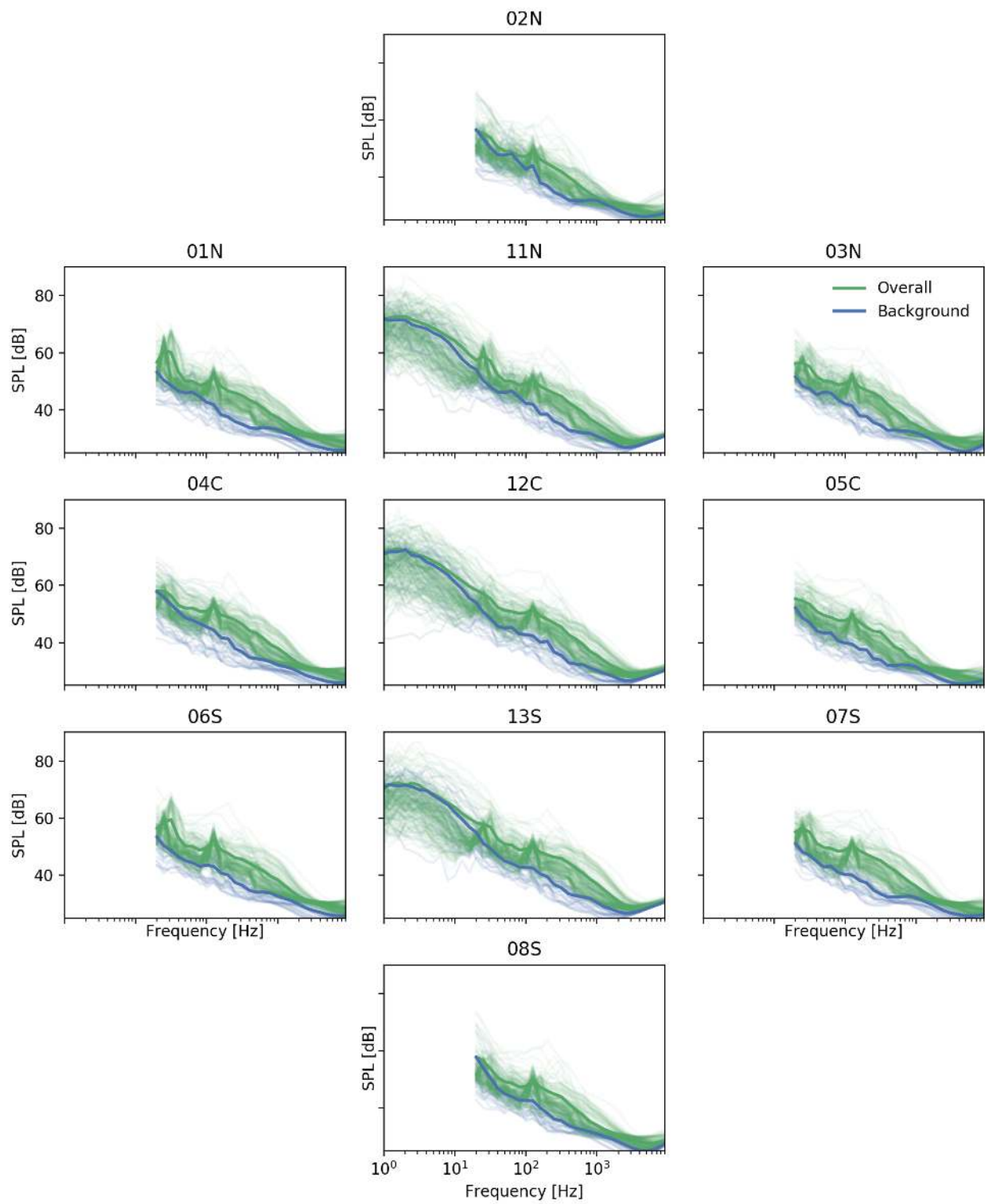


Figure 27. Overall and background spectra at 6 m/s for all microphones.

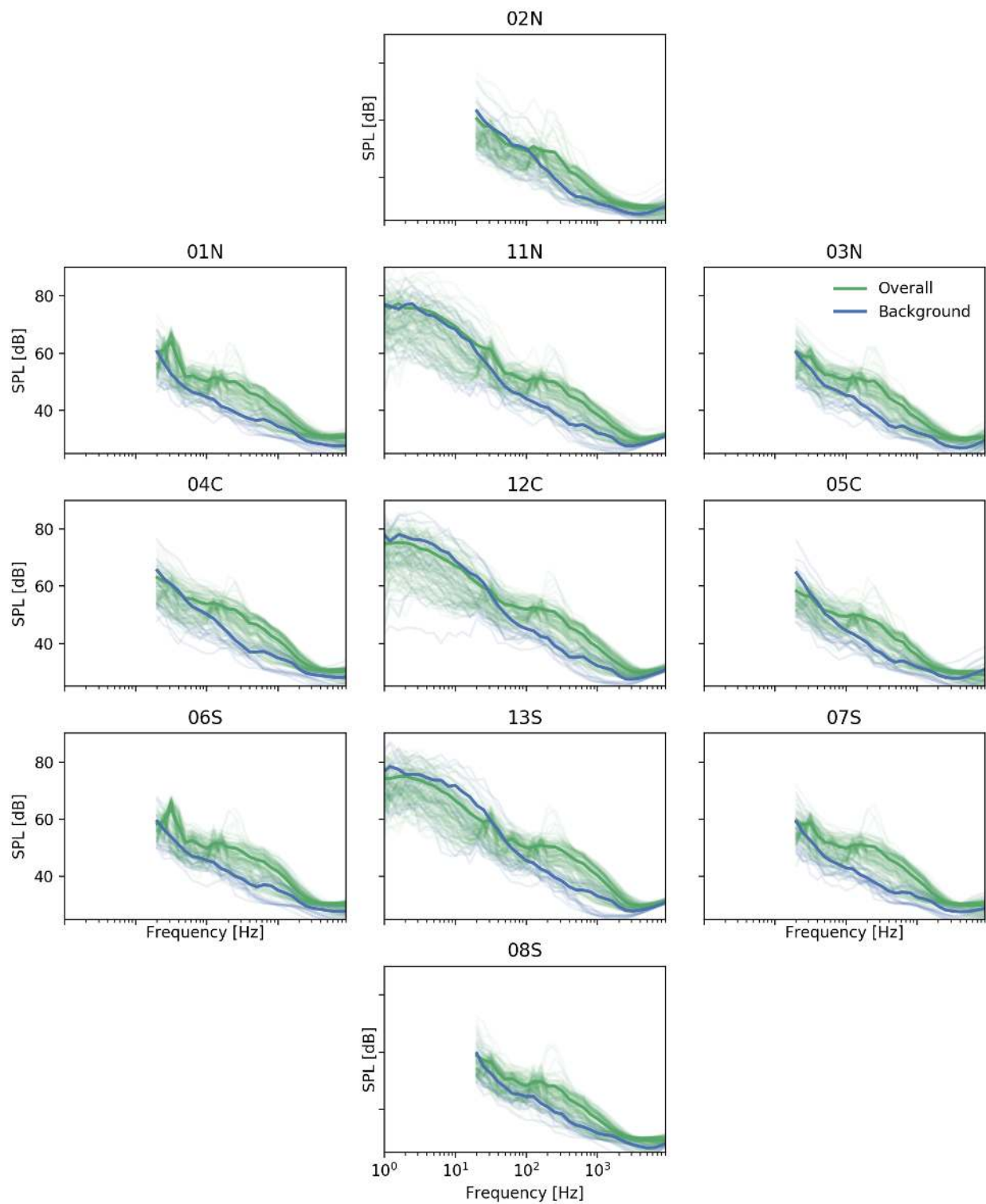


Figure 28. Overall and background spectra at 7 m/s for all microphones.

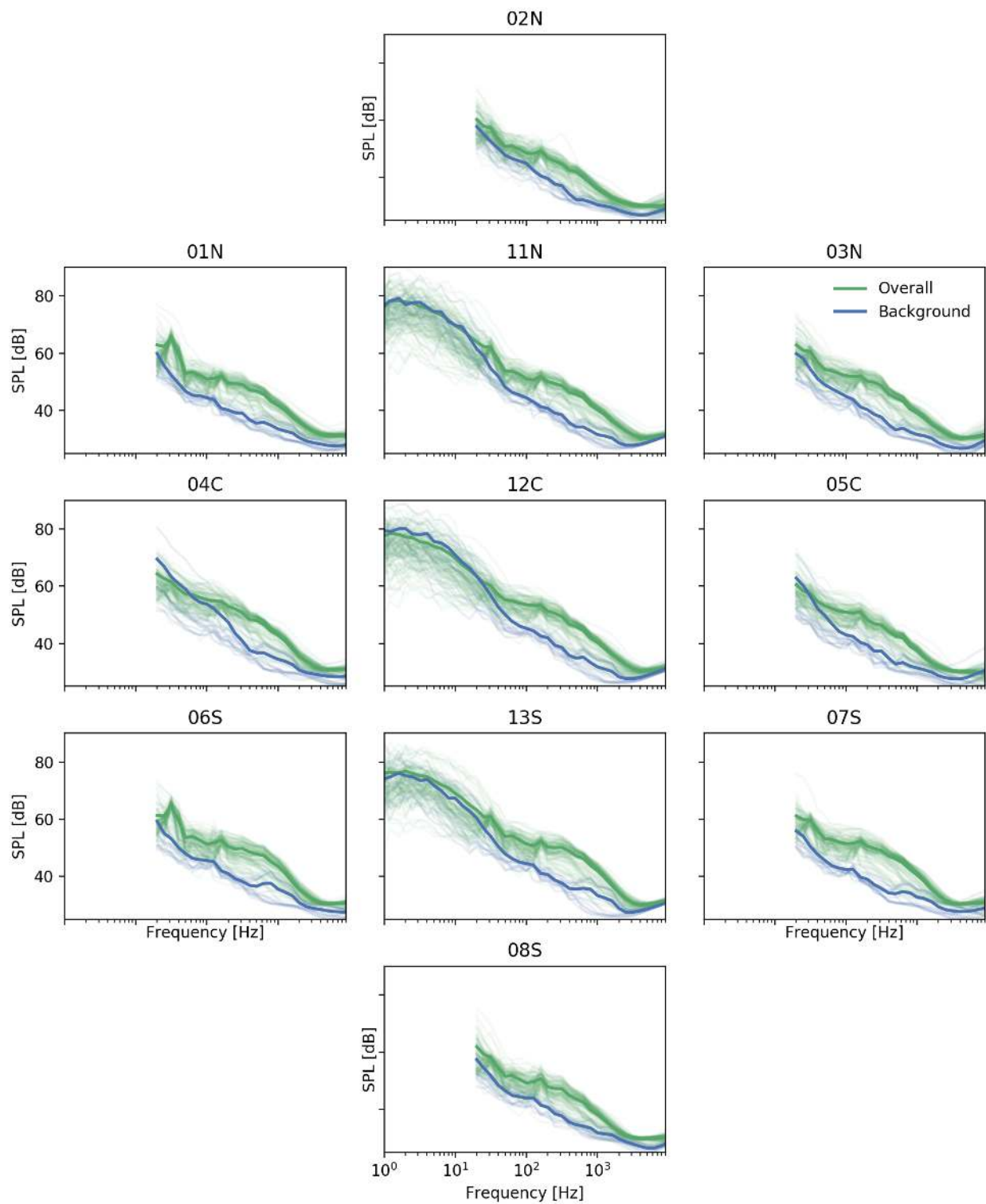


Figure 29. Overall and background spectra at 8 m/s for all microphones.

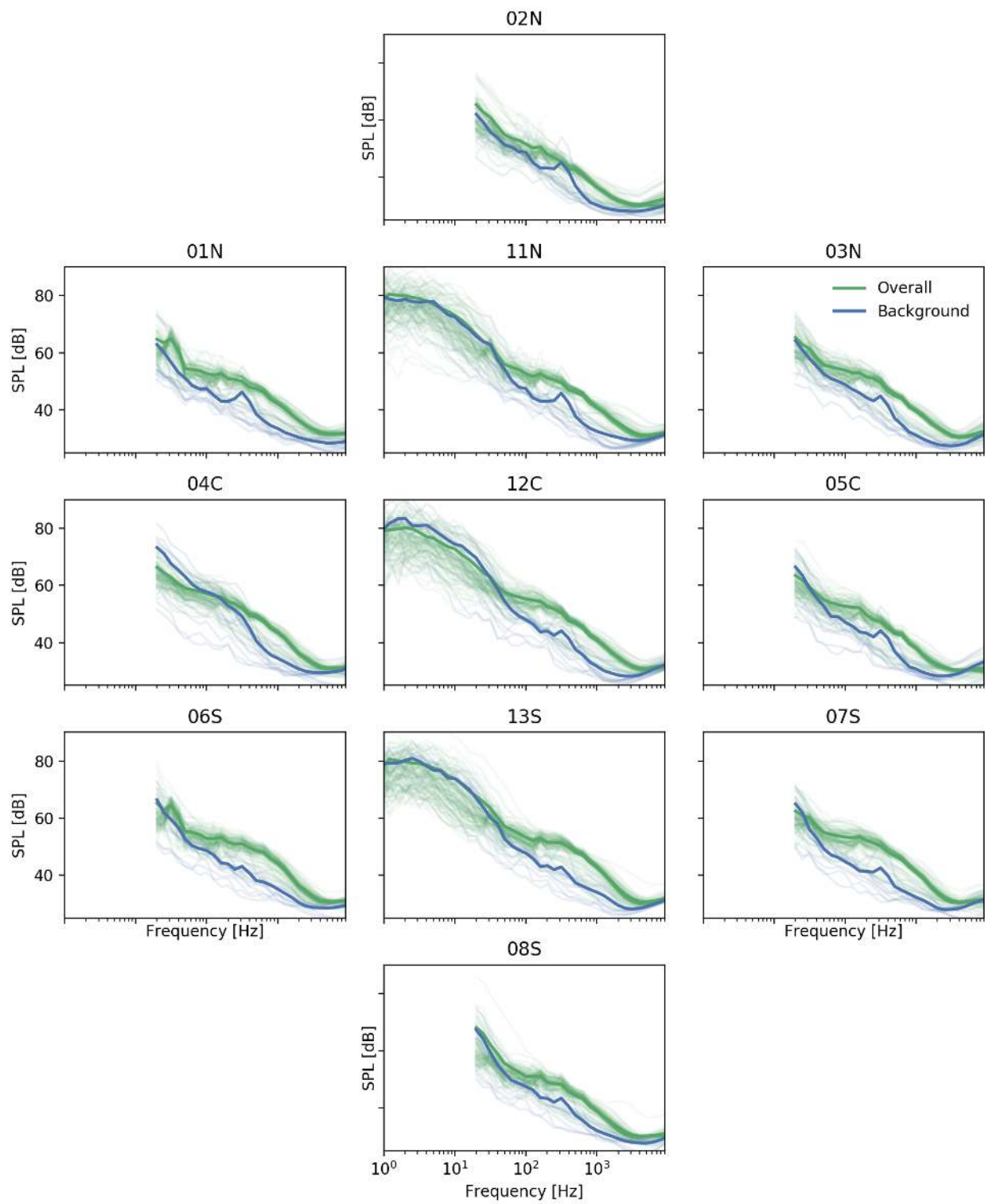


Figure 30. Overall and background spectra at 9 m/s for all microphones.

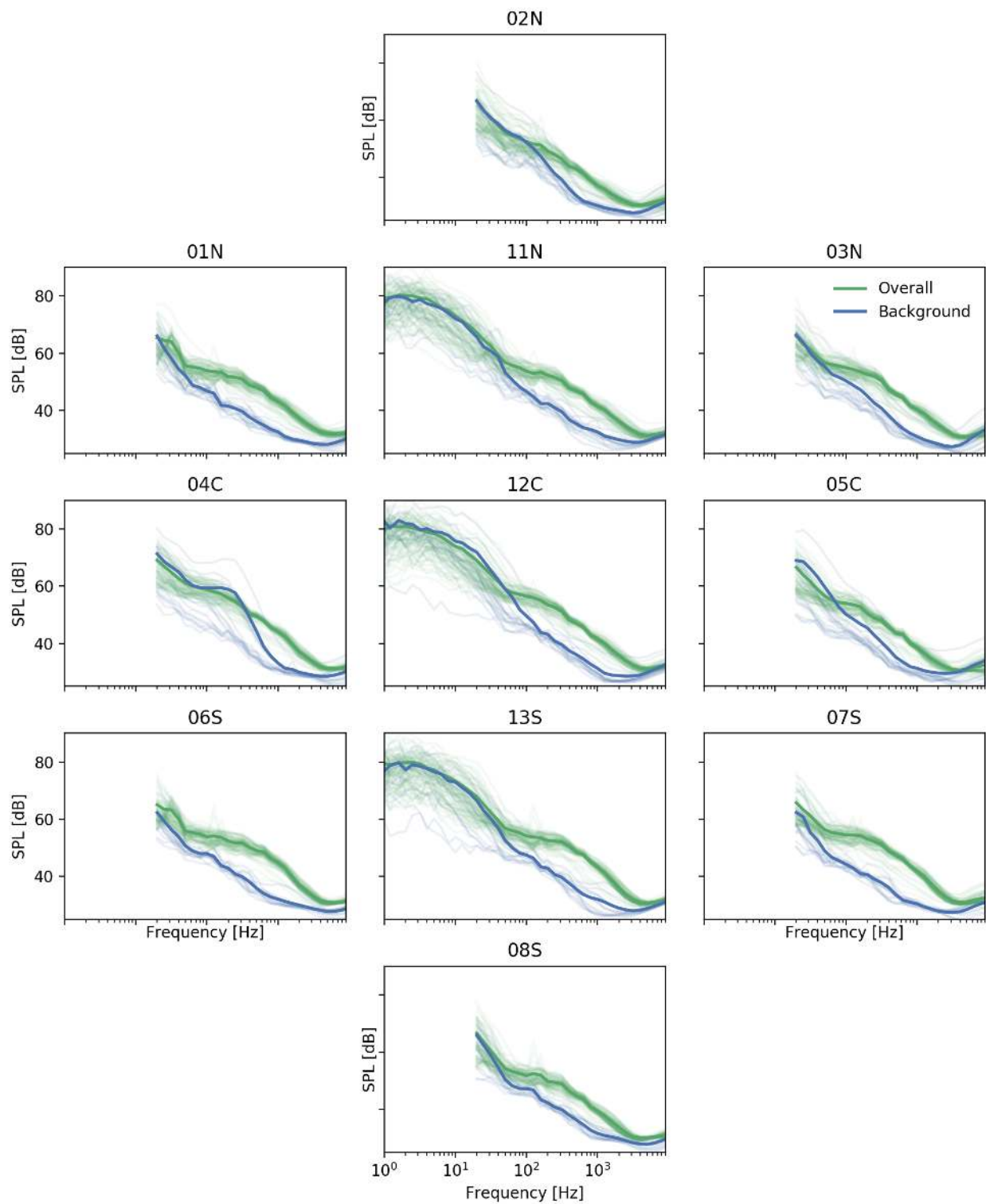


Figure 31. Overall and background spectra at 10 m/s for all microphones.

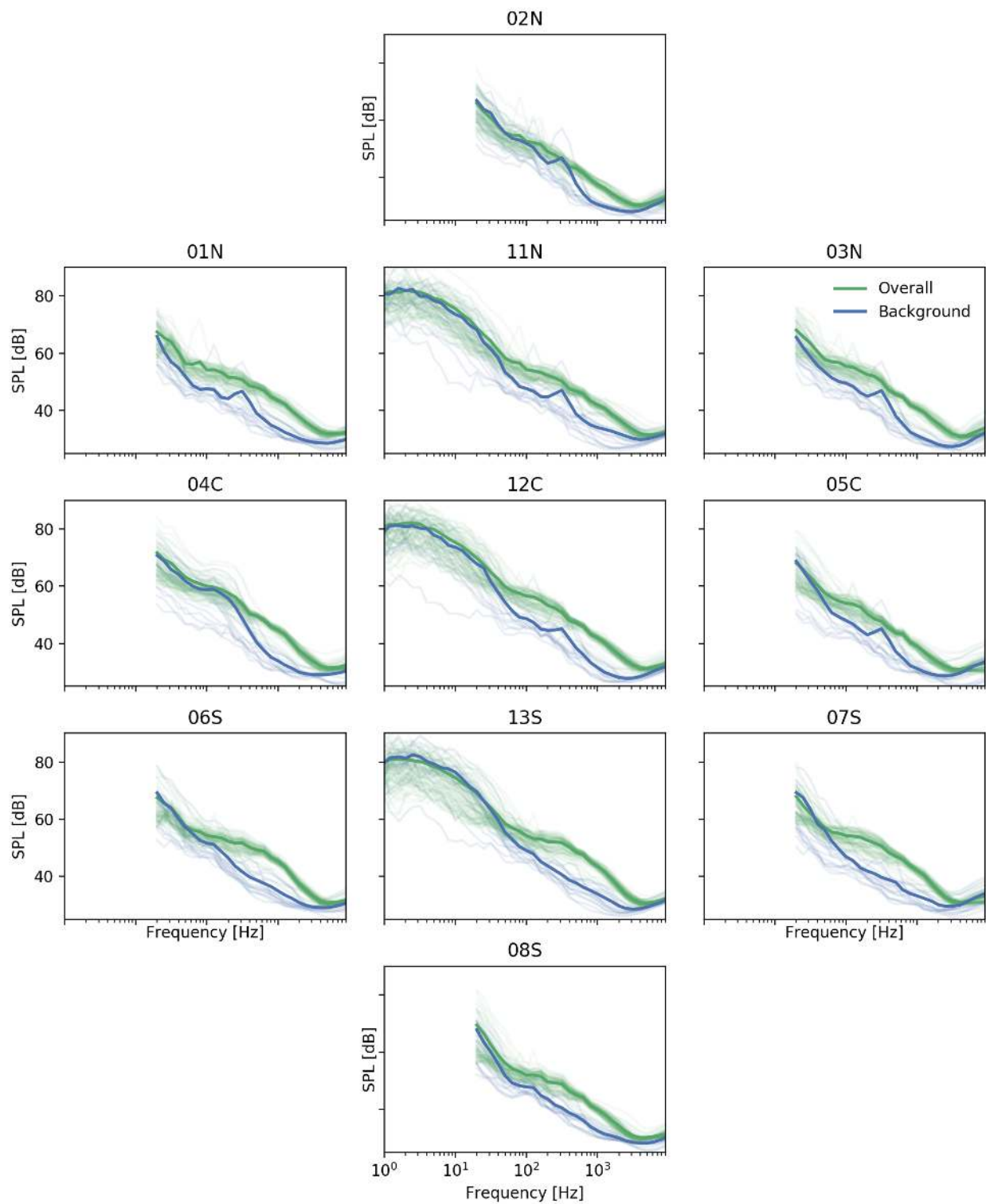


Figure 32. Overall and background spectra at 11 m/s for all microphones.

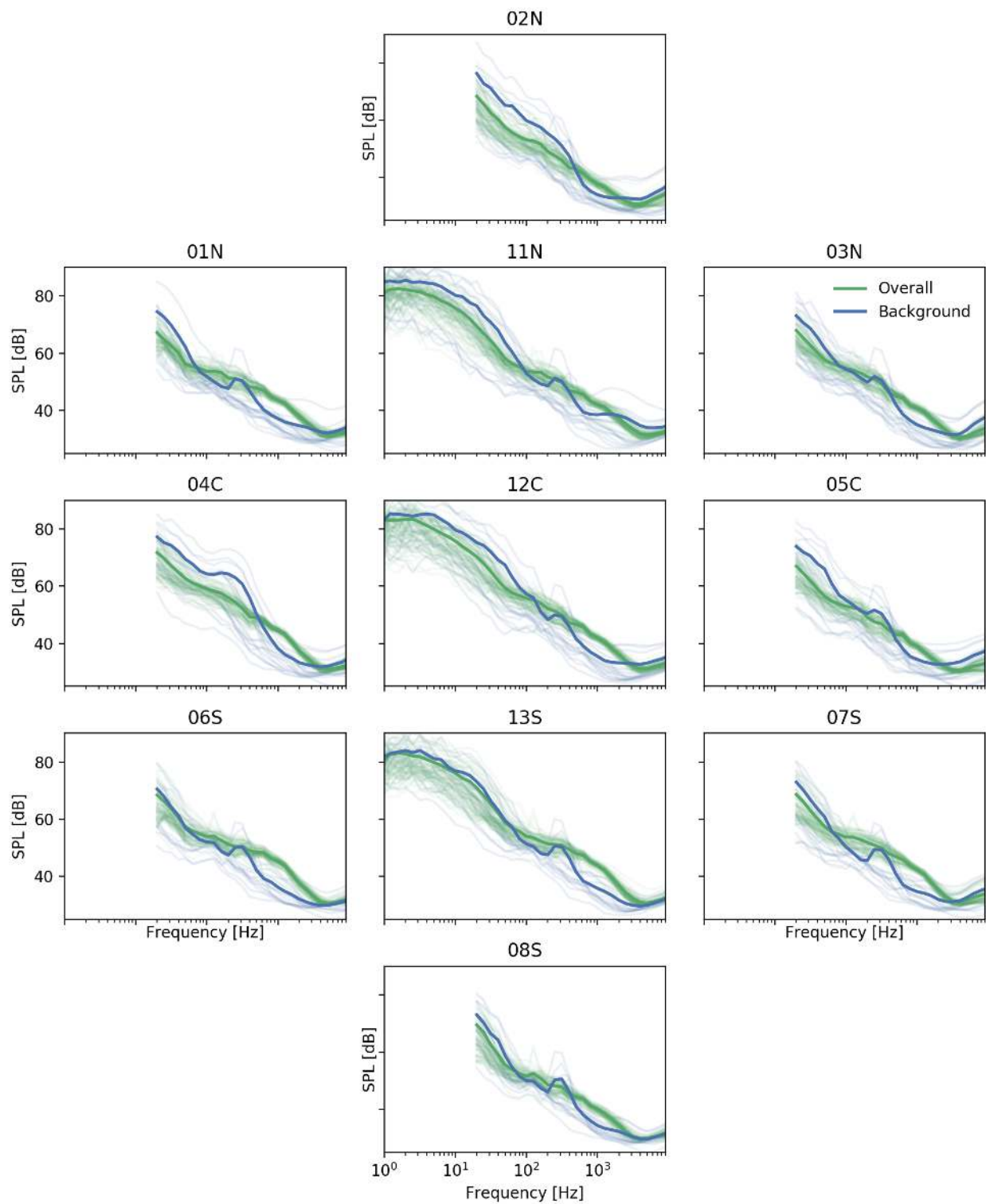


Figure 33. Overall and background spectra at 12 m/s for all microphones.

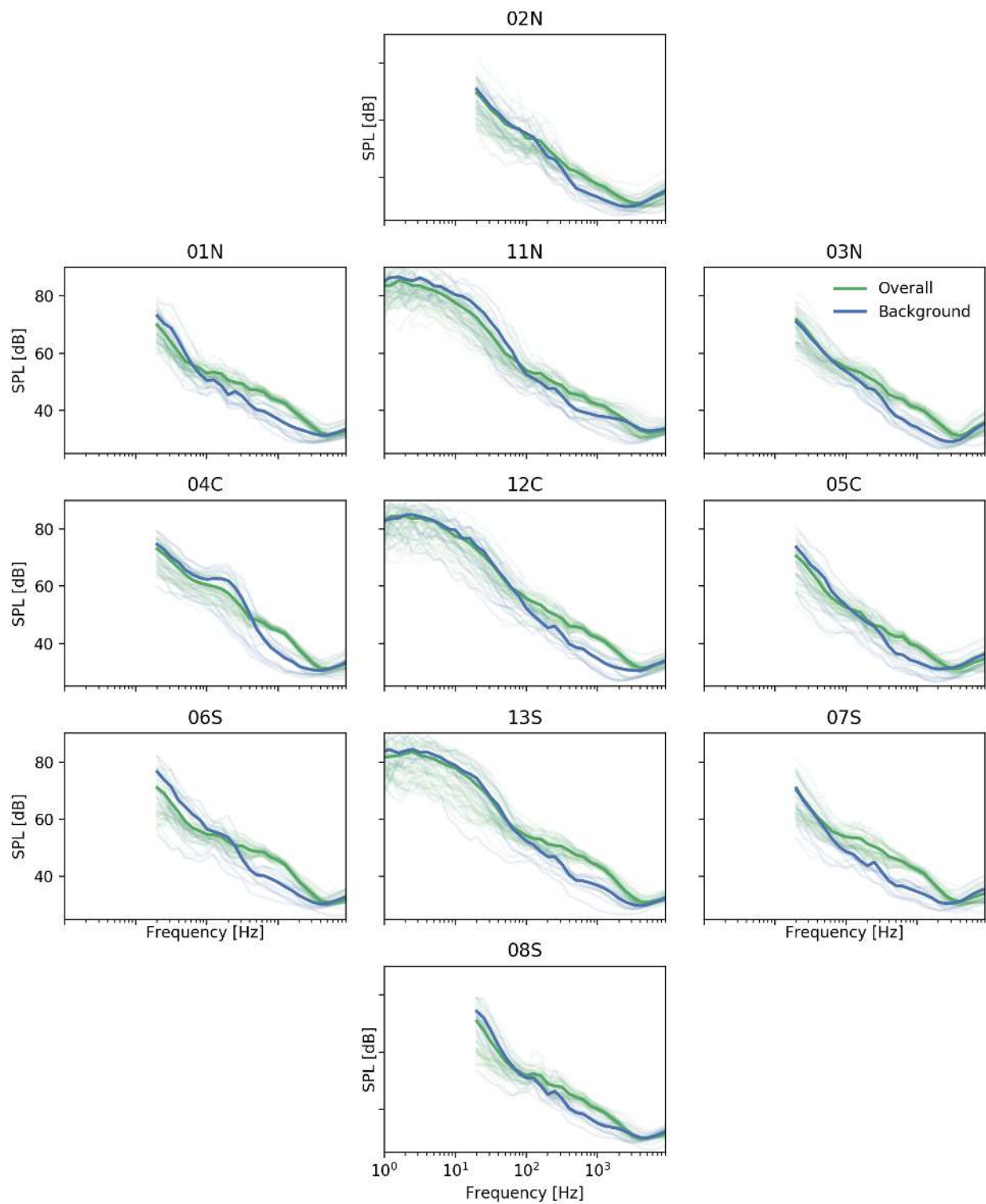


Figure 34. Overall and background spectra at 13 m/s for all microphones.

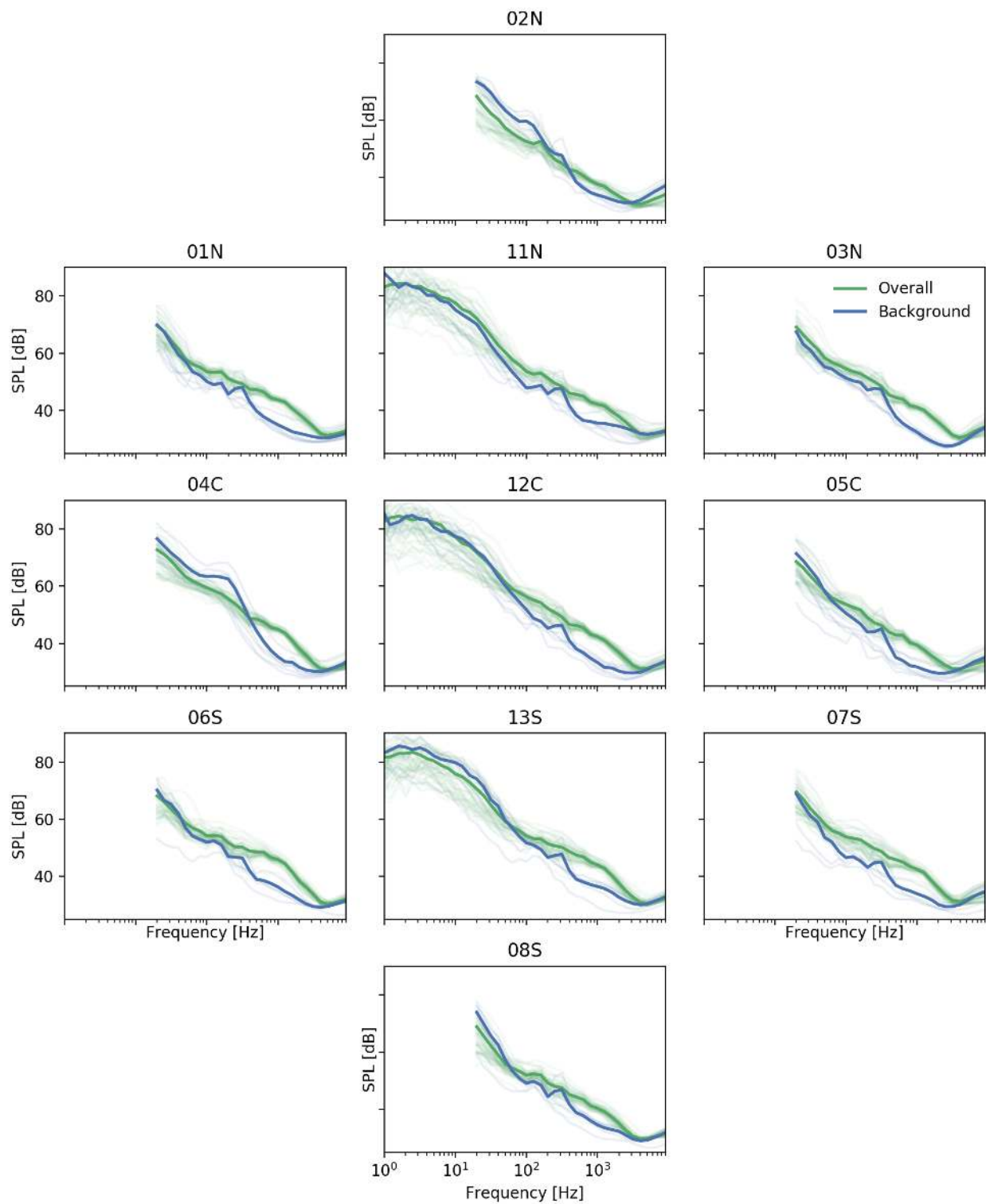


Figure 35. Overall and background spectra at 14 m/s for all microphones.

Appendix B Data Channels

Table 4 provides a list and description of the data channels available in the public data set hosted on the A2e DAP. Data can be accessed at <https://a2e.energy.gov/projects/aawpc>.

Table 4. Data channel names, descriptions, and units for the public dataset

Channel Name	Description	Quantity	Unit	Coordinate
'MS_Excel_Times-tamp'	Microsoft excel format timestamp	time	datetime	turb
'LabVIEW_Times-tamp'	LabVIEW format times-tamp	time	datetime	turb
'Scan_Errors'	DAS status signal indicating communications errors	flag	flag	turb
'Late_Scans'	DAS status signal indicating communications errors	flag	flag	turb
'Hum1'	hub height humidity measured at met tower	humidity	RH	turb
'Temp1'	hub height temperature from the met tower	temperature	C	turb
'Hum2'	hub height humidity, redundant, measured at met tower	humidity	RH	turb
'Temp2'	hub height temperature, redundant, from the met tower	temperature	C	turb
'Windspeed_38m'	wind speed from met tower measured at 38m elevation	wind speed	m/s	turb
'Windspeed_55m'	wind speed from met tower measured at 55m elevation	wind speed	m/s	turb
'Windspeed_87m'	hub height wind speed from met tower measured at 87m	wind speed	m/s	turb
'WD1_87m'	hub height wind direction from met tower measured at 87m	wind direction	deg	turb
'Air_Press_2'	hub height air pressure, redundant, from met tower	air pressure	kPa	turb
'Air_Press_1'	hub height air pressure from met tower	air pressure	kPa	turb
'Wind_Direction_38m'	wind direction measured at 38m	wind direction	deg	turb
'WindSpeed_80m'	hub height wind speed from met tower measured at 80m	wind speed	m/s	turb
'Precipitation'	wetness leaf sensor at data shed	wetness	V	turb
'NPcommand'	Natural Power curtailment command signal from BSCS, 0V = no command, 13V = command issued	command signal	V	turb
'Tower_Base_Bend_1'	tower base strain bending measurement 1	strain	V/V	turb
'Tower_Base_Bend_2'	tower base strain bending measurement 2	strain	V/V	turb

'Tower_Base_Torque'	tower base strain torque measurement	strain	V/V	turb
'Active_Power'	turbine measured power to grid	power	kW	turb
'Reactive_Power'	turbine reactive power to grid	kVAR		turb
'Power_Factor'	power factor to grid	unitless		turb
'TowerTopBending_0'	tower top strain bending measurement 1	strain	V/V	turb
'TowerTopBending_90'	tower top strain bending measurement 2	strain	V/V	turb
'TowerTopTorque'	tower top strain torque measurement	strain	V/V	turb
'TowerTopDCAccel_NS'	tower top acceleration in the ~north-south orientation	acceleration	g	turb
'TowerTopDCAccel_EW'	tower top acceleration in the ~east-west orientation	acceleration	g	turb
'LSS_RPM'	low speed shaft rpm	speed	RPM	turb
'HSS_RPM'	high speed shaft rpm	speed	RPM	turb
'NacelleWindSpeed'	direct signal from the nacelle anemometer - not the same as the SCADA value	speed	m/s	turb
'Mainshaft_Downwind_Bend_0'	main shaft bending strain measurement 1	strain	V	turb
'Mainshaft_Downwind_Bend_90'	main shaft bending strain measurement 2	strain	V	turb
'Mainshaft_Downwind_Torque'	main shaft torque strain measurement	strain	V	turb
'AzimuthAO'	rotor azimuth position - analog measurement	position	deg	turb
'Blade_1_Flap'	blade 1 flap strain	strain	V/V	turb
'Blade_1_Edge'	blade 1 edge strain	strain	V/V	turb
'Blade_2_Flap'	blade 2 flap strain	strain	V/V	turb
'Blade_2_Edge'	blade 2 edge strain	strain	V/V	turb
'Blade_3_Flap'	blade 3 flap strain	strain	V/V	turb
'Blade_3_Edge'	blade 3 edge strain	strain	V/V	turb
'Pitch_Blade2'	blade 2 pitch angle	angle	deg	turb
'Azimuth'	rotor azimuth position - digital input	position	deg	turb
'Yaw_Encoder'	yaw position - this signal can read less than zero and greater than 360, must be unwrapped	position	deg	turb
'Pitch_Blade1'	blade 1 pitch angle	angle	deg	turb
'WD_Mod_Active'	Flag to indicate modified wind direction signal	flag	bool	turb
'WD_Nacelle'	wind direction measured at nacelle	angle	deg	turb
'WD_Nacelle_Mod'	Modified wind direction measured at nacelle	angle	deg	turb

'EGD_AI_Cu-TorqueAct'	SCADA generator torque	torque		turb
'EGD_AI_In_Grid-MonRealPowerAct'	SCADA turbine active power	power	W	turb
'EGD_AI_In_-PitchAngleCurrent1'	SCADA blade 1 pitch	angle	deg	turb
'EGD_AI_In_-PitchAngleCurrent2'	SCADA blade 2 pitch	angle	deg	turb
'EGD_AI_In_-PitchAngleCurrent3'	SCADA blade 3 pitch	angle	deg	turb
'EGD_DI_In_TB-DiscBrakeClosed'	SCADA rotor brake disk closed/open status signal	flag	bool	turb
'EGD_In_RotorSpd'	SCADA rotor speed, LSS	rotational speed	rpm	turb
'EGD_In_WindSpd'	SCADA nacelle wind speed - matches 'SCADA_-nacelleWS' signal	wind speed	m/s	turb
'EGD_OpCtl_-TurbineFullState'	SCADA turbine status signal, not used	flag	flag	turb
'EGD_OpCtl_TurbineOperationState'	SCADA turbine status signal, not used	flag	flag	turb
'EGD_OpCtl_-TurbineStatus'	SCADA turbine status signal used to identify operational status and curailments. 12 = curtailed, 2 = normal op, 7 = weather conditions/low wind	flag	flag	turb
'EGD_Out_CalcTrbineStateSCADA'	SCADA turbine status signal, not used	flag	flag	turb
'EGD_Out_TurbineStatusSCADA'	SCADA turbine status signal, not used	flag	flag	turb
'EGD_Yaw_PositionToNorth'	SCADA yaw position - does not measure relative to true north!	angle	deg	turb
01N_LAeq	A-Weighted Equivalent Sound Pressure Level at Mic 01N	A-weighted Equivalent Sound Pressure Level	dBa	01N
02N_LAeq	A-Weighted Equivalent Sound Pressure Level at Mic 02N	A-weighted Equivalent Sound Pressure Level	dBa	02N
03N_LAeq	A-Weighted Equivalent Sound Pressure Level at Mic 03N	A-weighted Equivalent Sound Pressure Level	dBa	03N
04C_LAeq	A-Weighted Equivalent Sound Pressure Level at Mic 04C	A-weighted Equivalent Sound Pressure Level	dBa	04C
05C_LAeq	A-Weighted Equivalent Sound Pressure Level at Mic 05C	A-weighted Equivalent Sound Pressure Level	dBa	05C
06S_LAeq	A-Weighted Equivalent Sound Pressure Level at Mic 06S	A-weighted Equivalent Sound Pressure Level	dBa	06S

07S_LAeq	A-Weighted Equivalent Sound Pressure Level at Mic 07S	A-weighted Equivalent Sound Pressure Level	dBA	07S
08S_LAeq	A-Weighted Equivalent Sound Pressure Level at Mic 08S	A-weighted Equivalent Sound Pressure Level	dBA	08S
11N_LAeq	A-Weighted Equivalent Sound Pressure Level at Mic 11N	A-weighted Equivalent Sound Pressure Level	dBA	11N
12C_LAeq	A-Weighted Equivalent Sound Pressure Level at Mic 12C	A-weighted Equivalent Sound Pressure Level	dBA	12C
13S_LAeq	A-Weighted Equivalent Sound Pressure Level at Mic 13S	A-weighted Equivalent Sound Pressure Level	dBA	13S
01N_third_octave_-spectrum_A	A-weighted third octave band spectra Level at Mic 01N	A-weighted Equivalent Sound Pressure Level	dBA	01N
02N_third_octave_-spectrum_A	A-weighted third octave band spectra Level at Mic 02N	A-weighted Equivalent Sound Pressure Level	dBA	02N
03N_third_octave_-spectrum_A	A-weighted third octave band spectra Level at Mic 03N	A-weighted Equivalent Sound Pressure Level	dBA	03N
04C_third_octave_-spectrum_A	A-weighted third octave band spectra Level at Mic 04C	A-weighted Equivalent Sound Pressure Level	dBA	04C
05C_third_octave_-spectrum_A	A-weighted third octave band spectra Level at Mic 05C	A-weighted Equivalent Sound Pressure Level	dBA	05C
06S_third_octave_-spectrum_A	A-weighted third octave band spectra Level at Mic 06S	A-weighted Equivalent Sound Pressure Level	dBA	06S
07S_third_octave_-spectrum_A	A-weighted third octave band spectra Level at Mic 07S	A-weighted Equivalent Sound Pressure Level	dBA	07S
08S_third_octave_-spectrum_A	A-weighted third octave band spectra Level at Mic 08S	A-weighted Equivalent Sound Pressure Level	dBA	08S
11N_third_octave_-spectrum_A	A-weighted third octave band spectra Level at Mic 11N	A-weighted Equivalent Sound Pressure Level	dBA	11N
12C_third_octave_-spectrum_A	A-weighted third octave band spectra Level at Mic 12C	A-weighted Equivalent Sound Pressure Level	dBA	12C
13S_third_octave_-spectrum_A	A-weighted third octave band spectra Level at Mic 13S	A-weighted Equivalent Sound Pressure Level	dBA	13S
01N_Leq	Equivalent Sound Pressure Level at Mic 01N	Equivalent Sound Pressure Level	dB	01N
02N_Leq	Equivalent Sound Pressure Level at Mic 02N	Equivalent Sound Pressure Level	dB	02N

03N_Leq	Equivalent Sound Pressure Level at Mic 03N	Equivalent Sound Pressure Level	dB	03N
04C_Leq	Equivalent Sound Pressure Level at Mic 04C	Equivalent Sound Pressure Level	dB	04C
05C_Leq	Equivalent Sound Pressure Level at Mic 05C	Equivalent Sound Pressure Level	dB	05C
06S_Leq	Equivalent Sound Pressure Level at Mic 06S	Equivalent Sound Pressure Level	dB	06S
07S_Leq	Equivalent Sound Pressure Level at Mic 07S	Equivalent Sound Pressure Level	dB	07S
08S_Leq	Equivalent Sound Pressure Level at Mic 08S	Equivalent Sound Pressure Level	dB	08S
11N_Leq	Equivalent Sound Pressure Level at Mic 11N	Equivalent Sound Pressure Level	dB	11N
12C_Leq	Equivalent Sound Pressure Level at Mic 12C	Equivalent Sound Pressure Level	dB	12C
13S_Leq	Equivalent Sound Pressure Level at Mic 13S	Equivalent Sound Pressure Level	dB	13S
01N_G (infra)	G-weighted Infrasound Sound Pressure Level (below 20Hz) at Mic 01N	G-weighted Infrasound Sound Pressure Level (below 20Hz)	dBG	01N
02N_G (infra)	G-weighted Infrasound Sound Pressure Level (below 20Hz) at Mic 02N	G-weighted Infrasound Sound Pressure Level (below 20Hz)	dBG	02N
03N_G (infra)	G-weighted Infrasound Sound Pressure Level (below 20Hz) at Mic 03N	G-weighted Infrasound Sound Pressure Level (below 20Hz)	dBG	03N
04C_G (infra)	G-weighted Infrasound Sound Pressure Level (below 20Hz) at Mic 04C	G-weighted Infrasound Sound Pressure Level (below 20Hz)	dBG	04C
05C_G (infra)	G-weighted Infrasound Sound Pressure Level (below 20Hz) at Mic 05C	G-weighted Infrasound Sound Pressure Level (below 20Hz)	dBG	05C
06S_G (infra)	G-weighted Infrasound Sound Pressure Level (below 20Hz) at Mic 06S	G-weighted Infrasound Sound Pressure Level (below 20Hz)	dBG	06S
07S_G (infra)	G-weighted Infrasound Sound Pressure Level (below 20Hz) at Mic 07S	G-weighted Infrasound Sound Pressure Level (below 20Hz)	dBG	07S
08S_G (infra)	G-weighted Infrasound Sound Pressure Level (below 20Hz) at Mic 08S	G-weighted Infrasound Sound Pressure Level (below 20Hz)	dBG	08S
11N_G (infra)	G-weighted Infrasound Sound Pressure Level (below 20Hz) at Mic 11N	G-weighted Infrasound Sound Pressure Level (below 20Hz)	dBG	11N
12C_G (infra)	G-weighted Infrasound Sound Pressure Level (below 20Hz) at Mic 12C	G-weighted Infrasound Sound Pressure Level (below 20Hz)	dBG	12C
13S_G (infra)	G-weighted Infrasound Sound Pressure Level (below 20Hz) at Mic 13S	G-weighted Infrasound Sound Pressure Level (below 20Hz)	dBG	13S

01N_A (LF)	A-weighted Low-Frequency Sound Pressure Level (20-200Hz) at Mic 01N	A-weighted Low-Frequency Sound Pressure Level (20-200Hz)	dBA	01N
02N_A (LF)	A-weighted Low-Frequency Sound Pressure Level (20-200Hz) at Mic 02N	A-weighted Low-Frequency Sound Pressure Level (20-200Hz)	dBA	02N
03N_A (LF)	A-weighted Low-Frequency Sound Pressure Level (20-200Hz) at Mic 03N	A-weighted Low-Frequency Sound Pressure Level (20-200Hz)	dBA	03N
04C_A (LF)	A-weighted Low-Frequency Sound Pressure Level (20-200Hz) at Mic 04C	A-weighted Low-Frequency Sound Pressure Level (20-200Hz)	dBA	04C
05C_A (LF)	A-weighted Low-Frequency Sound Pressure Level (20-200Hz) at Mic 05C	A-weighted Low-Frequency Sound Pressure Level (20-200Hz)	dBA	05C
06S_A (LF)	A-weighted Low-Frequency Sound Pressure Level (20-200Hz) at Mic 06S	A-weighted Low-Frequency Sound Pressure Level (20-200Hz)	dBA	06S
07S_A (LF)	A-weighted Low-Frequency Sound Pressure Level (20-200Hz) at Mic 07S	A-weighted Low-Frequency Sound Pressure Level (20-200Hz)	dBA	07S
08S_A (LF)	A-weighted Low-Frequency Sound Pressure Level (20-200Hz) at Mic 08S	A-weighted Low-Frequency Sound Pressure Level (20-200Hz)	dBA	08S
11N_A (LF)	A-weighted Low-Frequency Sound Pressure Level (20-200Hz) at Mic 11N	A-weighted Low-Frequency Sound Pressure Level (20-200Hz)	dBA	11N
12C_A (LF)	A-weighted Low-Frequency Sound Pressure Level (20-200Hz) at Mic 12C	A-weighted Low-Frequency Sound Pressure Level (20-200Hz)	dBA	12C
13S_A (LF)	A-weighted Low-Frequency Sound Pressure Level (20-200Hz) at Mic 13S	A-weighted Low-Frequency Sound Pressure Level (20-200Hz)	dBA	13S
01N_Lin	Sound Pressure Level (1Hz-20kHz) at Mic 01N	Equivalent Sound Pressure Level (1-20000Hz)	dB	01N
02N_Lin	Sound Pressure Level (1Hz-20kHz) at Mic 02N	Equivalent Sound Pressure Level (1-20000Hz)	dB	02N
03N_Lin	Sound Pressure Level (1Hz-20kHz) at Mic 03N	Equivalent Sound Pressure Level (1-20000Hz)	dB	03N
04C_Lin	Sound Pressure Level (1Hz-20kHz) at Mic 04C	Equivalent Sound Pressure Level (1-20000Hz)	dB	04C
05C_Lin	Sound Pressure Level (1Hz-20kHz) at Mic 05C	Equivalent Sound Pressure Level (1-20000Hz)	dB	05C
06S_Lin	Sound Pressure Level (1Hz-20kHz) at Mic 06S	Equivalent Sound Pressure Level (1-20000Hz)	dB	06S
07S_Lin	Sound Pressure Level (1Hz-20kHz) at Mic 07S	Equivalent Sound Pressure Level (1-20000Hz)	dB	07S
08S_Lin	Sound Pressure Level (1Hz-20kHz) at Mic 08S	Equivalent Sound Pressure Level (1-20000Hz)	dB	08S
11N_Lin	Sound Pressure Level (1Hz-20kHz) at Mic 11N	Equivalent Sound Pressure Level (1-20000Hz)	dB	11N

12C_Lin	Sound Pressure Level (1Hz-20kHz) at Mic 12C	Equivalent Sound Pressure Level (1-20000Hz)	dB	12C
13S_Lin	Sound Pressure Level (1Hz-20kHz) at Mic 13S	Equivalent Sound Pressure Level (1-20000Hz)	dB	13S
01N_third_octave_- spectrum	Third octave band spectra Level at Mic 01N	Third octave spectra	dB	01N
02N_third_octave_- spectrum	Third octave band spectra Level at Mic 02N	Third octave spectra	dB	02N
03N_third_octave_- spectrum	Third octave band spectra Level at Mic 03N	Third octave spectra	dB	03N
04C_third_octave_- spectrum	Third octave band spectra Level at Mic 04C	Third octave spectra	dB	04C
05C_third_octave_- spectrum	Third octave band spectra Level at Mic 05C	Third octave spectra	dB	05C
06S_third_octave_- spectrum	Third octave band spectra Level at Mic 06S	Third octave spectra	dB	06S
07S_third_octave_- spectrum	Third octave band spectra Level at Mic 07S	Third octave spectra	dB	07S
08S_third_octave_- spectrum	Third octave band spectra Level at Mic 08S	Third octave spectra	dB	08S
11N_third_octave_- spectrum	Third octave band spectra Level at Mic 11N	Third octave spectra	dB	11N
12C_third_octave_- spectrum	Third octave band spectra Level at Mic 12C	Third octave spectra	dB	12C
13S_third_octave_- spectrum	Third octave band spectra Level at Mic 13S	Third octave spectra	dB	13S
Speed (cup_ 130 m)	Wind speed measured by a cup anememometer at 130 m	wind speed	m/s	met
Speed (cup_ 122 m)	Wind speed measured by a cup anememometer at 122 m	wind speed	m/s	met
Speed (cup_ 105 m)	Wind speed measured by a cup anememometer at 105 m	wind speed	m/s	met
Speed (cup_ 87 m)	Wind speed measured by a cup anememometer at 87 m	wind speed	m/s	met
Speed (cup_ 80 m)	Wind speed measured by a cup anememometer at 80 m	wind speed	m/s	met
Speed (cup_ 55 m)	Wind speed measured by a cup anememometer at 55 m	wind speed	m/s	met
Speed (cup_ 38 m)	Wind speed measured by a cup anememometer at 38 m	wind speed	m/s	met
Speed (cup_ 30 m)	Wind speed measured by a cup anememometer at 30 m	wind speed	m/s	met
Speed (cup_ 10 m)	Wind speed measured by a cup anememometer at 10 m	wind speed	m/s	met
Speed (cup_ 3 m)	Wind speed measured by a cup anememometer at 3 m	wind speed	m/s	met
Speed Gradient Richardson (38_- 87_ 122 m)	Speed Gradient Richardson Number	Ri	[-]	met

Speed Gradient Richardson (3_10_38_87_122 m)	Speed Gradient Richardson Number	Ri	[-]	met
Speed Gradient Richardson (3_10_38_87 m)	Speed Gradient Richardson Number	Ri	[-]	met
Speed Gradient Richardson (10_38 m)	Speed Gradient Richardson Number	Ri	[-]	met
Speed Ux (sonic_119m)	Wind speed measured by a sonic anememometer at 119m	wind speed	m/s	met
Speed Uy (sonic_119m)	Wind speed measured by a sonic anememometer at 119m	wind speed	m/s	met
Speed Uz (sonic_119m)	Wind speed measured by a sonic anememometer at 119m	wind speed	m/s	met
Speed (sonic_119m)	Wind speed measured by a sonic anememometer at 119m	wind speed	m/s	met
Total Speed (sonic_119m)	Wind speed measured by a sonic anememometer at 119m	wind speed	m/s	met
Cup Equivalent Speed (sonic_119m)	Wind speed measured by a sonic anememometer at 119m	wind speed	m/s	met
Advection Speed (sonic_119m)	Wind speed measured by a sonic anememometer at 119m	wind speed	m/s	met
Speed Ux (sonic_100m)	Wind speed measured by a sonic anememometer at 100m	wind speed	m/s	met
Speed Uy (sonic_100m)	Wind speed measured by a sonic anememometer at 100m	wind speed	m/s	met
Speed Uz (sonic_100m)	Wind speed measured by a sonic anememometer at 100m	wind speed	m/s	met
Speed (sonic_100m)	Wind speed measured by a sonic anememometer at 100m	wind speed	m/s	met
Total Speed (sonic_100m)	Wind speed measured by a sonic anememometer at 100m	wind speed	m/s	met
Cup Equivalent Speed (sonic_100m)	Wind speed measured by a sonic anememometer at 100m	wind speed	m/s	met
Advection Speed (sonic_100m)	Wind speed measured by a sonic anememometer at 100m	wind speed	m/s	met

Speed Ux (sonic_-74m)	Wind speed measured by a sonic anememometer at 74m	wind speed	m/s	met
Speed Uy (sonic_-74m)	Wind speed measured by a sonic anememometer at 74m	wind speed	m/s	met
Speed Uz (sonic_-74m)	Wind speed measured by a sonic anememometer at 74m	wind speed	m/s	met
Speed (sonic_74m)	Wind speed measured by a sonic anememometer at 74m	wind speed	m/s	met
Total Speed (sonic_-74m)	Wind speed measured by a sonic anememometer at 74m	wind speed	m/s	met
Cup Equivalent Speed (sonic_74m)	Wind speed measured by a sonic anememometer at 74m	wind speed	m/s	met
Advection Speed (sonic_74m)	Wind speed measured by a sonic anememometer at 74m	wind speed	m/s	met
Speed Ux (sonic_-61m)	Wind speed measured by a sonic anememometer at 61m	wind speed	m/s	met
Speed Uy (sonic_-61m)	Wind speed measured by a sonic anememometer at 61m	wind speed	m/s	met
Speed Uz (sonic_-61m)	Wind speed measured by a sonic anememometer at 61m	wind speed	m/s	met
Speed (sonic_61m)	Wind speed measured by a sonic anememometer at 61m	wind speed	m/s	met
Total Speed (sonic_-61m)	Wind speed measured by a sonic anememometer at 61m	wind speed	m/s	met
Cup Equivalent Speed (sonic_61m)	Wind speed measured by a sonic anememometer at 61m	wind speed	m/s	met
Advection Speed (sonic_61m)	Wind speed measured by a sonic anememometer at 61m	wind speed	m/s	met
Speed Ux (sonic_-41m)	Wind speed measured by a sonic anememometer at 41m	wind speed	m/s	met
Speed Uy (sonic_-41m)	Wind speed measured by a sonic anememometer at 41m	wind speed	m/s	met
Speed Uz (sonic_-41m)	Wind speed measured by a sonic anememometer at 41m	wind speed	m/s	met

Speed (sonic_41m)	Wind speed measured by a sonic anememometer at 41m	wind speed	m/s	met
Total Speed (sonic_41m)	Wind speed measured by a sonic anememometer at 41m	wind speed	m/s	met
Cup Equivalent Speed (sonic_41m)	Wind speed measured by a sonic anememometer at 41m	wind speed	m/s	met
Advection Speed (sonic_41m)	Wind speed measured by a sonic anememometer at 41m	wind speed	m/s	met
Speed Ux (sonic_15m)	Wind speed measured by a sonic anememometer at 15m	wind speed	m/s	met
Speed Uy (sonic_15m)	Wind speed measured by a sonic anememometer at 15m	wind speed	m/s	met
Speed Uz (sonic_15m)	Wind speed measured by a sonic anememometer at 15m	wind speed	m/s	met
Speed (sonic_15m)	Wind speed measured by a sonic anememometer at 15m	wind speed	m/s	met
Total Speed (sonic_15m)	Wind speed measured by a sonic anememometer at 15m	wind speed	m/s	met
Cup Equivalent Speed (sonic_15m)	Wind speed measured by a sonic anememometer at 15m	wind speed	m/s	met
Advection Speed (sonic_15m)	Wind speed measured by a sonic anememometer at 15m	wind speed	m/s	met
Direction (Vane_130 m)	Wind direction measured by a vane at 130	wind direction	deg	met
Std. Dev. Direction (Vane_130 m)	Wind direction measured by a vane at Direction	wind direction	deg	met
Direction (Vane_122 m)	Wind direction measured by a vane at 122	wind direction	deg	met
Std. Dev. Direction (Vane_122 m)	Wind direction measured by a vane at Direction	wind direction	deg	met
Direction (Vane_105 m)	Wind direction measured by a vane at 105	wind direction	deg	met
Std. Dev. Direction (Vane_105 m)	Wind direction measured by a vane at Direction	wind direction	deg	met
Direction (Vane_87 m)	Wind direction measured by a vane at 87	wind direction	deg	met
Std. Dev. Direction (Vane_87 m)	Wind direction measured by a vane at Direction	wind direction	deg	met
Direction (Vane_80 m)	Wind direction measured by a vane at 80	wind direction	deg	met

Std. Dev. Direction (Vane_ 80 m)	Wind direction measured by a vane at Direction	wind direction	deg	met
Direction (Vane_ 55 m)	Wind direction measured by a vane at 55	wind direction	deg	met
Std. Dev. Direction (Vane_ 55 m)	Wind direction measured by a vane at Direction	wind direction	deg	met
Direction (Vane_ 38 m)	Wind direction measured by a vane at 38	wind direction	deg	met
Std. Dev. Direction (Vane_ 38 m)	Wind direction measured by a vane at Direction	wind direction	deg	met
Direction (Vane_ 30 m)	Wind direction measured by a vane at 30	wind direction	deg	met
Std. Dev. Direction (Vane_ 30 m)	Wind direction measured by a vane at Direction	wind direction	deg	met
Direction (Vane_ 10 m)	Wind direction measured by a vane at 10	wind direction	deg	met
Std. Dev. Direction (Vane_ 10 m)	Wind direction measured by a vane at Direction	wind direction	deg	met
Direction (Vane_ 3 m)	Wind direction measured by a vane at 3	wind direction	deg	met
Std. Dev. Direction (Vane_ 3 m)	Wind direction measured by a vane at Direction	wind direction	deg	met
Direction (sonic_ - 119m)	Wind direction measured by a sonic anememometer at 119m	wind direction	deg	met
Direction (sonic_ - 100m)	Wind direction measured by a sonic anememometer at 100m	wind direction	deg	met
Direction (sonic_ - 74m)	Wind direction measured by a sonic anememometer at 74m	wind direction	deg	met
Direction (sonic_ - 61m)	Wind direction measured by a sonic anememometer at 61m	wind direction	deg	met
Direction (sonic_ - 41m)	Wind direction measured by a sonic anememometer at 41m	wind direction	deg	met
Direction (sonic_ - 15m)	Wind direction measured by a sonic anememometer at 15m	wind direction	deg	met
Stability parameter z/L (119m)	Monin-ObuKhov similarity parameter at 119m	MO stability parameter	[-]	met
Stability parameter z/L (100m)	Monin-ObuKhov similarity parameter at 100m	MO stability parameter	[-]	met
Stability parameter z/L (74m)	Monin-ObuKhov similarity parameter at 74m	MO stability parameter	[-]	met
Stability parameter z/L (61m)	Monin-ObuKhov similarity parameter at 61m	MO stability parameter	[-]	met
Stability parameter z/L (41m)	Monin-ObuKhov similarity parameter at 41m	MO stability parameter	[-]	met
Stability parameter z/L (15m)	Monin-ObuKhov similarity parameter at 15m	MO stability parameter	[-]	met

Ti (cup_ 130 m)	Turbulence intensity measured by a cup anemometer at 130 m	turbulence intensity	%	met
Ti (cup_ 122 m)	Turbulence intensity measured by a cup anemometer at 122 m	turbulence intensity	%	met
Ti (cup_ 105 m)	Turbulence intensity measured by a cup anemometer at 105 m	turbulence intensity	%	met
Ti (cup_ 87 m)	Turbulence intensity measured by a cup anemometer at 87 m	turbulence intensity	%	met
Ti (cup_ 80 m)	Turbulence intensity measured by a cup anemometer at 80 m	turbulence intensity	%	met
Ti (cup_ 55 m)	Turbulence intensity measured by a cup anemometer at 55 m	turbulence intensity	%	met
Ti (cup_ 38 m)	Turbulence intensity measured by a cup anemometer at 38 m	turbulence intensity	%	met
Ti (cup_ 30 m)	Turbulence intensity measured by a cup anemometer at 30 m	turbulence intensity	%	met
Ti (cup_ 10 m)	Turbulence intensity measured by a cup anemometer at 10 m	turbulence intensity	%	met
Ti (cup_ 3 m)	Turbulence intensity measured by a cup anemometer at 3 m	turbulence intensity	%	met
Cup Equivalent Ti (sonic_119m)	Turbulence intensity at 119m	turbulence intensity	%	met
Cup Equivalent Ti (sonic_100m)	Turbulence intensity at 100m	turbulence intensity	%	met
Cup Equivalent Ti (sonic_74m)	Turbulence intensity at 74m	turbulence intensity	%	met
Cup Equivalent Ti (sonic_61m)	Turbulence intensity at 61m	turbulence intensity	%	met
Cup Equivalent Ti (sonic_41m)	Turbulence intensity at 41m	turbulence intensity	%	met
Cup Equivalent Ti (sonic_15m)	Turbulence intensity at 15m	length	m	met
Integral Length Scale (u) (119m)	Turbulence integral length scale at 119m	length	m	met
Integral Length Scale (u) (100m)	Turbulence integral length scale at 100m	length	m	met
Integral Length Scale (u) (74m)	Turbulence integral length scale at 74m	length	m	met
Integral Length Scale (u) (61m)	Turbulence integral length scale at 61m	length	m	met
Integral Length Scale (u) (41m)	Turbulence integral length scale at 41m	length	m	met

Integral Length Scale (u) (15m)	Turbulence integral length scale at 15m	length	m	met
Turbine Operating	Flag to indicate operation of wind turbine	flag	bool	met
Yaw_Position_-Normal	flag to indicate normal operation of yaw position signal	flag	bool	met
Direction Valid	flag to indicate validity of wind direction from nacelle anemometer	flag	bool	met
WindSpeed_80m_-round	Wind speed rounded to nearest integer value	wind speed	m/s	met
yawPos	yaw setting (WD_Nacelle_-Mod - WD_Nacelle)	angle	deg	met
Windspeed_AeroA_-10m	Wind speed from 10 m met mast	wind speed	m/s	auxmet
Yaw_Offset_Cmd	Wind direction offset supplied for yaw control	angle	deg	turb
Yaw_Offset_Cmd_-Bin	flag to indicate activity of yaw controller	flag	bool	turb

PRODUCT DATA

Signal Conditioner Type 1708

Single-channel, battery powered for classical and CCLD input

Type 1708 provides signal conditioning, amplification and gain control for Brüel & Kjær classical microphones as well as CCLD* transducers. It is designed for easy use, both in the field and in the lab, featuring a built-in rechargeable battery optimized for in situ measurements.



Uses and Features

Uses

- Condition signals by applying gains and filters
- Provide reliable power to:
 - Classical microphone assemblies, prepolarized or polarized
 - CCLD transducers

Features

- ± 60 V supply covers the maximum dynamic range of all classical microphones and preamplifiers
- 8 mA supply for compatibility with all CCLD transducers
- Charge injection calibration (CIC) via an external generator

- Built-in Li-Ion battery, provides up to 9 h of operating time for classical microphones (up to 15 h for CCLD)
- 5 V DC adaptor for powering/charging via mains
- Power cable with USB connector for powering/charging via computer
- Wide range of gains ($\times 0.1$, $\times 1$, $\times 10$ and $\times 100$) to amplify analogue signal before external digital conversion, improving noise floor
- Linear, 22.4 Hz to 22.4 kHz, and A-weighting (type 0) filters for removing unwanted frequencies
- Easy-to-use switches for changing settings quickly
- LED displays for quick verification of status

Description

Type 1708 is a single-channel signal conditioner for classical microphone/preamplifier combinations as well as CCLD transducers.

Located on the front panel are the power switch, setting selectors (power supply, filter, and gain) and the LED status displays (battery, overload). The input connectors (LEMO for classical microphones, BNC for CCLD and/or direct), a BNC output connector, an SMB connector for CIC, and a coaxial connector for powering/charging the battery are located on the back panel.

Fig. 1
Left: Front panel
Right: Back panel



* CCLD: Constant current line drive, also known as DeltaTron® (IEPE compatible)

Transducer Power Supply

For powering both classical and CCLD transducers, there are two power supply options: polarization voltage (P_{vol}) or CCLD. Polarization voltage can be set to either 0 or 200 V, and CCLD provides an 8 mA constant current.

CCLD power has many manufacturer specific names such as DeltaTron®, ICP® (Integrated Circuit Piezoelectric), IEPE (Integrate Electronics Piezoelectric) and ISOTRON®. Type 1708 is compatible with transducers using any of the above trade names.

Gain and Filtering

Type 1708 includes analogue gain and filtering. Adding a gain before converting the signal from analogue to digital can improve the system's noise floor. Likewise, selecting a filter can remove unwanted frequencies before conversion.

Type 1708 Gain Settings:

×0.1 (−20 dB), ×1 (0 dB), ×10 (+20 dB), ×100 (+40 dB)

Type 1708 Filters:

Linear, 22.4 Hz to 22.4 kHz, A-weighting (type 0)

Fig. 2
Mains power adaptor ZG-0473 includes plug adaptor set and attached power cable AO-1429 with coaxial to USB connectors



Type 1708 Powering Options

Type 1708 features a DC coaxial (EIAJ-02) connector for powering/charging the built-in battery using either the provided mains power adaptor or a computer's USB port.

The rechargeable battery has at least 500 cycles, each lasting for about 9 hours of operation (depending on the settings), which is more convenient than replacing non-rechargeable batteries and reduces the cost of ownership.





Family of Brüel & Kjær Signal Conditioners

Table 1 Feature comparison of Brüel & Kjær signal conditioners

	1708	1704-A	2690-A	2829	5935-L
Mains (AC) Power	✓	✓	✓	✓	✓
USB Power	✓	✓			
Battery Power	✓	✓	Optional		✓
Number of Channels per Unit	1	1 or 2	1 to 4	4	2
Manual Control	✓	✓	✓		✓
Computer Control			✓		
Read Transducer Electronic Data Sheet (TEDS)			✓	Via external connector	
Uni (Fine) Gain Adjustment			✓		✓
Multiplexer Output			✓	✓	✓
Maximum Frequency (kHz, at filters −5% point)	>350	55	100	–	100
Maximum Gain (dB)	40	40	80	–	50
Minimum Gain (dB)	−20	0	−20	0	0
A-weighting (type 0)	✓	✓	✓		✓
Single and Double Integration Filters			✓	✓	✓
Constant Current Supply (mA)	✓	✓	✓	✓	✓

Compliance with Standards

Type 1708 is designed for use in systems with cable length <30 m.

   	<p>The CE marking is the manufacturer's declaration that the product meets the requirements of the applicable EU directives</p> <p>RCM mark indicates compliance with applicable ACMA technical standards – that is, for telecommunications, radio communications, EMC and EME</p> <p>China RoHS mark indicates compliance with administrative measures on the control of pollution caused by electronic information products according to the Ministry of Information Industries of the People's Republic of China</p> <p>WEEE mark indicates compliance with the EU WEEE Directive</p>
Safety	EN/IEC 61010–1: Safety requirements for electrical equipment for measurement, control and laboratory use ANSI/UL 61010–1: Safety requirements for electrical equipment for measurement, control and laboratory use
EMC Emission	EN/IEC 61000–6–3: Generic emission standard for residential, commercial and light industrial environments EN/IEC 61000–6–4: Generic emission standard for industrial environments CISPR 22: Radio disturbance characteristics of information technology equipment. Class B Limits FCC Rules, Part 15: Complies with the limits for a Class B digital device This ISM device complies with Canadian ICES–001 (standard for interference-causing equipment)
EMC Immunity	EN/IEC 61000–6–1: Generic standards – Immunity for residential, commercial and light industrial environments EN/IEC 61000–6–2: Generic standards – Immunity for industrial environments EN/IEC 61326: Electrical equipment for measurement, control and laboratory use – EMC requirements Note: Effect of radiated RF, 80–1000 MHz 80% AM 1 kHz 10 V/m: <300 µV Note: The above is only guaranteed using accessories listed in this Product Data sheet
Temperature	IEC 60068–2–1 & IEC 60068–2–2: Environmental Testing. Cold and Dry Heat Operating Temperature: –20 to +50 °C (–4 to 122 °F) Storage Temperature: –25 to +70 °C (–13 to +158 °F)
Humidity	IEC 60068–2–78: Damp Heat: 93% RH (non-condensing at 40 °C (104 °F))
Mechanical	Non-operating: IEC 60068–2–6: Vibration: 0.3 mm, 20 m/s ² , 10 – 500 Hz IEC 60068–2–27: Shock: 1000 m/s ² IEC 60068–2–29: Bump: 1000 bumps at 250 m/s ²
Enclosure	IEC 60529: Protection provided by enclosures: IP 20

Specifications – Type 1708

CONNECTORS

Input:

- Classical: LEMO
- CCLD: BNC

Output: BNC

External generator: SMB

Battery power supply: Coaxial EIAJ-02

BATTERY

Number of battery charging cycles (down to 80%): 500

Time to charge (in off mode), mains (AC) or USB: 5 hours

PHYSICAL

Dimensions: 110 × 140 × 36 mm (4.33 × 5.51 × 1.42 in)

Weight: 320 g (11.29 oz)

Temperature range:

- Operating: –20 to +50 °C (–4 to +122 °F)
- Charging: 10 to 40 °C (50 to 104 °F)

FILTERING AND GAIN

Filters:

- Linear
- 22.4 Hz to 22.4 kHz
- A-weighting

Gain:

- ×0.1 (–20 dB)
- ×1 (0 dB)
- ×10 (+20 dB)
- ×100 (+40 dB)

	Unit	Gain				
		×0.1 (–20 dB)	×1 (0 dB)	×10 (+20 dB)	×100 (+40 dB)	
Amplifier Gain	at 1 kHz	dB	–20 ± 0.05	0 ± 0.05	20 ± 0.05	40 ± 0.05
Gain Tolerance	10 Hz 100 kHz	dB	±0.2	±0.1	±0.1	±0.2
Excitation Voltage	Classical	V	±60	±15	±15	±15
	CCLD	V		25	25	25
Excitation Current	CCLD	mA	8 ± 2			
Maximum Input Voltage (peak)		V	±58	±10	±0.1	±0.010
Input Protection*		V	From ±58	–14.5 to +25	–14.5 to +25	–14.5 to +25
Maximum Non-destructive Input		V	±100	±100	±100	±100
Maximum Output Voltage (peak)		V	6	10	10	10
Overload Level		V	±55	±11	±1.1	±0.11
Output Impedance		Ω	50	50	50	50

		Unit	Gain			
			×0.1 (−20 dB)	×1 (0 dB)	×10 (+20 dB)	×100 (+40 dB)
Cable Fault Voltage Levels	CCLD overload levels		% CCLD current disconnected	Input voltage below +2.5 V: cable short-circuited Input voltage above +21 V: open circuit		
Total Harmonic Distortion	at 1 kHz 1 V_{rmsout}	dB	>70, Typ.: 80	>80, Typ.: 90	>80, Typ.: 90	>80, Typ.: 90
Output DC Offset		mV	Max.: 3.5, Typ.: 1	Max.: 3.5, Typ.: 1	Max.: 3.5, Typ.: 1	Max.: 3.5, Typ.: 1
Charge Injection Calibration (CIC)[†]			Yes	Yes	Yes	Yes
Frequency Range (−3 dB, max. slew rate 10 V/μs)	Lower Limit	Hz	<1, Typ.: 0.7	<1, Typ.: 0.7	<1, Typ.: 0.7	<1, Typ.: 0.7
	Upper Limit	kHz	>450	>450	>450	>350
Spectral Output Noise, Linear	1 Hz	$\mu\text{V}/\sqrt{\text{Hz}}$	<0.2, Typ.: 0.07	<0.2, Typ.: 0.06	<1.5, Typ.: 0.3	<10, Typ.: 3
	10 Hz		<0.2, Typ.: 0.05	<0.1, Typ.: 0.02	<0.5, Typ.: 0.1	<5, Typ.: 1
	100 Hz		<0.07, Typ.: 0.04	<0.05, Typ.: 0.01	<0.15, Typ.: 0.07	<1.5, Typ.: 0.7
	1 kHz		<0.07, Typ.: 0.035	<0.02, Typ.: 0.01	<0.15, Typ.: 0.07	<1.5, Typ.: 0.7
	10 kHz		<0.02, Typ.: 0.013	<0.02, Typ.: 0.01	<0.15, Typ.: 0.07	<1.5, Typ.: 0.7
	100 kHz		<0.02, Typ.: 0.013	<0.02, Typ.: 0.01	<0.15, Typ.: 0.07	<1.5, Typ.: 0.7
Broadband Electrical Output Noise, Linear	1 Hz to 10 kHz	μV_{rms}	<4, Typ.: 2.5	<3, Typ.: 1.2	<8, Typ.: 6.7	<70, Typ.: 63
	1 Hz to 100 kHz		<6, Typ.: 4	<5, Typ.: 3.5	<25, Typ.: 22	<250, Typ.: 200
	1 Hz to 150 kHz[‡]		<7.5, Typ.: 5	<6.5, Typ.: 4.5	<32, Typ.: 28	<320, Typ.: 250
Broadband Output Noise	Acoustic Bandpass, Linear	μV_{rms}	<4, Typ.: 2.6	<3, Typ.: 1.6	<12, Typ.: 10	<100, Typ.: 94
	Acoustic Bandpass, Internal		<8, Typ.: 6.5	<8, Typ.: 6	<15, Typ.: 12	<110, Typ.: 95
	A-weighting, Post-processing		<4, Typ.: 2.4	<3, Typ.: 1.4	<10, Typ.: 7.6	<80, Typ.: 73
	A-weighting, Internal		<10, Typ.: 7	<10, Typ.: 7	<12, Typ.: 10	<80, Typ.: 74
Phase Difference, Device to device (typ. values), Linear weighting (without filters)	100 kHz		±5°	±5°	±10°	±15°
	1 Hz		±2°	±2°	±2.5°	±2.5°
Max. Amplitude Difference, Device to device, Linear weighting (without filters)	100 kHz	dB	±0.4	±0.1	±0.2	±0.5
	1 Hz		±0.15	±0.1	±0.15	±0.11
Battery Life (Typical)	CCLD mode	h	15	15	15	15
	With Preamplifier Type 2669 (±15 V supply)		9.5	9.5	9.5	9.5
	With Preamplifier Type 2669 (±60 V supply)		4			
	After low-battery level	min	30	45	45	45

* If the signal input level exceeds the measuring range significantly, the input will go into protection mode for 0.5 s. Overload will be detected, input impedance will be increased and the signal attenuated. Input signal is cut when it exceeds ±60 V.

† It is possible to calibrate the input of preamplifier using charge injection by connecting an external generator via the SMB connector. During CIC, the CIC switch and the overload diode must be set to 'On'. When not in use, CIC switch must be 'Off'.

‡ Power supply switching frequency: between 170 and 180 kHz

Ordering Information

Type 1708 Signal Conditioner

ACCESSORIES

ZG-0473 Power supply wall adaptor, 5 V
AO-1429 Power cable, DC

CALIBRATION SERVICES

1708-CVI Initial Accredited Calibration, Type 1708 with microphone
1708-CVF Accredited Calibration, Type 1708 with microphone

Brüel & Kjær and all other trademarks, service marks, trade names, logos and product names are the property of Brüel & Kjær or a third-party company.

Brüel & Kjær Sound & Vibration Measurement A/S
DK-2850 Nærum · Denmark · Telephone: +45 77 41 20 00 · Fax: +45 45 80 14 05
www.bksv.com · info@bksv.com
Local representatives and service organizations worldwide

Although reasonable care has been taken to ensure the information in this document is accurate, nothing herein can be construed to imply representation or warranty as to its accuracy, currency or completeness, nor is it intended to form the basis of any contract. Content is subject to change without notice – contact Brüel & Kjær for the latest version of this document.

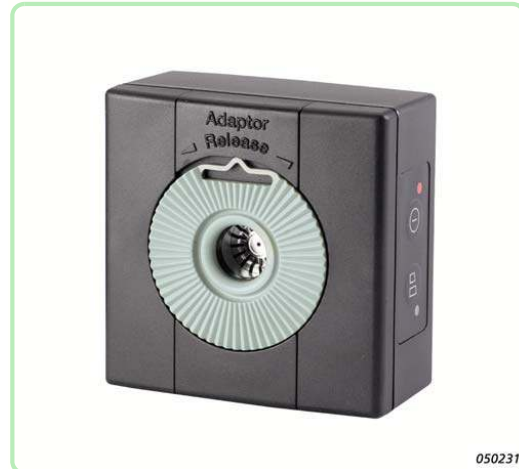
Brüel & Kjær 



PRODUCT DATA

Sound Calibrator Type 4231

Sound Calibrator Type 4231 is a handy, portable sound source for calibration of sound level meters and other sound measurement equipment. The calibrator is very robust and stable, and conforms to EN/IEC 60942 (2003) Class LS and Class 1, and ANSI S1.40–2006.



Uses and Features

Uses

- Calibration of sound level meters and other sound measurement equipment

Features

- Conforms to EN/IEC 60942 (2003) Class LS and Class 1, and ANSI S1.40–2006
- Robust, pocket-sized design with highly stable level and frequency
- Calibration accuracy ± 0.2 dB
- 94 dB SPL or 114 dB SPL for calibration in noisy environments
- Extremely small influence of static pressure and temperature
- Sound pressure independent of microphone equivalent volume
- 1 kHz calibration frequency for correct calibration level independent of weighting network
- Fits Brüel & Kjær 1" microphones (1/2", 1/4" and 1/8" microphones with adaptor)
- Switches off automatically when removed from the microphone

Brüel & Kjær 

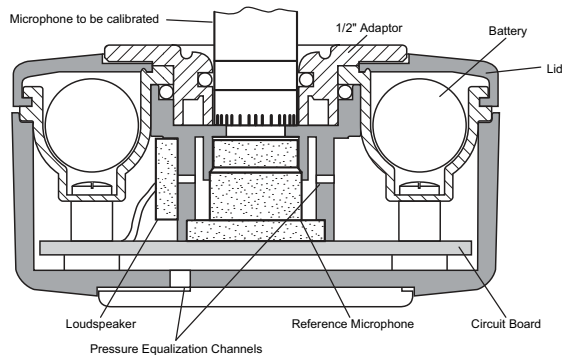
Sound Calibrator Type 4231

Sound Calibrator Type 4231 is a pocket-sized, battery operated sound source for quick and direct calibration of sound level meters and other sound measuring systems. It fits Brüel & Kjær 1" microphones and using the removable adaptor, 1/2" microphones. With optional adaptors, it can be used for 1/4" and 1/8" microphones as well.

The calibration frequency is 1000 Hz (the reference frequency for the standardized international weighting networks), so the same calibration value is obtained for all weighting networks (A, B, C, D and Linear). The calibration pressure of 94 ± 0.2 dB re 20 Pa is equal to 1 Pa or 1 N/m^2 . The +20 dB level step gives 114 dB SPL, which is convenient for calibration in noisy environments, or for checking linearity.

The design of Type 4231 is based on a feed-back arrangement to ensure a highly stable sound pressure level and ease of use. The feed-back loop uses a condenser microphone (see Fig. 1), which is specially developed for this purpose.

Fig. 1
Cross-sectional view of Sound Calibrator Type 4231. The feed-back loop is based on a high-quality condenser microphone to ensure a very stable sound pressure level



This microphone is optimized to have extremely high stability and independence of variations in static pressure and temperature around the 1 kHz calibration frequency. The result of this is a user-friendly calibrator where exact fitting of the microphone is not critical and the effects of changes in temperature and static pressure are negligible.

Fig. 2
Type 4231 fitted to Hand-held Analyzer Type 2250. The calibrator's centre of gravity is positioned very close to the microphone, giving a stable set-up




The calibrator gives a continuous sound pressure level when fitted on a microphone (see Fig. 2) and activated.

The sensitivity of the sound measuring equipment can then be adjusted until it indicates the correct sound pressure level.

The calibrator is automatically switched off when removed from the microphone.

A leather protection case, which does not need to be removed to use the calibrator, is supplied.

Compliance with Standards

	<p>The CE marking is the manufacturer's declaration that the product meets the requirements of the applicable EU directives RCM mark indicates compliance with applicable ACMA technical standards – that is, for telecommunications, radio communications, EMC and EME China RoHS mark indicates compliance with administrative measures on the control of pollution caused by electronic information products according to the Ministry of Information Industries of the People's Republic of China WEEE mark indicates compliance with the EU WEEE Directive</p>
Safety	<p>EN/IEC 61010-1: Safety requirements for electrical equipment for measurement, control and laboratory use. ANSI/UL 61010-1: Safety requirements for electrical equipment for measurement, control and laboratory use.</p>
EMC Emission	<p>EN/IEC 61000-6-3: Generic emission standard for residential, commercial and light industrial environments. EN/IEC 61000-6-4: Generic emission standard for industrial environments. CISPR 22: Radio disturbance characteristics of information technology equipment. Class B Limits. FCC Rules, Part 15: Complies with the limits for a Class B digital device. EN/IEC 60942: Instrumentation Standard – Electroacoustics – Sound Calibrators.</p>
EMC Immunity	<p>EN/IEC 61000-6-1: Generic standards – Immunity for residential, commercial and light industrial environments. EN/IEC 61000-6-2: Generic standards – Immunity for industrial environments. EN/IEC 61326: Electrical equipment for measurement, control and laboratory use – EMC requirements. EN/IEC 60942: Instrumentation Standard – Electroacoustics – Sound Calibrators. Note: The above is only guaranteed using accessories listed in this Product Data sheet.</p>
Temperature	<p>IEC 60068-2-1 & IEC 60068-2-2: Environmental Testing. Cold and Dry Heat. Operating Temperature: -10 to +50 C (14 to 122 F) Storage Temperature: -25 to +70 C (-13 to +158 F)</p>
Humidity	<p>IEC 60068-2-78: Damp Heat: 90% RH (non-condensing at 40 C (104 F)).</p>
Mechanical	<p>Non-operating: IEC 60068-2-6: Vibration: 0.3 mm (10 to 58 Hz), 20 m/s² (58–500 Hz) IEC 60068-2-27: Shock: 1000 m/s² IEC 60068-2-29: Bump: 3000 bumps at 400 m/s²</p>
Enclosure	<p>IEC 60529: Protection provided by enclosures: IP 50 with leather protection case.</p>

Specifications – Sound Calibrator Type 4231

STANDARDS SATISFIED

EN/IEC 60942 (2003), Class LS and Class 1, Sound Calibrators
 ANSI S1.40 – 2006, Specification for Acoustic Calibrators Class LS and Class 1

SOUND PRESSURE LEVELS

94.0 dB ±0.2 dB (Principal SPL) or
 114.0 dB ±0.2 dB re 20 Pa at reference conditions

FREQUENCY

1 kHz ±0.1%

SPECIFIED MICROPHONE

Size according to IEC 61094-4:

- 1" without adaptor
- 1/2" with adaptor UC 0210 (supplied)
- 1/4" with adaptor DP 0775 (optional)
- 1/8" with adaptor DP 0774 (optional)

EQUIVALENT FREE-FIELD LEVEL

(0 incidence, re Nominal Sound Pressure Level)
 -0.15 dB for 1/2" Brüel & Kjær microphones. See the Type 4231 User Manual for other microphones

EQUIVALENT RANDOM INCIDENCE LEVEL

(re Nominal Sound Pressure Level)
 +0.0 dB for 1", 1/2", 1/4" and 1/8" Brüel & Kjær microphones

NOMINAL EFFECTIVE COUPLER VOLUME

> 200 cm³ at reference conditions

DISTORTION

< 1%

LEVEL STABILITY

Short-term: Better than 0.02 dB (as specified in IEC 60942)

One Year: Better than 0.05 dB ($\sigma = 96\%$)

Stabilization Time: < 5 s

REFERENCE CONDITIONS

Temperature: 23 C ±3 C (73 ±5 F)

Pressure: 101 ±4 kPa

Humidity: 50%, -10% +15% RH

Effective Load Volume: 0.25 cm³

ENVIRONMENTAL CONDITIONS

Pressure: 65 to 108 kPa

Humidity: 10 to 90% RH (non-condensing)

Effective Load Volume: 0 to 1.5 cm³

INFLUENCE OF ENVIRONMENTAL CONDITIONS (Typical)

Temperature Coefficient: ±0.0015 dB/ C

Pressure Coefficient: +8 × 10⁻⁴ dB/kPa

Humidity Coefficient: 0.001 dB/% RH

POWER SUPPLY

Batteries: 2 × 1.5 V IEC Type LR6 ("AA" size)

Lifetime: Typically 200 hours continuous operation with alkaline batteries at 23 C (73 F)

Battery Check: When Type 4231 stops working continuously, and only operates when the On/Off button is held in, the batteries should be replaced

DIMENSIONS AND WEIGHT

(Without case)

Height: 40 mm (1.5")

Width: 72 mm (2.8")

Depth: 72 mm (2.8")

Weight: 150 g (0.33 lb), including batteries

Note: All values are typical at 25 C (77 F), unless measurement uncertainty or tolerance field is specified. All uncertainty values are specified at 2σ (that is, expanded uncertainty using a coverage factor of 2)

Ordering Information

Type 4231 Sound Calibrator

includes the following accessories:

- KE-0317: Leather Case
- 2 × QB-0013: Alkaline Battery Type LR6
- UC-0210: Adaptor for 1/2" microphones

Optional Accessories

DP-0775 Adaptor for 1/4" microphones

DP-0774 Adaptor for 1/8" microphones

DP-0887 Adaptor for Head and Torso Simulator Type 4128

Brüel & Kjær reserves the right to change specifications and accessories without notice. © Brüel & Kjær. All rights reserved.

HEADQUARTERS: Brüel & Kjær Sound & Vibration Measurement A/S · DK-2850 Nærum · Denmark
Telephone: +45 7741 2000 · Fax: +45 4580 1405 · www.bksv.com · info@bksv.com

Local representatives and service organisations worldwide

Brüel & Kjær 

BP1311-17 2014-04



Product Data



Falcon™ Range 1/2" Microphone Preamplifier — Type 2669

USES:

- Sound measurements with Brüel & Kjær 1/2" (1", 1/4" and 1/8" with adaptor) and compatible microphones
- General-purpose preamplifier and high-impedance input probe for Brüel & Kjær measuring instruments

FEATURES:

- Full electromagnetic compatibility (EMC)
- Detachable, thin cable for easy installation

- Compact LEMO connector at preamplifier
- Patented charge-injection calibration technique for on-site calibration of the whole measuring channel including the microphone
- Wide dynamic range
- Very low inherent noise, high input impedance
- Low output impedance and high output current allows use with long extension cables
- Wide working temperature range
- Falcon™ Range product with a three-year guarantee

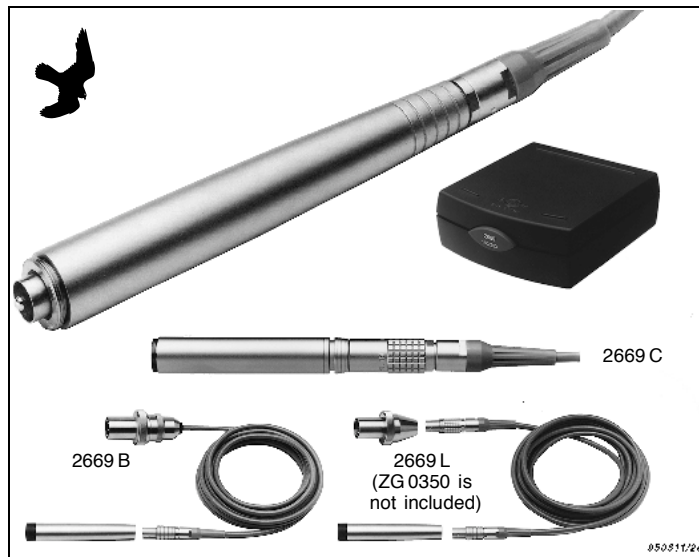
1/2" Microphone Preamplifier Type 2669 is a Falcon™ Range product for making precision acoustic measurements with Brüel & Kjær's wide range of condenser microphones. You can connect 1/2" microphones directly and 1", 1/4" and 1/8" types using adaptors. The preamplifier, cable and its connectors all fulfil EMC requirements. You can verify the condition of the microphone, preamplifier and cable on-site using its patented charge-injection calibration technique. The preamplifier's low output impedance allows the use of long extension cables without problems.

Description

This 1/2" Falcon™ Range microphone preamplifier operates over a wide range of temperature, humidity and other environmental conditions. It is available in three versions: the cylindrical Type 2669 C and the conical Types 2669 L and 2669 B. Apart from the shape of the housing, the only difference is the connectors. The conical form is optimized with respect to acoustical properties, whereas the cylindrical form will fit existing specialized holders.

The preamplifier has a very high input impedance presenting virtually no load to the microphone. The high output voltage together with an extremely low inherent noise level gives a wide dynamic range.

The low output impedance and high output current capability means



that you can use long cables between the preamplifier and your measuring instrument without loss of signal quality. Furthermore, this Falcon™ Range microphone preamplifier comes with an extended guarantee period of three years. It is supplied in an elegant and strong plastic box made from recyclable materials.

EMC Certification

The preamplifier complies with EMC (electromagnetic compatibility) requirements specified in EN 50082-1 (residential, commercial and light in-

dustry) as well as in EN 50082-2 (industrial environment). These are generic European standards for electrical noise immunity, to ensure that instruments do not interfere with each other. To get the full benefit of this certification, the preamplifier must be connected to an instrument which also complies with EMC requirements.

Charge-injection Calibration

This is a patented technique for verifying the entire measurement set-up

including the microphone, preamplifier and connecting cable (see box below).

Microphones and Sockets

You can fit 1/2" microphones directly and 1", 1/4" and 1/8" microphones using adaptors DB 0375, UA0035 and UA0036 respectively.

Preamplifier Type 2669 L is delivered with a cable which fits the LEMO preamplifier input socket on new Brüel & Kjær instruments (as well as instruments from Hewlett-Packard and Nortronic). Adaptor ZG 0350 is available for converting it to traditional 7-pin Brüel & Kjær preamplifier sockets. Alternatively, Type 2669 B is available for direct use with traditional Brüel & Kjær instruments. This cable has the same diameter and flexibility, but is equipped with a traditional Brüel & Kjær plug. Both types are fitted with a LEMO 0B connector at the preamplifier.

In contrast the cylindrical Type 2669 C is fitted with a LEMO 1B connector, which means that it can be connected directly to LEMO to LEMO extension cables. Type 2669 C is supplied without a cable.

Power Supply

You can use a dual (plus/minus) or single power supply for the preamplifier. When using a balanced power supply, the offset voltage at the output — and at the preamplifier guard ring — will be almost zero. This protects you against harmless, but unpleasant, electrical shocks if you accidentally mount or remove the microphone with power on, and gives a faster stabilisation time for a measurement set-up.

Detachable Cable (2669L and B)

The 4 mm thick connecting cable is made of silicone and is very flexible. It has a wide working temperature range (-60°C to 150°C). It has a small high-quality connector at the preamplifier end for easy detachment during installation.

Accessories

In addition to the previously mentioned adaptors for 1", 1/4" and 1/8" microphones, other useful accessories are available. The Coaxial Input Adaptor JJ 2617 is used for measuring electrical signals by connecting the preamplifier directly to cables with microplugs (Cables AO0038, AO0122). The Flexible Extension Rod UA0196 gives directional flexi-

bility to the microphone and increases the distance between the microphone and the preamplifier. This allows continuous exposure of the microphone to high temperatures (up to 150°C, 302°F) while avoiding electrical noise otherwise generated by the preamplifier at high temperatures. For short periods the UA0196 tolerates temperatures up to 300°C (572°F). Microphone Holder UA 1317 is used for mounting the preamplifier on a tripod without compromising the acoustical properties of the preamplifier. It can hold all Brüel & Kjær 1/2" preamplifiers. Adaptor DP 0901 is supplied with the preamplifier for use with holders that require a cylindrical shaped preamplifier.

Characteristics

The small and large signal frequency response of the preamplifier depend on the capacitance of the microphone connected to its input and the capacitive load (for example, extension cables) connected to the output.

Small Signal Frequency Response

The curves in Fig. 1 show the low-frequency response of the preamplifier.

Brüel & Kjær's Patented Charge-injection Calibration Technique

The Charge-injection Calibration (CIC) technique is a method for remotely verifying the condition of the entire measurement set-up including the microphone. This is a great improvement over the traditional insert-voltage calibration method which virtually ignores the state of the microphone. The CIC technique is very sensitive to any change in the microphone's capacitance which is a reliable

indicator of the microphone's condition.

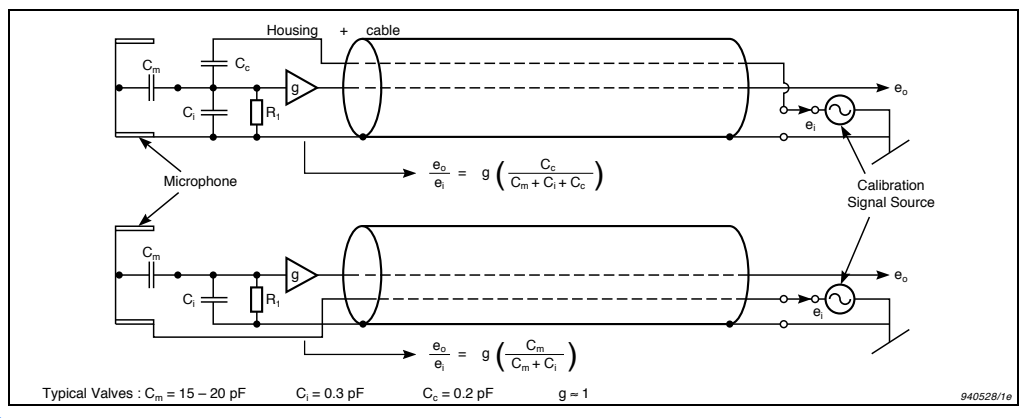
The technique works by introducing a small but accurately defined capacitance C_c (typically 0.2 pF) with a very high leakage resistance (greater than 50000 GΩ) into the circuit of the preamplifier, see below (upper diagram). C_i and R_i represent the preamplifier's high input impedance and g its gain (≈ 1).

For a given calibration signal e_i , the output e_o of this arrangement will change measurably, even for small changes in the microphone's capacitance C_m . The CIC technique is about 100 times more sensi-

tive than the insert-voltage calibration arrangement shown in the lower diagram.

In the extreme case where there is significant leakage between the microphone's diaphragm and its backplate (C_m becomes very large), the signal output will change by tens of decibels compared with only tenths of a decibel using the insert-voltage method.

Another important CIC feature is that, unlike the insert-voltage technique, it is far less sensitive to external electrical fields.



er for various microphone capacitances. These capacitances (47 pF, 15 pF and 6.2 pF) are typical for 1", 1/2" and 1/4" microphones respectively. Note that they do not show or take into account the lower cut-off frequencies of the microphones. The effects of various capacitive output loads (cable length) on the high-frequency response are also shown. The curves in Fig.1 apply for signal levels within the large signal limits in Table 2.

Large Signal Frequency Response

The capacitive load of extension cables on the output of the preamplifier influences its frequency response and available output voltage. If the specified maximum output current of the preamplifier is exceeded, the signal will be distorted. The curves in Fig.2 show the upper distortion limits (3%) as a function of preamplifier output voltage, frequency and capacitive loading (cable length). The curves are shown for total supply voltages of 120 VDC and 28 VDC (± 60 VDC and ± 14 VDC dual supply voltages respectively).

Noise

Fig.3 shows typical noise frequency spectra when loading the preamplifier with 6.4 pF and 15 pF microphone capacities. The low noise of the preamplifier ensures that the noise floor for a microphone/preamplifier assembly is determined mainly by the associated microphone over most of the frequency range. The preamplifier can work at temperatures up to 150°C, but reduced specifications for noise and output capability will apply.

More information on preamplifiers and other Falcon™ Range products are given in the Microphone Handbook BA5105.

Extension Cables

Extension Cable	AO0414/15 /16	AO 0027	AO 0028/29
Connectors	LEMO	Brüel & Kjær	
Length	3/10/30 m	3 m	10/30 m
Diameter	4 mm	6 mm	9 mm
Capacitance	290/960 /2900 pF	300 pF	570/ 1700 pF

Table 1 Extension cables

All the extension cables with LEMO connectors (see Table 1) are fully EMC certified. The preamplifier can be used with traditional cables with Brüel & Kjær connectors, but EMC compatibility is not guaranteed. The

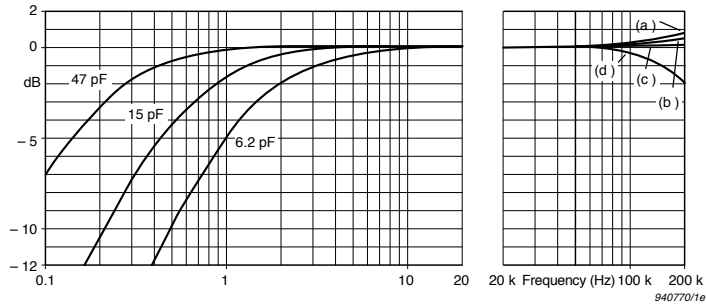


Fig.1 Small signal frequency response of the preamplifier at low frequencies for various microphone capacitances and at high frequencies for various capacitive loads which are (a) 10 nF (b) 3 nF (c) with the 3 m cable supplied (d) 30 nF

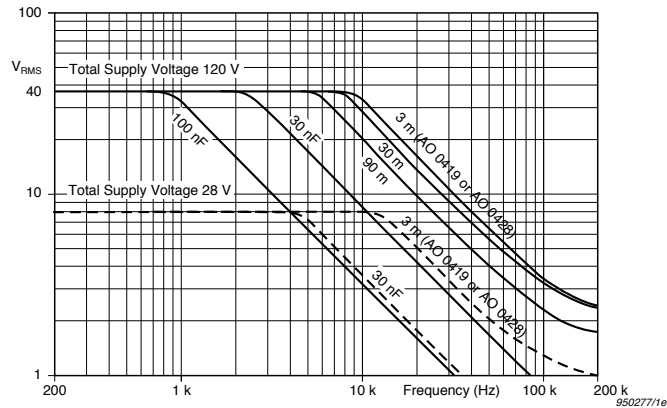


Fig.2 Upper distortion limit (3%) as a function of preamplifier output voltage and frequency for various capacitive loads. The full-drawn curves are valid for a preamplifier powered with 120 VDC (± 60 VDC) and the dotted curves are for 28 VDC (± 14 VDC)

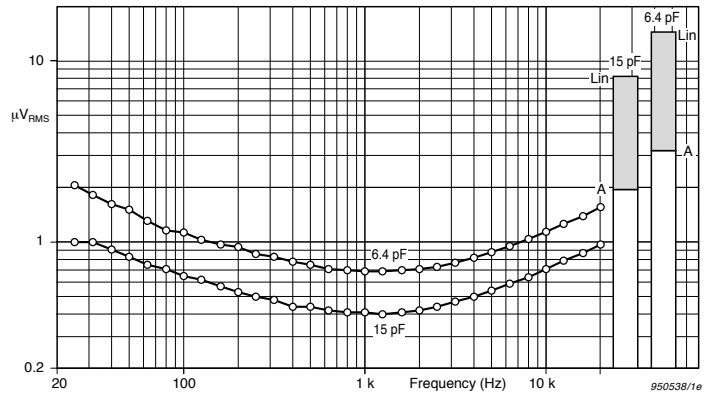


Fig.3 Typical noise frequency spectra in μ V measured with 6.4 pF and 15 pF microphone capacities. The spectra are measured in 1/3-octave bands with levels at centre frequencies indicated by circles. The bar graphs represent broad-band (22.4 Hz to 300 kHz) and A-weighted noise levels for both microphone capacities

cables in Table 1 have a working temperature range from -20 to $+80^\circ\text{C}$. They are very robust, have low capacitance and extremely good shield-

ing so that several of them can be connected in series without loss of signal quality.

Specifications 2669

FREQUENCY RESPONSE (re 1 kHz):

3 Hz to 200 kHz, ±0.5 dB. See Fig. 1

ATTENUATION: 0.35 dB (max.)

PHASE LINEARITY:

±3° from 20 Hz to 100 kHz

PHASE MATCHING: 0.3° at 50 Hz

INPUT IMPEDANCE: 15 GΩ || 0.45 pF

OUTPUT IMPEDANCE: 25 Ω (max.)

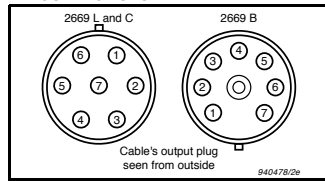
CONNECTOR TYPE:

LEMO type FGJ.OB.307 at preamp. (2669 L & B)

LEMO type FGG.1B.307 (2669 L), or Brüel & Kjør JP0715 (2669 B) to measuring device

LEMO type FWG.1B.307 at preamp. (2669 C)

PIN CONNECTIONS:



Pin	LEMO (L & C)	Brüel & Kjør (B)
1	Calibration input	Ground
2	Signal ground	Pol. voltage
3	Pol. voltage	Calibration input
4	Signal output	Signal output
5	Not connected	Power supply positive
6	Power supply positive	Not connected
7	Power supply negative/ground	Not connected
Casing	Connected to instrument chassis	

MAX. OUTPUT CURRENT: 20 mA (peak)

Note: The max. output current can be limited by the power supply

CURRENT CONSUMPTION: 3 mA plus output current

MAX. OUTPUT VOLTAGE:

Maximum output voltage V_{p-p} is equal to total supply voltage minus 10 V

OUTPUT SLEW RATE: 2 V/μs

DISTORTION (THD):

Less than -80 dB at 25 V out, 1 kHz

NOISE:

≤ 8.2 μV Lin. 20 Hz - 300 kHz

≤ 10.0 μV Lin. 20 Hz - 300 kHz (max.)

≤ 1.9 μV A weighted

≤ 2.2 μV A weighted (max.)

POWER SUPPLY, DUAL: ±14 V to ±60 V

POWER SUPPLY, SINGLE: 28 V to 120 V

OUTPUT DC OFFSET:

= 1 V for a dual supply, or

= 1/2 the voltage of a single supply

CALIBRATION INPUT:

Charge insert capacity: 0.2 pF

Max. 10 V RMS, input impedance: 1 nF

DIMENSIONS:

Diameter: 12.7 mm (0.5")

Length: 110 mm (4.3"), (2669 L and B)

120 mm (4.7"), (2669 C)

Weight: 40 g (1.41 oz) (preamplifier only)

Note: All values are typical at 25°C (77°F), unless measurement uncertainty is specified. All uncertainty values are specified at 2σ (i.e. expanded uncertainty using a coverage factor of 2). The above are valid for 15 pF mic. capacitance and a 3 metre cable unless otherwise specified.

COMPLIANCE WITH STANDARDS:

	CE-mark indicates compliance with: EMC Directive and Low Voltage Directive.
Safety	EN 61010-1 and IEC 1010-1: Safety requirements for electrical equipment for measurement, control and laboratory use.
EMC Immunity	EN 50082-1: Generic immunity standard. Part 1: Residential, commercial and light industry. EN 50082-2: Generic immunity standard. Part 2: Industrial environment. Note: The above is guaranteed only with extension cables AO 0414, AO 0415 and AO 0416.
Temperature	IEC 68-2-1 & IEC 68-2-2: Environmental Testing. Cold and Dry Heat. Operating Temperature: -20 to +60°C (-4 to +140°F), (150°C (302°F) with increase in noise) Storage Temperature: -25 to +70°C (-13 to +158°F)
Humidity	IEC 68-2-3: 95% RH (non-condensing at 40°C (104°F))
Enclosure	IEC 529: IP 20
Mechanical	Non-operating: IEC 68-2-6: Vibration: 0.3 mm, 20 m/s ² , 10-500 Hz IEC 68-2-27: Shock: 1000 m/s ² IEC 68-2-29: Bump: 4000 bumps at 400 m/s ²
Reliability	MI-HDBK 217F, GB (Part-Stress): MTBF >40000 hours (max. 2.5% errors/1000 h)

Charge Injection Calibration Technique patented according to US Patent No. 5,400,297. The patent includes the measurement method and its implementation.

Ordering Information

Type 2669 L 1/2" Microphone Preamplifier (LEMO connector)

Includes the following accessories:

DP 0901: 1/2" Cylindrical Adaptor
AO 0419: Microphone Cable 3 m (9.8 ft.) or as a special order:

EL 4006-AC 0219-x: Microphone Cable length x m (specified by customer)

Type 2669 B 1/2" Microphone Preamplifier (Brüel & Kjør connector)

Includes the following accessories:

DP 0901: 1/2" Cylindrical Adaptor
AO 0428: Microphone Cable 3 m (9.8 ft.) or as a special order:

EL 4005-AC 0219-x: Microphone Cable length x m (specified by customer)

Type 2669 C 1/2" Microphone Preamplifier (no cable included)

Optional Accessories

ZG 0350: LEMO to 7-pin Brüel & Kjør adaptor

JJ 2617: Input Adaptor (51 pF). Is screwed directly onto a preamplifier for connection to microplug cables

UA 0196: Flexible Extension Rod

DB 0375: 1/2" to 1" Adaptor

UA 0035: 1/2" to 1/4" Adaptor

UA 0036: 1/2" to 1/8" Adaptor

UA 1317: 1/2" Microphone Holder

BA 5105: Microphone Handbook

WB 0850: Insert Junction Adaptor for Type 2669 B/2669 L with Adaptor ZG 0350. For Charge-injection Calibration

Extension Cables

LEMO to LEMO:

AO 0414: 3 m (9.8 ft.)

AO 0415: 10 m (32.8 ft.)

AO 0416: 30 m (98.4 ft.)

EL 4004-AC 0079-x: Length x m (specified by customer)

AR 0014: Flat Cable, 0.5 m (1.64 ft)

Brüel & Kjør reserves the right to change specifications and accessories without notice

Brüel & Kjør

WORLD HEADQUARTERS:

DK-2850 Naerum · Denmark · Telephone: +45 45 80 05 00 · Fax: +45 45 80 14 05 · Internet: <http://www.bk.dk> · e-mail: info@bk.dk

Australia (02) 9450-2066 · Austria 00 43-1-865 74 00 · Belgium 016/44 92 25 · Brazil (011) 246-8166 · Canada: (514) 695-8225 · China 10 6841 9625 / 10 6843 7426

Czech Republic 02-67 021100 · Finland 90-229 3021 · France (01) 69 90 69 00 · Germany 0610 3/908-5 · Holland (030) 6039994 · Hong Kong 254 8 7486

Hungary (1) 215 83 05 · Italy (02) 57 60 4141 · Japan 03-3779-8671 · Republic of Korea (02) 3473-0605 · Norway 66 90 4410 · Poland (0-22) 40 93 92 · Portugal (1) 47114 53

Singapore (65) 275-8816 · Slovak Republic 07-37 6181 · Spain (91) 36810 00 · Sweden (08) 71127 30 · Switzerland 01/94 0 09 09 · Taiwan (02) 713 9303

United Kingdom and Ireland (0181) 954-236 6 · USA 1 - 800 - 332 - 2040

Local representatives and service organisations worldwide

BP 1422-13

96/09

PRODUCT DATA

TEDS Microphones

A TEDS (Transducer Electronic Data Sheet) microphone is a cartridge and a preamplifier assembled and sealed in a clean environment. The assembly has one type and serial number. Individual TEDS microphone information is programmed in a data chip inside the preamplifier. TEDS microphones are available with CCLD as well as classical preamplifiers. TEDS is standardized in compliance with IEEE 1454.4.



Uses and Features

Uses

- General sound measurements
- Measurement of dynamic pressure fluctuations

Features

- Plug-and-play
- Frequency: 1 Hz to 180 kHz
- Dynamic Range: 6.5 dB to 192 dB

Brüel & Kjær's TEDS Microphones

TEDS Microphone Benefits

The most important benefit of a TEDS microphone is that the actual identity and loaded sensitivity of the cartridge are programmed in the TEDS and thereby readily available for documentation and application purposes. For many Brüel & Kjær TEDS microphones, the individual frequency response is stored on a mini-CD under the S/N ratio of the microphone. During the manufacturing process the unit is sealed in a clean environment, thus eliminating contamination that could later result in reduced performance.

TEDS Templates

All Brüel & Kjær TEDS microphones, except Types 4957, 4958 and 4959, use a template that complies with IEEE P1454.4 V 0.9. A mapping that complies with IEEE 1454.4 V 1.0 is available free of charge for new TEDS microphones.

Data Transmission

Generally, there are two ways that data from the TEDS chip can be transmitted to the analyzer. The simpler way, class 2, uses a separate wire to transmit the data. For classical, LEMO type TEDS preamplifiers, pin 5 is often used for TEDS data transmission. In single-wire systems, like that used with CCLD, the same conductor is used both for signal and data transmission. This is made possible by using an electronic switch to control the mode of the wire (TEDS data or signal mode).

Selecting the Right TEDS Microphone

Brüel & Kjær offers a wide range of TEDS microphones, most of which are based on combined cartridges and preamplifiers that are available as individual units. The first selection criterion is often determined by the front-end input type: classical or CCLD. The second criterion can be the type of sound field for which the microphone is optimized.

Customer-specific TEDS Microphones

Customer-specific solutions can be made, so if you do not see what you are looking for please ask your local Brüel & Kjær sales office for a quote on a customized solution.

Common Specifications

The following pages contain short-form data for the TEDS microphones offered by Brüel & Kjær. For detailed specifications, please see the individual Product Data. Unless otherwise stated all specifications in this Product Data are valid under the following conditions:

CCLD Input Types	24 V compliance voltage
Classical Input Types	120 V _{DC} supply
Dynamic Range Low Limit	Noise floor dB A
Dynamic Range High Limit	3% distortion limit in dB SPL RMS rounded to nearest integer The undistorted peak level will normally be 3 dB higher
Cartridge Sensitivity	Nominal
TEDS Microphone Sensitivity	Stated as the nominal cartridge sensitivity except for small cartridges where the loaded sensitivity differs considerably from the open-circuit sensitivity

Most microphones come with an individual data CD and a calibration chart that includes the typical frequency response. Any microphones that do not include a CD and/or frequency response graph are noted below under each table.

Temperature Range

The read/write temperature range of the TEDS chip is guaranteed by the chip manufacturer up to 85 °C (185 °F) only, but the TEDS chip will survive the full specified temperature range of the TEDS microphone/preamplifier without any damage.

Standard preamplifier Types 2669, 2670, 2671 and 2699 go to 80 °C (176 °F). High-temperature preamplifier Type 1706 goes to 125 °C (257 °F). Remember also to use cables with the correct temperature range.

Cable Length

TEDS will normally work with cables up to 100 m (328 ft).

Sound Field

In the sections that follow, the microphone specifications are organized by the type of sound field that the microphones are designed to measure.

Free-field TEDS Microphones

Free-field microphones are designed to have a flat frequency response in a free field. At higher frequencies, reflections and diffractions cause a pressure increase in front of the diaphragm. If not corrected for, this would result in an increased output voltage from the microphone. Free-field optimization means that the frequency response of the microphone has been designed in such a way that a flat free-field frequency response at 0° angle of incidence is achieved.

Free-field microphones are commonly used for sound measurement in an anechoic chamber or far away from reflecting buildings, etc. Another application area for free-field microphones is general electroacoustic purposes, like loudspeaker and microphone measurements.

Table 1 Free-field TEDS microphones with Type 4188 ½" cartridge

Input	Microphone	Preamplifier	mV/Pa	dB re 1 V/Pa	±2 dB Frequency Range (Hz)	Dynamic Range (dB)
Classical	Type 4188-C/L-001	Type 2669-C/L	31.6	-30	8 to 12.5 k	15.8 to 146
CCLD	Type 4188-A-021	Type 2671	31.6	-30	20 to 12.5 k	19 to 138

Type 4188 is suited for free-field measurements where an extra-robust prepolarized microphone with medium sensitivity is required
Type 4188 TEDS microphones do not come with a data CD nor with typical frequency response on the calibration chart

Table 2 Free-field TEDS microphones with Type 4189 ½" cartridge

Input	Microphone	Preamplifier	mV/Pa	dB re 1 V/Pa	±2 dB Frequency Range (Hz)	Dynamic Range (dB)
Classical	Type 4189-B/C/L-001	Type 2669-B/C/L	50	-26	6.3 to 20 k	15.2 to 146
CCLD	Type 4189-A-021	Type 2671	50	-26	20 to 20 k	16.5 to 134
CCLD	Type 4189-A-031	Type 2699	50	-26	A-weighted*	18 to 131
CCLD	Type 4189-W-003	Type 2671-W-001	50	-26	6.3 to 20 k	16.5 to 134
CCLD	Type 4189-H-041	Type 1706	50	-26	6.3 to 20 k	16.5 to 134

Type 4189 is suited for free-field measurements where a high-sensitivity prepolarized microphone with full 20 kHz bandwidth is preferred
*For more information on A-weighting, see Type 2699 Product Data BP2009

Table 3 Free-field TEDS microphones with Type 4190 ½" cartridge

Input	Microphone	Preamplifier	mV/Pa	dB re 1 V/Pa	±2 dB Frequency Range (Hz)	Dynamic Range (dB)
Classical	Type 4190-B/C/L-001	Type 2669-B/C/L	50	-26	3.15 to 20 k	15 to 148

Type 4190 is designed for free-field measurements where a high-sensitivity externally polarized microphone with full 20 kHz bandwidth is preferred

Table 4 Free-field TEDS microphones with Type 4191 ½" cartridge

Input	Microphone	Preamplifier	mV/Pa	dB re 1 V/Pa	±2 dB Frequency Range (Hz)	Dynamic Range (dB)
Classical	Type 4191-B/C/L-001	Type 2669-B/C/L	12.5	-38	3.15 to 40 k	21.4 to 162

Type 4191 is designed for free-field measurements where a wideband externally polarized microphone is required

Table 5 Free-field TEDS microphones with Type 4939 ½" cartridge

Input	Microphone	Preamplifier	mV/Pa	dB re 1 V/Pa	±2 dB Frequency Range (Hz)	Dynamic Range (dB)
Classical	Type 4939-A-011	Type 2670	4	-48	4 to 100 k	35 to 164
Classical	Type 4939-C/L-002	Type 2669-C/L with UA-0035	3.5	-49	4 to 100 k	35 to 164

Type 4939 is designed for free-field measurements where a high-frequency, high-level externally polarized microphone is required

Table 6 Free-field TEDS microphones with Type 4954 ¼" cartridge

Input	Microphone	Preamplifier	mV/Pa	dB re 1 V/Pa	±2 dB Frequency Range (Hz)	Dynamic Range (dB)
Classical	Type 4954-A-011	Type 2670	2.8	-51	3 to 80 k	34 to 164
CCLD	Type 4954-A	Integral with SMB	2.8	-51	16 to 80 k	40 to 159
CCLD	Type 4954-B	Integral with 10-32 UNF	2.8	-51	16 to 80 k	40 to 159

Type 4954 is designed for free-field measurements where a high-frequency, high-level prepolarized microphone is required

Table 7 Free-field TEDS microphones with Type 4966 ½" cartridge

Input	Microphone	Preamplifier	mV/Pa	dB re 1 V/Pa	±2 dB Frequency Range (Hz)	Dynamic Range (dB)
CCLD	Type 4966-H-041	Type 1706	50	-26	6.3 to 20 k	16.5 to 134

Type 4966 is suited for free-field measurements where a high-sensitivity prepolarized microphone with full 20 kHz bandwidth is preferred

Pressure-field TEDS Microphones

Pressure-field microphones are optimized to have a flat frequency response in a pressure field. They are used for measurements in small, closed couplers or close to hard, reflective surfaces.

Table 8 Pressure-field TEDS microphones with Type 4192 ½" cartridge

Input	Microphone	Preamplifier	mV/Pa	dB re 1 V/Pa	±2 dB Frequency Range (Hz)	Dynamic Range (dB)
Classical	Type 4192-B/C/L-001	Type 2669-B/C/L	12.5	-38	3.15 to 20 k	20.7 to 162

Type 4192 is designed for pressure-field measurements where a high-sensitivity externally polarized microphone with full 20 kHz bandwidth is preferred

Table 9 Repolarized pressure-field TEDS microphones with Type 4956 ¼" cartridge

Input	Microphone	Preamplifier	mV/Pa	dB re 1 V/Pa	±2 dB Frequency Range (Hz)	Dynamic Range (dB)
CCLD	Type 4956-W-001	Type 2671-W-001	12.5	-38	3.5 to 20 k	26.5 to 135

Type 4956 is designed for pressure-field measurements where a high-frequency, high-level externally polarized microphone is required

Table 10 Pressure-field TEDS microphones with Type 4938 ¼" cartridge

Input	Microphone	Preamplifier	mV/Pa	dB re 1 V/Pa	±2 dB Frequency Range (Hz)	Dynamic Range (dB)
Classical	Type 4938-A-011	Type 2670	1.4	-57	4 to 70 k	42 to 172
Classical	Type 4938-B/C/L-002	Type 2669-B/C/L with UA-0035	1.4	-57	4 to 70 k	42 to 172

Type 4938 is designed for pressure-field measurements where a high-frequency, high-level externally polarized microphone is required

Table 11 Pressure-field TEDS microphones with Type 4944 ¼" cartridge

Input	Microphone	Preamplifier	mV/Pa	dB re 1 V/Pa	±2 dB Frequency Range (Hz)	Dynamic Range (dB)
Classical	Type 4944-A	Integral with SMB	0.9	-61	16 to 70 k	48 to 169
Classical	Type 4944-B	Integral with 10-32 UNF	0.9	-61	16 to 70 k	48 to 169

Type 4944 is designed for pressure-field measurements where a high-frequency, high-level prepolarized microphone is required

Table 12 Pressure-field TEDS microphones with Type 4138 1/8" cartridge

Input	Microphone	Preamplifier	mV/Pa	dB re 1 V/Pa	±2 dB Frequency Range (Hz)	Dynamic Range (dB)
Classical	Type 4138-A-015	Type 2670 with UA-0160	0.56	-65	6.5 to 140 k	52.2 to 168
Classical	Type 4138-B/C/L-006	Type 2669-B/C/L with UA-0036	0.8	-62	6.5 to 140 k	52.2 to 168

Type 4138 is designed for pressure-field measurements where an absolute maximal frequency range is required. This microphone is externally polarized. Type 4138 TEDS microphones do not come with a data CD nor with typical frequency response on the calibration chart.

Diffuse-field TEDS Microphones

Diffuse-field microphones, also called random-incidence microphones, are designed to have a flat response to signals arriving simultaneously from all directions – that is, a random or diffuse field. They should be used in all situations where the sound field is diffuse, and where several sources contribute to the sound pressure at the measurement position. Applications include indoor measurements where the sound is reflected by walls, ceilings and objects in the room, including in reverberation chambers, and in-cabin measurements.

Table 13 Diffuse-field TEDS microphones with Type 4942 1/2" cartridge

Input	Microphone	Preamplifier	mV/Pa	dB re 1 V/Pa	±2 dB Frequency Range (Hz)	Dynamic Range (dB)
Classical	Type 4942-B/C/L-001	Type 2669-B/C/L	50	-26	6.3 to 16 k	15.2 to 146
CCLD	Type 4942-A-021	Type 2671	50	-26	20 to 16 k	18 to 134
CCLD	Type 4942-A-031	Type 2699	50	-26	A-weighted	18 to 131
CCLD	Type 4942-H-041	Type 1706	50	-26	6.3 to 20 k	18 to 134

Type 4942 is designed for diffuse-field measurements where a high-sensitivity prepolarized microphone with wide bandwidth is preferred.

Table 14 Diffuse-field TEDS microphones with Type 4943 1/2" cartridge

Input	Microphone	Preamplifier	mV/Pa	dB re 1 V/Pa	±2 dB Frequency Range (Hz)	Dynamic Range (dB)
Classical	Type 4943-B/C/L-001	Type 2669-B/C/L	50	-26	3.15 to 10 k	15.9 to 148

Type 4943 is designed for diffuse-field measurements where a high-sensitivity externally polarized microphone is preferred.

Special TEDS Microphones

A number of special TEDS microphones are available:

- Infrasound Microphone Type 4193
- High-intensity Pressure-field Microphones Type 4941
- Aerospace Surface Microphone Type 4948
- Automotive Surface Microphone Type 4949
- Low-noise Free-field Microphone Type 4955
- Low-noise Free-field Microphone Type 4955-A, for hand-held analyzers such as Type 2250/2270
- 10 kHz Array Microphone Type 4957
- 20 kHz Array Microphone Type 4958
- Short 20 kHz Array Microphone Type 4959
- Multi-field Microphone Type 4961

Table 15 Special TEDS Microphones

Input	Microphone	Preamplifier	mV/Pa	dB re 1 V/Pa	±2 dB Frequency Range (Hz)	Dynamic Range (dB)
Classical	Type 4193-B/C/L-004	Type 2669-B/C/L with UC-0211	2	-54	0.1 to 20 k	29 to 148
Classical	Type 4941-A-011	Type 2670	0.08	-82	4 to 20 k	73.5 to 184
Classical	Type 4941-C-002	Type 2669-C with UA-0035	0.08	-82	4 to 20 k	75.8 to 184
Classical	Type 4955	Integral	1100	0.8	10 to 16 k	6.5 to 110
Classical	Type 4955-A	Integral	1100	0.8	10 to 16 k	6.5 to 110
CCLD	Type 4948	Integral	1.4	-57	5 to 20 k*	55 to 160
CCLD	Type 4949	Integral	11.2	-39	5 to 20 k*	30 to 140
CCLD	Type 4957	Integral	11.2	-39	50 to 10 k	32 to 134
CCLD	Type 4958	Integral	11.2	-39	10 to 20 k	28 to 140
CCLD	Type 4959	Integral	11.2	-39	50 to 20 k	32 to 134
CCLD	Type 4961	Integral	60	-24.5	12 to 20 k	20 to 130

* ±3 dB pressure response limits

Types 4941, 4957, 4958 and 4959 microphones do not come with an individual data CD nor with typical frequency response on the calibration chart

Ordering Information

If you do not see what you are looking for, please ask your local Brüel & Kjær sales office for a quote on a customized solution.

Order No.	Mini CD Incl.	Description
Type 4101-A	No	Binaural Microphone
Type 4138-A-015	No	Pressure-field 1/8" Mic. Type 4138, Preamp. Type 2670, Adaptor UA-0160
Type 4138-B-006*	No	Pressure-field 1/8" Mic. Type 4138, Preamp. Type 2669-B, Adaptor UA-0036
Type 4138-C-006	No	Pressure-field 1/8" Mic. Type 4138, Preamp. Type 2669-C, Adaptor UA-0036
Type 4138-L-006	No	Pressure-field 1/8" Mic. Type 4138, Preamp. Type 2669-L, Adaptor UA-0036
Type 4188-C-001	No	Prepolarized Free-field 1/2" Mic. Type 4188, Preamp. Type 2669-C
Type 4188-L-001	No	Prepolarized Free-field 1/2" Mic. Type 4188, Preamp. Type 2669-L
Type 4188-A-021	No	Prepolarized Free-field 1/2" Mic. Type 4188, Preamp. Type 2671
Type 4189-B-001*	Yes	Prepolarized Free-field 1/2" Mic. Type 4189, Preamp. Type 2669-B
Type 4189-C-001	Yes	Prepolarized Free-field 1/2" Mic. Type 4189, Preamp. Type 2669-C
Type 4189-L-001*	Yes	Prepolarized Free-field 1/2" Mic. Type 4189, Preamp. Type 2669-L
Type 4189-A-021	Yes	Prepolarized Free-field 1/2" Mic. Type 4189, Preamp. Type 2671
Type 4189-A-031	Yes	Prepolarized Free-field 1/2" Mic. Type 4189, Preamp. Type 2699
Type 4189-H-041	Yes	Prepolarized Free-field 1/2" Mic. Type 4189, Preamp. Type 1706
Type 4189-W-003	Yes	Prepolarized Free-field 1/2" Mic. Type 4189, Preamp. Type 2671-W-001
Type 4190-B-001*	Yes	Free-field 1/2" Mic. Type 4190, Preamp. Type 2669-B
Type 4190-C-001	Yes	Free-field 1/2" Mic. Type 4190, Preamp. Type 2669-C
Type 4190-L-001	Yes	Free-field 1/2" Mic. Type 4190, Preamp. Type 2669-L
Type 4190-L-002	Yes	Free-field 1/2" Mic. Type 4190, Preamp. Type 2669-L, Adaptor UA-1260
Type 4191-B-001*	Yes	Free-field 1/2" Mic. Type 4191, Preamp. Type 2669-B
Type 4191-C-001	Yes	Free-field 1/2" Mic. Type 4191, Preamp. Type 2669-C
Type 4191-L-001	Yes	Free-field 1/2" Mic. Type 4191, Preamp. Type 2669-L
Type 4192-B-001*	Yes	Pressure-field 1/2" Mic. Type 4192, Preamp. Type 2669-B
Type 4192-C-001	Yes	Pressure-field 1/2" Mic. Type 4192, Preamp. Type 2669-C
Type 4192-L-001	Yes	Pressure-field 1/2" Mic. Type 4192, Preamp. Type 2669-L
Type 4193-B-004*	Yes	Pressure-field 1/2" Mic. Type 4193, Preamp. Type 2669-B, Adaptor UC-0211
Type 4193-C-004	Yes	Pressure-field 1/2" Mic. Type 4193, Preamp. Type 2669-C, Adaptor UC-0211
Type 4193-L-004	Yes	Pressure-field 1/2" Mic. Type 4193, Preamp. Type 2669-L, Adaptor UC-0211
Type 4938-A-011	Yes	Pressure-field 1/4" Mic. Type 4938, Preamp. Type 2670
Type 4938-C-002	Yes	Pressure-field 1/4" Mic. Type 4938, Preamp. Type 2669-C, Adaptor UA-0035
Type 4938-L-002	Yes	Pressure-field 1/4" Mic. Type 4938, Preamp. Type 2669-L, Adaptor UA-0035
Type 4939-A-011	Yes	Free-field 1/4" Mic. Type 4939, Preamp. Type 2670
Type 4939-C-002	Yes	Free-field 1/4" Mic. Type 4939, Preamp. Type 2669-C, Adaptor UA-0035
Type 4939-L-002	Yes	Free-field 1/4" Mic. Type 4939, Preamp. Type 2669-L, Adaptor UA-0035
Type 4941-A-011	No	High-level Pressure-field 1/4" Mic. Type 4941, Preamp. Type 2670
Type 4941-C-002	No	High-level Pressure-field 1/4" Mic. Type 4941, Preamp. Type 2669-C, Adaptor UA-0035
Type 4942-B-001*	Yes	Prepolarized Diffuse-field 1/2" Mic. Type 4942, Preamp. Type 2669-B
Type 4942-C-001	Yes	Prepolarized Diffuse-field 1/2" Mic. Type 4942, Preamp. Type 2669-C
Type 4942-L-001	Yes	Prepolarized Diffuse-field 1/2" Mic. Type 4942, Preamp. Type 2669-L
Type 4942-A-021	Yes	Prepolarized Diffuse-field 1/2" Mic. Type 4942, Preamp. Type 2671
Type 4942-A-031	Yes	Prepolarized Diffuse-field 1/2" Mic. Type 4942, Preamp. Type 2699
Type 4942-H-041	Yes	Prepolarized Diffuse-field 1/2" Mic. Type 4942, Preamp. 1706

Order No.	Mini CD Incl.	Description
Type 4943-B-001*	Yes	Diffuse-field 1/2" Mic. Type 4943, Preamp. Type 2669-B
Type 4943-C-001	Yes	Diffuse-field 1/2" Mic. Type 4943, Preamp. Type 2669-C
Type 4943-L-001	Yes	Diffuse-field 1/2" Mic. Type 4943, Preamp. Type 2669-L
Type 4944-A	No	Pressure-field 1/4" Mic. Type 4944 with SMB socket
Type 4944-B	No	Pressure-field 1/4" Mic. Type 4944 with 10–32 UNF socket
Type 4948	No	Aerospace Surface Microphone
Type 4949	No	Automotive Surface Microphone
Type 4954-A	No	Free-field 1/4" Mic. Type 4954 with SMB socket
Type 4954-B	No	Free-field 1/4" Mic. Type 4954 with 10–32 UNF socket
Type 4954-A-011	Yes	1/4" Prepolarized Free-field Mic. Type 4954, Preamp. Type 2670
Type 4955	Yes	1/2" Low-noise Free-field Microphone
Type 4955-A	Yes	1/2" Low-noise Free-field Microphone for hand-held analyzers such as Type 2250/2270
Type 4956-W-001	Yes	Prepolarized Pressure-field 1/2" Mic. Type 4956 with Preamp. Type 2671-W-001
Type 4957†	No	10 kHz Array Microphone
Type 4958‡	No	20 kHz Precision Array Microphone
Type 4959	No	Short 20 kHz Array Microphone
Type 4966-H-041	Yes	Prepolarized Free-field 1/2" Mic. Type 4966 with Preamp. Type 1706
Other TEDS Related Equipment		
BZ-5294	–	TEDS Editor Kit
ZZ-0245	–	In-line TEDS Adaptor for CCLD Transducer without TEDS
Type 2467-A	–	1 mV/pC Charge to CCLD Converter with TEDS
Type 2647-B	–	10 mV/pC Charge to CCLD Converter with TEDS
Type 2647-C	–	0.1 mV/pC Charge to CCLD Converter with TEDS

* These types are delivered with a LEMO to Brüel & Kjær cable AO-0428. This cable does **NOT** support TEDS

† TEDS to IEEE 1454.4, V1.0, UDID No. 127–0–0–0U

‡ TEDS to IEEE 1454.4, V1.0, UDID No. 127–0–0–1 U with complex transfer function

© Brüel & Kjær. All rights reserved.
2016-11
BP 2225 – 15



Brüel & Kjær and all other trademarks, service marks, trade names, logos and product names are the property of Brüel & Kjær or a third-party company.

Brüel & Kjær Sound & Vibration Measurement A/S
DK-2850 Nærum · Denmark · Telephone: +45 77 41 20 00 · Fax: +45 45 80 14 05
www.bksv.com · info@bksv.com
Local representatives and service organizations worldwide

Although reasonable care has been taken to ensure the information in this document is accurate, nothing herein can be construed to imply representation or warranty as to its accuracy, currency or completeness, nor is it intended to form the basis of any contract. Content is subject to change without notice – contact Brüel & Kjær for the latest version of this document.



PRODUCT DATA

1/2" Prepolarized Infrasond Microphone Type 4964

Type 4964 is designed for high-precision, acoustic measurements where an infrasond microphone with high sensitivity is required. Being prepolarized, Type 4964 can be used with both CCLD and classical preamplifiers.

Uses

- General noise measurements
- Wind turbine measurements
- Sonic boom measurements

Features

- Sensitivity: 50 mV/Pa
- Frequency: 0.02 Hz – 20 kHz (± 3 dB)
- Dynamic Range: 14.6 – 146 dB
- Temperature: –30 to +150 C (–22 to +302 F)
- Polarization: Pre-polarized



Use of Free-field Microphones

Free-field means that the frequency response at 0 degrees incidence is flat. Free-field microphones are commonly used, for example, for recording sound measurements in anechoic chambers and far away from reflecting buildings. Another area for free-field microphones is for general electroacoustic measurement purposes like loudspeaker and microphone measurements.

At infrasond and frequencies below a few kHz, the pressure and free-field response are the same. At higher frequencies, reflections and diffractions cause pressure to increase in front of a microphone's diaphragm. Type 4964 has been optimized for free-field, and designed for use with the protection grid in place.

Type 4964 is also suited for use in class 1 sound level meters and for all high-precision acoustic measurements where a robust and stable free-field microphone with an upper frequency of 20 kHz is required.

Manufacturing and Stability

A press-fitted, stainless-steel diaphragm ensures superior long-term stability and mechanical robustness – Type 4964 will withstand the 1 m drop test of IEC 60068–2–32.

All Brüel & Kjær measuring microphones are assembled in a clean room. This ensures that the microphones maintain their inherent low noise floor and high stability, even when used in environments with a combination of high humidity and high temperature.

Polarization Voltage

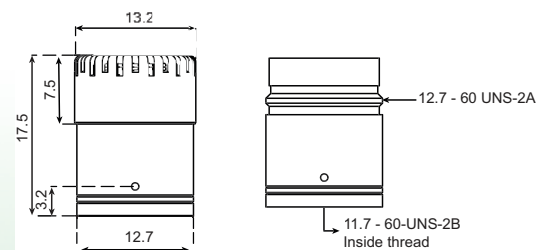
Being prepolarized, Type 4964 is especially well-suited for battery operated equipment and operation in environments with high humidity.

Individual Calibration Data

Each Type 4964 comes with an individual calibration chart including information about the open-circuit sensitivity, the frequency response in a free field as well as the electrostatic actuator response.

An enclosed mini-CD contains the individual calibration data at 1/12-octave frequencies plus a wealth of technical information, such as the influence of different accessories, response in different sound fields and much more. Using the CD data and the REq-X feature of PULSE™, a real-time correction for different measurement situations, can increase measurement accuracy.

Fig. 1 Physical specifications of Type 4964



130188

Brüel & Kjær 

Specifications – Prepolarized Infrasound Microphone Type 4964 (valid for serial number 2495 387)

Specification	Value
IEC 61094–4 Type Designation	WS2F
Polarization Voltage (external)	0 V (prepolarized)
Open-circuit Sensitivity (250 Hz) [*]	50 mV/Pa, –26 dB ±1.5 dB re 1 V/Pa
0° Incidence Free-field Response [*]	0.04 Hz to 8 kHz: ±1 dB 0.03 Hz to 20 kHz: ±2 dB
Lower Limiting Frequency (–3 dB) [*]	0.01 to 0.05 Hz
Pressure Equalization Vent	Rear vented
Diaphragm Resonance Frequency	14 kHz (90° phase shift)
Cartridge Capacitance (Polarized) [†]	14 pF at 250 Hz
Equivalent Air Volume	46 mm ³ (250 Hz)
Pistonphone Correction	0.00 dB (with Type 4228 and DP-0776)
Cartridge Thermal Noise	14.6 dB(A), 15.3 dB(Lin)
Upper Limit of Dynamic Range [‡]	3% Distortion: >148 dB SPL Max. SPL: 158 dB (peak)
Environmental	
Operating Temperature Range	–30 to +150 C (–22 to +302 F)
Storage Temperature (in Microphone Box)	–30 to +70 C (–22 to +158 F) With mini-CD: +5 to +150 C (+41 to 122 F)
Temperature Coefficient (250 Hz)	–0.006 dB/K (–10 to +50°C/+14 to 122°F)
Pressure Coefficient	–0.01 dB/kPa
Operating Humidity Range	0 to 100% RH (without condensation)
Influence of Humidity	<0.1 dB in the absence of condensation
Vibration Sensitivity (<1000 Hz)	62.5 dB, ≈ SPL for 1 m/s ² axial vibration
Magnetic Field Sensitivity	6 dB SPL for 80 A/m, 50 Hz field
Estimated Long-term Stability	>1 dB/1000 years in dry air at 20°C (68°F) >2 hours/ dB in dry air at 150°C (302°F) >40 years/ dB in air at 20°C (68°F), 90% RH >1 dB/year in air at 50 C (122 F), 90% RH
Physical	
Thread for Preamplicifier Mounting	11.7 mm–60 UNS
Diameter with Grid	13.2 mm (0.52")
Diameter without Grid	12.7 mm (0.50")
Height with Grid	17.6 mm (0.69")
Height without Grid	16.3 mm (0.64")

^{*} Individually calibrated

[†] 137 dB (peak) with CCLD preamplicifier and 24 V supply and 140 (peak) with ±15 V supply

Ordering Information

Type 4964 ½" Prepolarized Infrasound Microphone Type 4964

Includes the following accessories:

- BC-0224: Calibration Chart[‡]
- BC-5002: Microphone Mini-CD[‡]

Optional Accessories	
Type 1706	½" CCLD High Temperature Preamplicifier
Type 2669	½" Microphone Preamplicifier
2671-W-001	½" CCLD Preamplicifier (version with LLF <1.2 Hz)
Type 2699	½" CCLD Preamplicifier, A-weighted
Type 4231	Sound Calibrator
Type 4228	Pistonphone
Type 4226	Multifunction Acoustic Calibrator
DP-0776	Calibration Adapter for ½" Microphones
UA-0033	Electrostatic Actuator
UA-1260	½" Angle Adaptor (approx. 80°)
UA-0386	Nose Cone for ½" Microphone
UA-0237	Windscreen for ½" microphone, 90 mm diameter
UA-0459	Windscreen for ½" Microphone, 65 mm diameter
Calibration Services	
4964-CAI	Accredited Initial Calibration
4964-CAF	Accredited Calibration
4964-CFF	Factory Standard Calibration



Compliance with EMC Directive and Low Voltage Directive of the EU
Compliance with the EMC requirements of Australia and New Zealand

[‡] State microphone serial number if re-ordering calibration data

Brüel & Kjær reserves the right to change specifications and accessories without notice. © Brüel & Kjær. All rights reserved.

HEADQUARTERS: Brüel & Kjær Sound & Vibration Measurement A/S · DK-2850 Nærum · Denmark
Telephone: +45 7741 2000 · Fax: +45 4580 1405 · www.bksv.com · info@bksv.com

Local representatives and service organisations worldwide

Brüel & Kjær

BP 2478-11 2013-05



PRODUCT DATA

½" Prepolarized Free-field Microphone Type 4966

Type 4966 is designed for high-precision, free-field measurements where a microphone with high sensitivity is required. Being prepolarized, Type 4966 can be used with both CCLD[‡] and classical Brüel & Kjær preamplifiers.



Uses

- Precision sound-measurements
- General purpose sound-measurements
- Electroacoustic measurements

Features

- Sensitivity: 50 mV/Pa
- Frequency: 5 Hz to 20 kHz
- Dynamic Range: 14.6 to 144 dB
- Temperature: -30 to +150 °C (-22 to +302 °F)

Description

Type 4966 is a robust and stable free-field microphone cartridge designed for high-precision acoustic measurements. It is developed and refined for measurements where a high sensitivity microphone with a full 20 kHz bandwidth is preferred and is optimized for use with the protection grid in place. Type 4966 is prepolarized, so it is well suited for use in battery-operated equipment and environments with high humidity.

Because this microphone is optimized for free-field environments, it has a flat free-field response at 0° incidence. This makes Type 4966 ideal for use in anechoic chambers or far away from reflective surfaces, such as buildings, and for general electroacoustic measurement purposes, such as loudspeaker and microphone measurements.

Manufacturing and Stability

The press-fitted, stainless-steel diaphragm of Type 4966 ensures superior long-term stability and mechanical robustness, withstanding the 1 m drop test according to IEC 60068-2-32.

All Brüel & Kjær measuring microphones are assembled in a clean room. This ensures that the microphones maintain their low noise floor and high stability even in environments with a combination of high humidity and high temperature.

TEDS Microphone

Type 4966-H-041 is a transducer electric data sheet (TEDS) combination of Type 4966 and High-temperature CCLD Microphone Preamplifier Type 1706. The TEDS template is based on IEEE P1451.4 and programmed with the loaded sensitivity of the actual cartridge. This combination can be used for measurements up to 125 °C (257 °F) making it suitable for

use in a broad range of applications. Brüel & Kjær offers a selection of cables, including cables for use at higher temperatures.

TEDS microphones are considered one unit because the cartridge is sealed to the preamplifier in production.

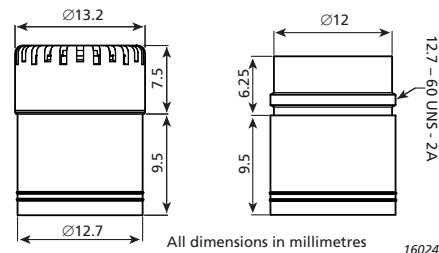
Individual Calibration Data

All calibration data for Brüel & Kjær transducers is now available electronically. Find calibration charts and correction factors at bksv.com/calibrationdata and select Search Calibrations.

Calibration charts include information about the open-circuit sensitivity, the frequency response in a free field and the electrostatic actuator response.

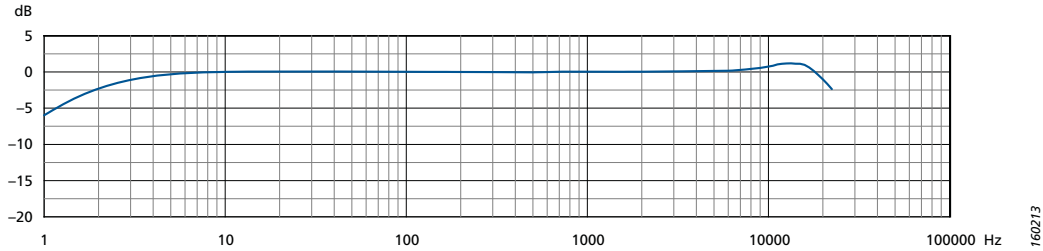
Correction factors contain individual calibration data at 1/12-octave frequencies and technical information, such as the influence of different accessories and the microphone's response in different sound fields. For example, use data and the REq-X feature of PULSE™ for a real-time correction under different measurement situations to increase measurement accuracy.

Fig. 1 Dimensions of Type 4966



[‡] CCLD: Constant current line drive, also known as DeltaTron® (IEPE compatible)

Fig. 2 Typical free-field response of the microphone cartridge with protection grid. The low-frequency response is valid when the vent is exposed to the sound field



Specifications – 1/2" Free-field Microphone Type 4966

Type No.	4966
General	
IEC 61094–4 Type Designation	WS2F
Polarization Voltage	0 V (prepolarized)
Open-circuit Sensitivity (250 Hz) [†]	50 mV/Pa, –26 ± 1.5 dB re 1 V/Pa
0° Incidence Free-field Response [*]	10 Hz to 8 kHz: ±1 dB 5 Hz to 20 kHz: ±2 dB
Lower Limiting Frequency (LLF)(–3 dB) [†]	1 to 3 Hz
Pressure Equalization Vent	Rear vented
Cartridge Capacitance [*]	14 pF at 250 Hz
Pistonphone Correction (Type 4228 with DP-0776)	0.00 dB
Cartridge Thermal Noise	14.9 dB(A), 15.4 dB(Lin)
Upper Limit of Dynamic Range (3% Distortion)	>144 dB SPL [†]
Max. Sound Pressure Level	158 dB (peak)
Environmental	
Operating Temperature Range	–30 to +150 °C (–22 to +302 °F)
Storage Temperature In Microphone Box	–30 to +70 °C (–22 to +158 °F)
With Mini-CD	5 to 50 °C (41 to 122 °F)
Temperature Coefficient (250 Hz)	+0.003 dB/K (–10 to +50 °C, 14 to 122 °F)
Pressure Coefficient	–0.012 dB/kPa
Operating Humidity Range	0 to 100% RH (without condensation)
Influence of Humidity	<0.1 dB in the absence of condensation
Vibration Sensitivity (<1000 Hz)	62.5 dB equivalent SPL for 1 m/s ² axial vibration
Magnetic Field Sensitivity	6 dB SPL for 80 A/m, 50 Hz field
Estimated Long-term Stability	<1 dB/1000 years in dry air at 20 °C (68 °F)
	<1 dB/2 hours in dry air at 150 °C (302 °F)
	<1 dB/40 years in 90% RH at 20 °C (68 °F)
	<1 dB/1 year in 90% RH at 50 °C (122 °F)

* Individually calibrated

† 137 dB (peak) with DeltaTron preamplifier and 24 V supply and 140 dB (peak) with ±15 V supply

All values are typical at 23 °C (73.4 °F), 101.3 kPa and 50% RH unless otherwise specified

Ordering Information

Type 4966 1/2" Prepolarized Free-field Microphone[‡]

TEDS COMBINATION

Type 4966-H-041 Type 4966 with Type 1706[‡]

OPTIONAL ACCESSORIES

Type 2669 1/2" Microphone Preamplifier
Type 1706 1/2" CCLD Microphone Preamplifier (LLF: <3 Hz)

Type 2671-W-001 1/2" CCLD Microphone Preamplifier (LLF: <1.2 Hz)

Type 2699 1/2" CCLD Microphone Preamplifier, A-weighted

Type 4231 Sound Calibrator
Type 4228 Pistonphone
Type 4226 Multifunction Acoustic Calibrator

DP-0776 Calibration Adaptor for 1/2" Microphones

UA-0033 Electrostatic Actuator
UA-1260 1/2" Angle Adaptor (approx. 80°)

UA-0386 Nose Cone, 1/2" microphone
UA-0237 Windscreen, 1/2" microphone, Ø 90 mm

UA-0459 Windscreen, 1/2" microphone, Ø 65 mm

CALIBRATION SERVICES

4966-CAI Accredited Initial Calibration
4966-CAF Accredited Calibration
4966-CFF Factory Standard Calibration

COMPLIANCE WITH STANDARDS



‡ Calibration data can be found at bksv.com

Brüel & Kjær and all other trademarks, service marks, trade names, logos and product names are the property of Brüel & Kjær or a third-party company.

Brüel & Kjær Sound & Vibration Measurement A/S
DK-2850 Nærum · Denmark · Telephone: +45 77 41 20 00 · Fax: +45 45 80 14 05
www.bksv.com · info@bksv.com
Local representatives and service organizations worldwide

Although reasonable care has been taken to ensure the information in this document is accurate, nothing herein can be construed to imply representation or warranty as to its accuracy, currency or completeness, nor is it intended to form the basis of any contract. Content is subject to change without notice – contact Brüel & Kjær for the latest version of this document.

Brüel & Kjær

160213
© Brüel & Kjær. All rights reserved.
BP 2536–13 2019-02
BP-2536–13
BP-2536–13